

IN VITRO AND IN SILICO FINDINGS ON CELL-CELL AND CELL-ECM
INTERACTIONS DURING CELLULAR AGGREGATION AND
REARRANGEMENT

by

CARLOS EDUARDO CAICEDO-CARVAJAL

A dissertation submitted to

The Graduate School-New Brunswick

Rutgers, The State University of New Jersey

and

The Graduate School of Biomedical Sciences

University of Medicine and Dentistry of New Jersey

In partial fulfillment of the requirements for the degree of

Doctor of Philosophy

Graduate Program in Biomedical Engineering

Written under the direction of

Troy Shinbrot, Ph.D.

Ramsey A. Foty, Ph.D.

And approved by

New Brunswick, New Jersey
October, 2009

ABSTRACT OF THE DISSERTATION

IN VITRO AND IN SILICO FINDINGS ON CELL-CELL AND CELL-ECM INTERACTIONS DURING CELLULAR AGGREGATION AND REARRANGEMENT

By

CARLOS E. CAICEDO-CARVAJAL

Dissertation Director:

Troy Shinbrot, Ph.D.

Ramsey A. Foty, Ph.D.

In this dissertation, we present in silico and in vitro work on the dynamics of cellular aggregation and rearrangement as cell-cell and cell-ECM interactions are systematically varied. Computationally, we explore the contributions of homotypic and heterotypic forces between cells and the ECM affect cellular self-assembly. We find that variation of homotypic and heterotypic forces generates both expected morphologies and previously unreported patterns. Among the newly discovered patterns are segmented states of alternating cell types, and an “onion” state, in which cells form multilayer-aggregates of two cell types. Experimentally we varied cell-ECM adhesive strength through selection of $\alpha 5 \beta 1$ -integrin receptor expression in Chinese Hamster Ovary (CHO) Cells at two soluble fibronectin (sFn) concentrations. Second, to describe dual adhesive relations, we used a CHO cell line variants coexpressing integrin and N-cadherin surface receptors. We found previously unreported complex behaviors of aggregates in these experiments. For example, we found that at constant sFn concentration, aggregate cohesion grows linearly

as $\alpha 5\beta 1$ receptor density is increased from low to moderate levels. However, further increase in receptor expression causes an abrupt drop in tissue cohesion. We propose that the observed biphasic property of these aggregates may be due to depletion of sFn below a critical value in the aggregate microenvironment at high $\alpha 5\beta 1$ expression level. We also found that a complicated interplay emerges when cell-ECM and cell-cell interactions mediate cellular aggregation and rearrangement. Thus, we describe two nodes of cellular interaction, cell-ECM and cell-cell/cell-ECM. For weak cell-ECM interactions, cells can still rearrange, and new cellular patterns (e.g. inverted structures) emerge. For high cell-ECM strengths, cells are bound to the matrix and cannot rearrange. For weak and high cell-ECM interactions, cell-cell governs final equilibrium configurations. We propose that these results have potential implications for embryonic development, for wound healing, and for cancer therapeutic applications.

Acknowledgements

As the sounds of pots and pans exponentially grew, I realized it was time to leave. This was the beginning of a transition in my life. Life is full of transitions and each transition brings two important gifts, the excitement of a new beginning and the people that would make a new beginning a reality. Ever since my arrival to the United States in the winter of 1994, I have witnessed the many extending hands that have made this new experience possible. It would be fair to give an account of those helping hands, on the prelude on this thesis work, and the everlasting contribution of valuable people in my life.

I would like to thank the following people:

Dr. Troy Shinbrot, it has been a learning experience all these years under your direction. You always kept everything on the bright side, even when situations were out of control and without a feasible solution. I appreciated your interest on every idea I presented to you, even the silly ones, because you always took them with great respect and attention. I take with great pride all your knowledge and ethics and I will make sure to transmit these learning experiences, as I venture into another new beginning.

Judith Dickerson, Dr. Nadir Kaddour, Dr. Peter Pappas, Dr. Alexis Thurman, Dean Bette Simmons, Mr. Martinez, Eduardo Lopez, Dr. Peter C. Kahn, Kamal Khan, and Dr. Muriel Grimmett, for defining the origin of what I have achieved today. Thanks for the leadership and the constant encouragement during my early years. Your positivism and willingness showed me that many things are possible through hard work and perseverance.

Dr. Joaquin Kohn, Dr. Thomas Papathomas, Dr. Martin Yarmush, Dr. Henrik Pedersen, Dr. Sharon Bourke, and Dr. Norbert Weber for materializing and helping me pursue the idea about graduate school. This has definitively been a valuable option in my life.

The Surgery Department at Robert Wood Johnson, Dr. Ramsey Foty, for being my co-advisor supporting part of this work and endlessly correcting my thesis, and Dr. Dongxuan Jia for the patience, great conversations, and providing experimental expertise in the laboratory. Dr. Eva-Maria Schoetz for stimulating scientific discussions and for later on opening the doors of her laboratory at Princeton University. Dr. Siobhan Corbett for help and guidance, Dr. Mohan Raj for providing cell lines and protocols, and Elaine Langerfeld, and Marie Macor for making the tough times enjoyable.

My classmates: Nick Tovar, Tamika Blassingame, Eric Balint, Eleina Panas, Marika Bergenstock and Normal Lapin, for those great moments and because we were there for each other when most needed.

The research group, “The Core”, Mehdi Doumi, Andrew Voyiadjis, and Kerri-Ann Norton, for all those great stimulating discussions about science and life. I definitively enjoyed your company during my graduate work.

The BME Fellows and friends at Rutgers, these valuable people, whom, I mainly encounter in the hallways, and we usually ended up laughing, sharing expertise, and exchanging thoughts about life. I am definitively happy to have met each of you. Jason Maikos, Harini Sundararaghavan, Garry Monteiro, Jocie Harris, Maria Pia Rossi, Shirley Masand, Mercedes Morales, Nuria Royo, Christopher Gaughan, Lavania Peddada, Kevin Nikitzuk, J.P., Norman Lapin, Salah Hemed, Alex Fok, Salah Somakia, Christ

Langhammer, Ian Gaudet, Jeremy Griffin, Roberto Delgado, Margareth Julias, and Danila Guzman.

The BME Faculty, Dr. Nada Bustany for teaching optics and opening the doors of her laboratory. Dr. William Craelius, Dr. David Shreiber, Dr. Kathryn Uhrich, and Dr. George Shoane for discussions and providing expertise during my graduate work. Outside Members: Dr. Emmanuel Diccico-Bloom and Dr. Siobhan Corbett for valuable expertise and suggestions.

I also had the opportunity to met people whom, sometimes when I wanted to get away from all the stress, either going over a pint, exercising, or a casual stress-free conversation, they all made it happen. Jose R. Fernandez, El-Mehdi Doumi, Mark Carmichael, Lucy Kwan, Meera Mani, Erik Semler, Anibal Sotocardalda, Tonye Briggs, Jean Paul Abboud, Ziad Saem-el-Dahr, Maziar Shirazi, Stephen Guzikowski, Anibal Valentin, France Gratacos, Napoleon Benavides, Kelvin Caban, Alana Toro-Ramos, Deena Midani, Patricia Irizarry-Barreto, Ana Ramos, Rosanna Grafals, and Jacqueline Florez-Otero.

I would like to thank the people who read my work and offered valuable advise on presentation and syntax, Dr. Kathryn Scarbrough and Evelyn Strombom.

The people who make paperwork enjoyable: Ursula Wolf, Perry Dominguez, Linda Johnson and Lawrence Stromberg.

Finally, I would like to thank the other mechanism that drives our dreams: funding. I thank the taxpayer money for partially paying my college education; I made sure it did not go to waste. The Educational Opportunity Fund (EOF) at Morris County College and Rutgers University, The Ronald McNair Fellowship (Rutgers University), The

Biotechnology Fellowship (Rutgers University), the Graduate School of Biological Sciences (UMDNJ), and the Engineering Research Center (ERC) at Rutgers.

Dedication

I would like to dedicate this work to my wife, Estelle Marie Ruidiaz-Santiago for her constant presence, understanding of odd working hours, patience through my rough times, and making my graduate school experience a complete event in my life. I would like to thank my mother, Leonor Carvajal for teaching me to pursue my dreams and achieve them. My father Miguel Angel Caicedo for teaching me that life is simple and that one has to irradiate calm to others, even when the situation seem far from positive or plausible to change. My stepmother Nina Caicedo and her son and daughters Larry, Sorany, and Sully San Martin, because they all showed me that in adversity, true friends would always come to your doorsteps. The Caicedo Family in South Carolina, for the great moments and the help provided during tough times. My family in Puerto Rico, Colombia, Florida and Louisiana, Ruidiaz-Santiago, Carvajal, Mora, and Betancourt-Laserna families for the constant support in my life. I would like to thank my brother Joffre Abdul-Rahim and Guillermo Monje for conversations and laughs on the weekends at mom's home. Finally, friends that have become family because they make you feel welcome, cared for, and are always there unconditionally. I would like to extend this dedication to my long-lasting friends, John Proano, Fernanda Proano, Javier Diaz and Norma Diaz. I always looked forward for those weekends when we all share laughs, playing with the kids in the backyard, and talked until the night fell asleep. "The Mosques": Jessica and Maritxa Reymundo, Eda Paola Angulo, Betiana Caprioli, and Jessica Segura for those great times of serious talks and fun times.

Table of Contents

ABSTRACT OF THE DISSERTATION	ii
ACKNOWLEDGEMENTS	iv
DEDICATION	viii
TABLE OF CONTENTS	ix
LIST OF TABLES	xi
LIST OF FIGURES	xii
Chapter 1	1
Historical and Experimental Perspective on Cellular Aggregation and Rearrangement.....	1
INTRODUCTION	2
BACKGROUND	10
IN SILICO ASPECT OF CELL INTERACTIONS	10
Historical Perspective of in silico Cellular Dynamics	11
Dissipative Particle Dynamics: Approximation to 3-D Cellular Interaction	13
BIOLOGICAL ASPECT OF CELLULAR BINDING	14
Short-Range Interactions: The Cadherin Paradigm	15
Long-Range Interactions: Cell-ECM Paradigm.....	20
Fibronectin: The Basic Unit of a Complex Substrate	24
$\alpha 5 \beta 1$ -Fibronectin Interactions are Required for Insoluble Fn Matrix Formation	28
The Effect of Integrin Receptor and ECM-ligand Concentration on Cell Migration	33
The Effect of Cellular Repulsion on Morphogenesis	35
DIFFERENTIAL ADHESION HYPOTHESIS (DAH): FROM CELL-CELL INTERACTIONS TO LARGE-SCALE TISSUE ASSEMBLY	36
DAH FRAMEWORK ON CELL-ECM CONTRIBUTIONS TO TISSUE MECHANICS	43
Tissue Self-Organization Requires Active Substrate Interactions.....	48
TWO-DIMENSION VS. 3-DIMENSION STRUCTURE IN EMBRYONIC DEVELOPMENT	49
Chapter 2	51
Computational Dynamics of Structure and Rearrangement: in silico 3D Cellular Morphogenesis.....	51
ABSTRACT	55
INTRODUCTION	56
MODEL DESCRIPTION.....	57
PHASE DIAGRAM	61
DISCUSSION	63
ACKNOWLEDGEMENT	67
APPENDIX: MODEL DETAILS.....	67
The mechanical system	67
Computational details	68
CHAPTER 2 BIBLIOGRAPHY	71

Chapter 3	76
Interplay Between $\alpha 5\beta 1$ Receptor Expression and Soluble Fibronectin Concentration Influences Tissue Visco-elasticity and Rearrangement	76
ABSTRACT	77
INTRODUCTION	78
RESULTS	82
Characterization of integrin receptor level expression and fibronectin matrix assembly.....	82
The interplay between $\alpha 5\beta 1$ receptor density and soluble fibronectin concentration promotes changes in tissue mechanical properties.	86
Increasing $\alpha 5\beta 1$ surface receptor affects surface tension in a biphasic manner.	92
$\alpha 5\beta 1$ expression and soluble fibronectin concentration influence aggregate compaction.....	95
The effect of $\alpha 5\beta 1$ integrin receptor expression on sFn concentration and insoluble Fn matrix.....	100
The effect of N-cadherin on $\alpha 5\beta 1$ -Fibronectin interactions.....	104
The influence of $\alpha 5\beta 1$ and $\alpha 5\beta 1$ /Ncad on cell rearrangement	108
DISCUSSION	114
Interplay between integrin receptor density and soluble fibronectin concentration influence tissue mechanical properties	115
Structure formation is affected by soluble fibronectin concentration history.....	116
Interplay between N-cadherin and $\alpha 5\beta 1$ -fibronectin interactions on aggregate mechanical properties	118
The effect integrin alone and integrin-cadherin adhesion on cellular rearrangement	119
METHODS	122
CHAPTER 3 BIBLIOGRAPHY.....	140
Chapter 4	144
Conclusions and Outlook	144
Bibliography	148
Curriculum Vitae	159

List of Tables

TABLE B-1. OVERVIEW OF CLASSICAL AND NON-CLASSICAL CADHERINS.	19
TABLE B-2. CHRONOLOGICAL ADVANCES OF CADHERIN-MEDIATED CELLULAR SELF- ASSEMBLY.....	42
TABLE B-3. CHRONOLOGICAL ADVANCES OF THE EFFECT OF CELL-ECM INTERACTIONS ON CELLULAR AGGREGATION.	44
TABLE 3-1. AGGREGATE SURFACE TENSION MEASUREMENTS AS A FUNCTION OF $\alpha 5\beta 1$ RECEPTOR DENSITY.	93
TABLE 3-2. AGGREGATE SURFACE TENSION MEASUREMENTS AS A FUNCTION OF $\alpha 5\beta 1$ RECEPTOR AND N-CAD EXPRESSION..	106
TABLE 3-3. SURFACE TENSION VALUES AND PERCENT LIQUIDITY.....	107

List of Figures

FIGURE B-1. STRUCTURE OF THE CADHERIN RECEPTOR.....	16
FIGURE B-2. REPRESENTATION OF 3 EPITHELIAL CELLS..	17
FIGURE B-3. DIAGRAM DESCRIBING TWO MAJOR TYPES OF ECM PROTEINS.....	23
FIGURE B-4. SOLUBLE FORM OF THE FIBRONECTIN DIMER.....	26
FIGURE B-5. HETERODIMERIC FORM OF THE INTEGRIN RECEPTOR.....	29
FIGURE B-6. INTEGRIN HETERODIMER CLUSTERING ON PLANAR SURFACES.....	31
FIGURE B-7. EFFECT OF COMPRESSIVE FORCES ON AGGREGATE GEOMETRY.....	41
FIGURE B-8. COMPARISON BETWEEN EMBRYONIC TISSUE AND CADHERIN ENGINEERED CELLS.....	47
FIGURE 2-1. SCHEMATICS OF INTERACTIONS BETWEEN CELLS.....	59
FIGURE 2-2. PHASE DIAGRAM FOR HOOKEAN ATTRACTION AND INVERSE R^2 REPULSION...	63
FIGURE 2-3. COMPARISON IN VITRO AND IN SILICO CELL ORGANIZATION PATTERNS.....	65
FIGURE 2-4. FLOW CHART OF IN SILICO MODEL.....	70
FIGURE 3-1. ANALYSIS BY FLOW CYTOMETRY OF $\alpha 5\beta 1$ EXPRESSION.....	83
FIGURE 3-2. ANALYSIS BY FLOW CYTOMETRY OF DUAL $\alpha 5\beta 1$ AND N-CAD RECEPTOR EXPRESSION.....	84
FIGURE 3-3. FIBRONECTIN MATRIX ASSEMBLY ON GLASS COVERSLEPS AFTER 24 HOURS...	85
FIGURE 3-4. RESPONSE OF CHO- $\alpha 5\beta 1$ (M) CELL AGGREGATES TO A COMPRESSIVE FORCE REFLECT MECHANICAL PROPERTIES.....	87
FIGURE 3-5. VISCOELASTIC PROPERTIES OF AGGREGATES.....	89
FIGURE 3-6. PLOTS OF AGGREGATE SURFACE TENSION VS. AGGREGATE VOLUME.....	91
FIGURE 3-7. BIPHASIC BEHAVIOR OF TISSUE SURFACE TENSION.....	95
FIGURE 3-8. AGGREGATION ASSAYS AS A FUNCTION OF INITIAL CELL SEEDING DENSITY AND CONSTANT TISSUE CULTURE MEDIA.....	98
FIGURE 3-9. CELL AGGREGATION AS A FUNCTION OF CELL SEEDING DENSITY AND $\alpha 5\beta 1$ RECEPTOR EXPRESSION.....	100
FIGURE 3-10. SFN CONCENTRATION AND RATE OF SFN UTILIZATION DURING AGGREGATION OF CHO- $\alpha 5\beta 1$ (M AND HH).....	102
FIGURE 3-11. FRESH TISSUE AGGREGATE IMMUNOSTAINING.....	103
FIGURE 3-12. PLOTS OF AGGREGATE SURFACE TENSION VS. AGGREGATE VOLUME.....	105
FIGURE 3-13. LACK OF REARRANGEMENT OF CELLS EXPRESSING DIFFERENT LEVELS OF $\alpha 5\beta 1$ INTEGRIN RECEPTOR.....	109
FIGURE 3-14. REARRANGEMENT DYNAMICS OF $\alpha 5\beta 1$ CELLS AND ITS PARENT CELL LINE, P3(GREEN).....	111
FIGURE 3-15. EXOTIC REARRANGEMENT DYNAMICS OF $\alpha 5\beta 1$ (HH).....	112
FIGURE 3-16. REARRANGEMENT DYNAMICS OF $\alpha 5\beta 1$ /N-CAD CELLS WITH CHO-P3 CELL.	113

Chapter 1

Historical and Experimental Perspective on Cellular Aggregation and Rearrangement

INTRODUCTION

The mammalian body plan arises as a consequence of complex interactions between cells, tissues, organs, and organ systems. Notwithstanding this complexity, development from an undifferentiated blastula into a more complex, three-layered organized embryo proceeds from a limited sequence of essentially straightforward processes. Cells divide, differentiate, interact, migrate, and die. Of these fundamental processes, cell-cell and cell-extracellular matrix (ECM) interactions play a critical role in establishing direct contact between cells and the microenvironment in which they exist. Specifically, cell surface adhesion proteins are thought to be powerful mediators of morphogenesis during the establishment of specific spatial relationships between cells, tissues, and organs. They do so through the integration of the external matrix and the internal cytoskeleton of each cell in order to maintain cohesion and active rearrangement during tissue remodeling. The expression and function of various cell surface adhesion systems, such as cadherins and integrins, impart to cells and tissues certain biomechanical properties that can be measured. One such property, tissue surface tension, has previously been shown to correlate strongly with tissue self-assembly [1-12]

Although recreating the evolution of structure and function of a complex living tissue from single cells to whole organ systems is complex, identifying a set of basic rules that can be exploited to generate structure is a more manageable task. This thesis will explore the impact of extracellular matrix-mediated adhesion on biomechanical tissue properties and their attendant effect on cellular rearrangement to establish a set of physical rules through which cells and tissues can interact to generate histologically complex structures.

Cellular aggregation has been widely studied. Initial experiments by Townes and Holtfreter in the 1950s showed that cells dissociated from embryos spontaneously reaggregate in culture to adopt their original anatomical positions [13]. In that work, it was demonstrated that cells have affinities that drive aggregation and rearrangement of dissociated cell mixtures. Subsequent work showed that a more precise definition of affinity, the Differential Adhesion Hypothesis (DAH), could explain the rearrangement behavior of embryonic mixtures of cells [2]. Differential adhesion between cells is regulated by separate families of membrane-bound adhesion receptor proteins depending on whether the interaction is cell-cell, cell-substrate or a combination of both adhesive mechanisms [8, 10, 14-16]. Direct cell-cell adhesion is largely mediated by a family of Ca^{2+} -dependent receptors from the cadherin family, which are normally expressed during development. Changes in the expression and function of these membrane-bound receptors are known to guide tissue structure through both cohesion and rearrangement. During development, as the original fertilized egg becomes highly partitioned, the cell adhesion receptors E-cadherin (E-cad) and P-cadherin (P-cad) increase their expression in order to drive tissue aggregation during cellular division [17]. Consequently, reducing Ca^{2+} during the morula stage results in the dissociation of the agglomerate of cells, halting the regular progression to a blastula [18].

In addition to direct cell-cell interactions, cells also interact with the ECM. This interaction is mediated by fibronectin, a fibroblast-secreted protein in the ECM with an RGD (Arg-Gly-Asp) motif recognized by the external domain of integrin receptors. Following binding, soluble fibronectin polymerizes into a network of fibrils that affect not only the mechanical properties of tissue, but cellular motility within that tissue as

well [19, 20]. At the cell receptor level, the assembly of fibrils depends on the clustering of the α and β integrin units and the interaction of the $\alpha\beta$ heterodimeric complex with soluble fibronectin [21]. This occurs, for example, during development, as a critical step in gastrulation, where optimal substrate deposition drives the internalization of the mesoderm [21, 22]. Thus involution of the mesodermal layer during gastrulation is arrested by addition of RGD peptides, or antibodies against fibronectin and the $\beta 1$ subunit [23, 24]. The previous examples, illustrate the importance of substrate-mediated as well as cell-cell adhesion mechanisms during development.

The role of adhesion as the driving force of cell aggregation and tissue assembly in morphogenesis led to the formulation of a theoretical framework articulated in the “Differential Adhesion Hypothesis” (DAH), developed by Malcolm Steinberg in 1963 [2]. The DAH simplifies the complex nature of cell adhesive relations and proposes a straightforward mechanism based on physical principles to partially explain self-assembly. According to the DAH, mixtures of cells are analogous to mixtures of miscible/immiscible fluids. Such mixtures follow thermodynamic relationships that ultimately determine whether cells intermix or segregate. Moreover, the specific relationship between the work of cohesion and the work of adhesion determines spatial relations between the cells. For example, when detergent is added to an immiscible water-oil blend, both the work of cohesion of the water and the work of adhesion between the two fluids are decreased, leading to improved bonding between water and oil molecules and consequent miscibility between the fluids. Analogously, two populations of cells will separate if they exhibit a large difference in cadherin cell surface receptor densities, and will intermix if this difference is small [11]. Broadly speaking, this effect

has been characterized by correlating visual outcomes of segregation and intermixing of cells with the site frequency distribution theoretical model of cadherin bonds between cells. Thus a higher frequency of bonds is seen between cells having more cadherin receptors than between cells having fewer receptors. Similarly, cells with more bonds are found to adhere more strongly than cells with fewer bonds. As in the case of surfactant in a water-oil mixture, a decrease in the work of adhesion and cohesion of one cell population can lead to a transition from separation or sorting-out (separation of cell types) to intermixing of cell populations.

More specifically, Steinberg and collaborators have shown that the work of cohesion in cellular systems is proportional to the expression of cadherin cell surface receptors and can be expressed in terms of a surface tension that plays the same role as in the case of miscible and immiscible liquids [4, 8]. For example, a liquid with a higher surface tension will tend to be encapsulated by a second liquid with lower surface tension. Similarly for tissues, cells with more cadherin links or bonds tend to “round-up” and internally “sort-out” with respect to cells that have fewer surface cadherin receptors. In this regard, it has been shown that a minimal receptor difference between two cell populations of 1.4-fold is enough to drive segregation within a time scale of hours [8, 11, 14]. Tissue surface tension relations have been experimentally determined using early embryonic tissues in which the contribution of cadherin-based adhesive relations has been exhaustively characterized. In these experiments, surface tensions have been found to be directly related to the ability of cells to rearrange and sort-out, with the more cohesive phase always becoming enveloped by the less cohesive phase [6] in agreement with DAH predictions.

Notwithstanding these successes involving cell-cell interactions, cell-substrate interactions add a number of complications whose roles remain to be elucidated. For example, Wiseman et al., reported that heart and liver tissue taken from 5-day chick embryos behaved differently when time in culture was a variable during tissue rearrangement experiments. Thus, 1.5 day-old cultured chick embryonic heart tissue adopted an external position compared with 2.5 day old liver embryonic tissue, while heart tissue adopted an internal position when left in culture for the same time as the embryonic liver tissue [25]. Importantly, in that system the ability of embryonic heart tissue to adopt either an internal or an external position (termed “tissue reversal”) was found to depend on whether or not insoluble fibronectin matrix formed in the process [26, 27].

The role of cell-substrate interactions is further complicated by the fact that for cell assemblies to round up, sort out, or otherwise self-organize, the individual cells involved must be able to rearrange to adopt a minimum energy state [28]. In particular, for some tissues (e.g. limb bud, pigmented epithelium, heart, and liver), long incubation times in the presence of high concentrations of soluble fibronectin have been shown to lead to transitions from liquid-like to solid-like behavior [29]. In a solid-like state, cells cannot rearrange - despite biomechanical stresses that may be present - and remain locked into pre-existing conformation. Consequently the meaningfulness of parallels between cadherin and integrin-ECM-based mechanisms for tissue self-assembly is suspect.

The effect of integrin expression on cellular self-assembly has recently been scrutinized in vitro. In these tests, Chinese hamster ovary (CHO) epithelial cells,

transfected to express the $\alpha 5$ integrin (CHO- $\alpha 5\beta 1$) and allowed to aggregate in the presence of 30 $\mu\text{g/ml}$ soluble fibronectin, rounded up into a sphere, a typical liquid-like behavior allowing measurement of aggregate surface tension [15]. Thus, apparently one can modify integrin receptor expression and fibronectin concentration, defining a substrate-mediated adhesion working range that imparts liquidity. Intriguingly, a close comparison between surface tensions of cells adhering only through cadherins and cells adhering by means of the ECM has shown that cell-ECM interactions deliver more cohesion on a per-receptor basis. Interestingly, in that work ECM-based cohesion tended to increase with time in culture, whereas cadherin-dependent cohesion remained constant for the same time period [15]. This suggests that dependency of cell-ECM interactions on time may be associated with the chemical and physical nature of soluble fibronectin polymerizing into a complex meshwork: a conjecture that we study further in this work. This would be distinct from the case of cadherin-based aggregation, where rearrangement and cohesion is driven by constant bond strengths that do not appear to significantly depend on history.

These results, while not yet conclusive, make a compelling case that tissue cohesion and rearrangement may differ significantly depending on the type of adhesion system driving the dynamics in ways that are controlled by details of the mechanism holding the cells together. We speculate that the differences in mechanism and time courses between integrin-mediated and cadherin-mediated adhesion may significantly affect their roles during development.

The added complexity seen in cell-ECM interactions may be associated with multiple factors, including that fibronectin matrix formation depends first on integrin

receptor expression, second on the concentration of soluble fibronectin available over time, and third on the stability of the insoluble matrix. In light of the multiplicity of complex phenomena driving the formation of integrin-fibronectin mediated adhesion, it is unclear what the DAH would predict for cellular assembly in the presence of cell-substrate interactions. Although the effects on cellular rearrangement of differential expression of cadherins have been well studied, no similar evaluations using cells that express different amounts of integrins apparently exist in the literature. Likewise, changes in cellular rearrangements caused by the introduction of known integrin variants that polymerize fibronectin at different rates have not been studied, and effects of a potential competition between cellular interactions mediated by integrins and by cadherins are as yet poorly understood. As a consequence of these complications, effects such as rounding up and sorting-out have not been evaluated for integrin-fibronectin cell interactions, and as we will show, the actual state reached when integrin expression is varied is considerably more complicated than the existing DAH model would suggest.

A more comprehensive understanding of how integrin-fibronectin interactions can influence tissue cohesion and cell aggregation requires a firm grasp of the science of cell-cell and cell-substrate interactions and their roles in the formation of biological structures. To this end, in the chapters following I will summarize general and specific effects of the ECM on tissue mechanics and cellular rearrangement. In Chapter 1, I will discuss the relevant background for this thesis, followed by Chapter 2, in which I will present an *in silico* model of cellular rearrangements mediated by short-(cadherin) and long-(integrin-Fn) range interactions between cells. Next, I will present detailed experimental evaluations of the effects of cell-ECM interactions on tissue structure and

rheology. In Chapter 3, I will present tissue surface measurements of cell aggregates with variable expressions of $\alpha 5 \beta 1$ surface receptor expression and soluble fibronectin concentrations. Also in Chapter 3, I will examine changes in the rearrangement behavior associated with variations in cell-cell and cell-substrate interactions, thus posing questions about the possible role of each cohesive system during cell rearrangement. Chapter 4 we conclude and pose future questions about the role of cell-ECM and cell-cell/cell-ECM on morphogenesis.

BACKGROUND

Cells, as fundamental units of living tissue, represent the simplest component of biological tissues, organs or organisms, and the goal of this thesis is to address the question of how cells aggregate and rearrange as a function of the integrin $\alpha 5 \beta 1$ receptor and insoluble fibronectin in the surrounding matrix. We are especially interested in the effect of cell-ECM contributions to tissue cohesion and whether differences in the level of cohesion mediate segregation of whole tissue fragments of heterogeneous cell suspensions. The goal in this chapter is to review current knowledge of how membrane bound receptors contribute to cell-cell and cell-substrate interactions as background to the aims of this thesis.

In silico Aspect of Cell Interactions

From a physical perspective, cells rearrange and organize through interactions with other cells and with their substrates. In the case of local, cell-cell interactions, the type and the number of membrane-bound receptors determine the interactions leading to cellular reorganization. On the other hand, cell-substrate interactions offer another type of behavior, which we propose to study here. In particular, the contribution of several forms of cellular interaction, i.e., $\alpha 5 \beta 1$, cadherin, Eph/ephrin, and others, are involved in active substrate assembly, cell-cell attraction, and cell-cell repulsion respectively. Hence the interplay between these forms of cellular interaction has an effect on the dynamics of cells during morphogenesis, and in silico studies provide a means of isolating precisely how given interactions affect subsequent dynamics.

Historical Perspective of in silico Cellular Dynamics

Computer modeling of biological events has proven to be valuable in elucidating the mechanisms that lead to developmental biological features such as fibroblast aggregation, cell sorting, and epithelial folding [30-33]. A principal strength of computational modeling lies on its ability to provide a direct link between underlying physical principles and biological problems of practical importance. In addition, modeling has demonstrated that simple computational rules can be formulated to mimic the complex dynamics seen in physiological systems [34, 35]. Steinberg's Differential Adhesion Hypothesis (DAH) is a notable example of a simple model that appears to correctly predict biological morphogenesis. Several groups have used a variety of approaches to model morphogenesis – some better known examples include the French flag model, and the elucidation of the role of negative feedback in biological patterning networks [36, 37]. One of the most prevalent classes of computational modeling of biological structures involves "Potts" models, which have been applied, among other problems, to reproduce cell sorting as predicted by the DAH [38, 39].

Potts models spatially discrete approximations in which an array of coupled gridpoints, analogous to cells, switch between integer states. Thus for example, a zero could represent a vacant gridpoint, a one could represent a gridpoint occupied by one type of cell, a two could represent a second type of cell, etc. By defining rules of interaction between neighboring gridpoints, one can model how cells might interact. Conway's game of life [35] is an early example of such a model. Two-dimensional Potts models simulate biological processes such as sorting, engulfment, and mixing of cell populations, and have served as a computational tool for the understanding of

mechanisms driving the rearrangement of cells [40-42]. Modifications included in Potts models of the DAH allow more detailed simulations of features such as the inhibition of coarsening in biological aggregates, the use of multiple connected gridpoints to define a single biological cell, and the proportionality between surface energy and cell type [42]. A merit of the two-dimensional Potts model is its ability to reproduce the kinetics of cell rearrangement in a simple and comprehensible manner [43]. For example, Extended Potts model has been used to show that full sorting of differentially adhesive cells may require membrane fluctuations [40, 42], a result supported by experimental work using cytochalasin-B treated cells [44]. However, neural retina and pigmented epithelium do partially sort under the presence of cytochalasin-D [44]. This represents more “passive” dynamics that could be independent of membrane fluctuations. Using a variation of Potts model, Large-Q-Potts model, with reduced membrane fluctuation (about 1/10 of membrane fluctuation causing complete sorting) cells achieved partial segregation of heterogeneous mixtures of cells for comparable times with membrane fluctuations [45]. Hence, just differences in adhesion allow the formation of small clusters that do not represent a true energy minimum of the system. In the same manner, internal contractive forces from the cytoskeleton are required to break a higher energy barrier in order to achieve total segregation of cell mixtures.

Potts models have well-known shortcomings, especially in the approximate manner with which they represent continuous cellular behavior as discrete processes. Thus a Potts model would represent the migration of a cell by switching states of gridpoints at the interface between two cells from one state to another rather than by modeling the motion of an entire body in response to biomechanical forces. Notwithstanding these

shortcomings, modified Potts models have undergone extensive development; notably, Agarwal has devised a Cell Programming Language (CPL) with the idea of defining each cell as a generator of instructions resembling genomic control of cell function. Each cell in the CPL is represented by a set of states or instructions having a temporal identity defined by features such as its proliferation and differentiation rates. This CPL model has been used to show that local differences in adhesion and random motion are the driving forces that lead to engulfment and segregation of cell populations [46].

Dissipative Particle Dynamics: Approximation to 3-D Cellular Interaction

The fundamental aim of Potts models is to simulate cell rearrangements using spatially discrete, state-based, approximations of neighboring cells that switch states but not positions. As an alternative, we propose implementation of a continuous model for the particle dynamics of cell motion in response to neighboring mechanical forces or following Newton's laws. Thus we define each cell as an autonomous mass that moves, interacts, reproduces, and undergoes apoptosis in response to stimuli from other cells, chemical gradients or forces associated between cells and the ECM. The purpose of particle dynamics, in the context of this thesis, is to understand how the dynamics of many-cell interactions through cell-cell and cell-ECM interactions influence morphogenesis. The advantage of modeling cells as particles is that stress-strain relations, comparable dynamics of cell movement, and physically-based constraints can be directly applied in such a way as to directly correspond to those observed in biological systems [47].

In summary, there are two major advantages of the particle dynamics approach proposed here. 1) The approach has the ability to modulate attractive and repulsive

interactions between cells as in the case of membrane-bound receptors on neighboring cells, and 2) cells are allowed behave viscoelastically, for example to interact through short-range or cell-cell and long-range or cell-ECM interactions. In the following sections, short-range and long-range interactions are described from the perspective of biological cells. Further details will be presented in the introduction of Chapter 3.

Biological Aspect of Cellular Binding

Cadherin-mediated binding or short-range interaction represents a basic level of coupling between neighboring cells, which we discuss in detail in the following section. Cell-cell adhesive interactions depend on the cadherin receptor number and intracellular activation of actin, tubulin, and vinculin polymerization to create linkage within the cell. Cellular rearrangements, therefore, rely on regulation of both the type and number of cadherin receptors, which, in turn, are subject to transcriptional control as well as to the biochemistry and dynamics of cytoskeletal polymerization within the cell. The combined effect of these processes is to render cells into a state of motion that leads to cellular rearrangement and energy minimization.

Beyond direct cell-cell cadherin links or short-range interactions, cell-mediated substrate deposition produce longer-range interactions between cells. These also play a role in aggregation and rearrangement within tissue structures, for extra-cellular matrix (ECM) deposition is a process that spans a larger range of temporal and spatial scales than cadherin interactions. For example, integrin receptor activation and clustering occurring at the nano-scale regulates fiber polymerization and matrix deposition, which in turn lead to macro-scale interactions between cells and their substrate. Therefore

$\alpha 5 \beta 1$ -mediated fibronectin deposition may offer far more complex dynamics and points of control that potentially affect the overall mechanics and rearrangement dynamics of whole tissues.

Beyond the contributions of membrane-bound receptors such as cadherins and integrins during cellular binding, other forms of membrane-bound receptors have the ability to exert repulsion between neighboring cells. This is the case of Eph/ephrin receptors that modulate both attractive and repulsive interactions through the cell membrane. A second form of cellular repulsion is produced through the interaction of negatively charged sialic acid moieties bound to cellular-adhesion receptors on cell surfaces. Unlike the modulation of repulsion of the Eph/ephrin system, which is essentially chemodiffusive in nature, this form of repulsion is simply electrostatic.

Short-Range Interactions: The Cadherin Paradigm

Cadherins are transmembrane receptors composed of an average of 735 amino acids. After translation, cadherins as polypeptides undergo a series of post-translational modifications, e.g., proteolytic cleavage, phosphorylation, and glycosylation. The external domain of cadherins, depicted in brief in Figure B-1, is composed of 3 to 5 units of approximately 110 amino acids [48]. These external units or repeats give cadherins the ability to bind Ca^{2+} [49], and also define their tissue specificity as summarized in Table B-1.

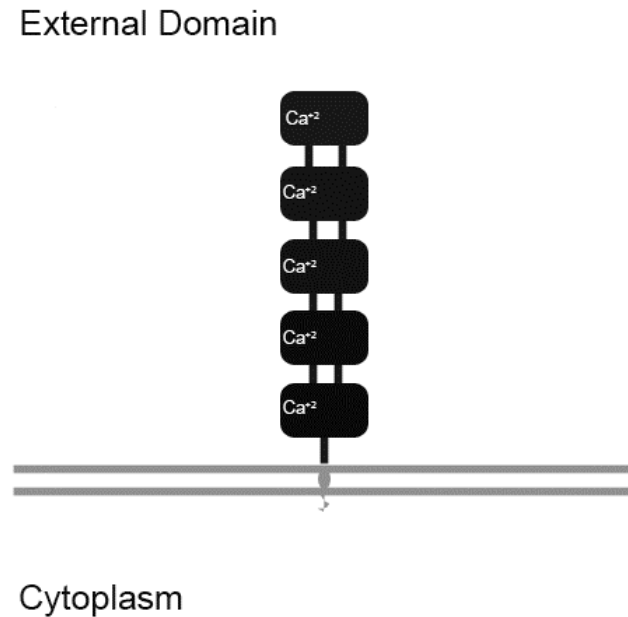


Figure B-1. Structure of the cadherin receptor. The cadherin receptor has 3 regions: external domain, transmembrane domain, and cytoplasmic domain. The external domain is composed of 3 to 5 units and the type of unit defined the different types of receptors known e.g. N-Cad, E-Cad, etc. These domains bind calcium ion in order to become activated and to avoid proteolytic degradation due to protease activity. There is also a transmembrane domain and a cytoplasmic tail that is in charge of relaying the external information into the cytoplasm. This site binds cytoplasmic proteins such as the (α , β , and γ) catenins.

In general, cell adhesion molecules (CAMs) have the ability to make several types of adhesive contacts between cells resulting in cell rearrangement [11], e.g. tight junctions, adhesion belts, desmosomes, and gap junctions [50-52]. These different types of contacts, dependent on cadherin bond half-life [53], clustering [54], and type of cytoskeletal link [55], providing specific cadherin-mediated adhesive functions during

development [56]. Figure B-2 is a schematic representation of an example of cadherin-mediated adhesive junctions that play important roles in epithelium stability.

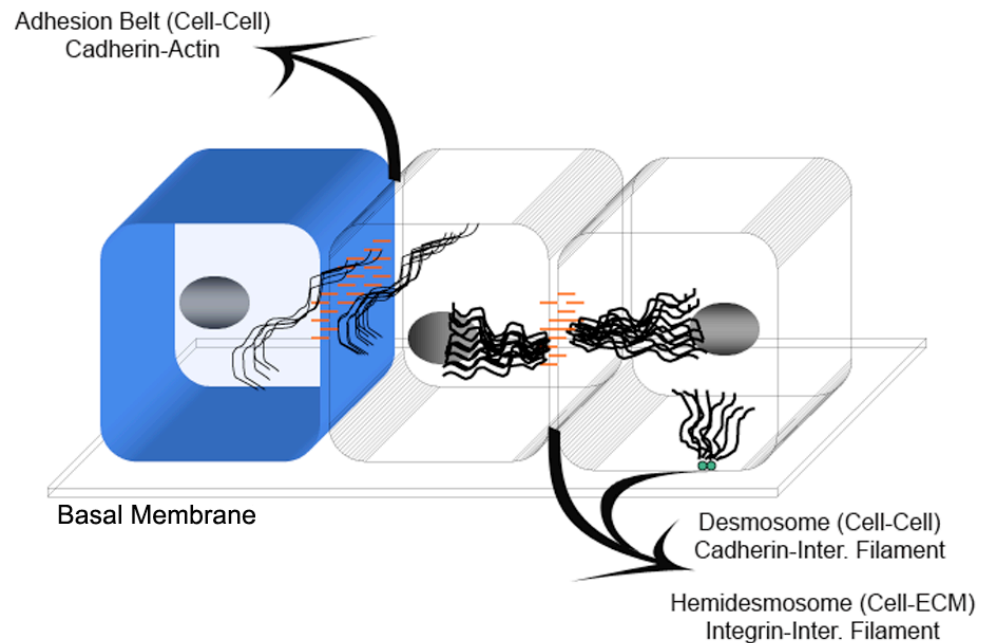


Figure B-2. Representation of 3 epithelial cells. Epithelial sheets use different types of adhesion structures to maintain stability. The adhesion belt and the desmosome are both cadherin cell-cell mediated adhesive systems. They are different in the type of cytoskeletal element controlling the cytoplasmic dynamics i.e. actin filaments for adhesion belt, and intermediate elements for desmosome type adhesive junction. Lastly, the hemidesmosomes are a type of adhesive junction that connects the ECM with the basal part of the cells. Integrins are known to mediate this type of interaction and intermediate filaments are the force generating elements.

Cadherin receptors can be sorted into two groups: classical and non-classical. During the early scrutiny of cell adhesion molecules, experimental observations of cell adhesion molecules such as Ca^{2+} requirement, and activation through cytoplasmic

proteins such as α - and β -catenins, defined this original set of adhesion molecules as classical cadherins [57, 58]. Any cadherin deviating from classical cadherins is defined to be non-classical. Table I gives an overview of the different types of cadherins, tissue expression, and in vivo effects of their own down-regulation [59]. Classical cadherins require Ca^{2+} to gain activity and create links with other cell surfaces. Calcium binds to the external domains of cadherins in a cooperative manner, such that more binding of calcium leads to more activation of the cadherin external domain, which is crucial for cell-cell binding [49].

One final type of adhesion molecule, N-CAM, belonging to the immunoglobulin (Ig) superfamily of proteins, and does not require the presence of Ca^{2+} to become active and form homotypic links on adjacent cell membranes [60]. N-CAM is the most abundant of this family of adhesion molecules. Alternative splicing of N-CAM mRNA transcript, in the same manner as antibody Ig production, makes at least 20 different forms of N-CAMs [61]. Some forms of N-CAMs have the ability to incorporate sialic acid or long chains of polysialic acid, which as we have mentioned are responsible for cellular repulsion due to electrostatic interaction between sialic acid moieties on adjacent cell surfaces [62, 63].

At their intracellular end, transmembrane cadherins have a short and highly conserved region involved in binding of the proteins, α - and β -catenins. The binding of α - and β -catenins with the cytoplasmic tail of cadherins activates downstream reactions such as actin-, and intermediate filament- polymerization [64].

Table B- 1. Overview of classical and non-classical cadherins. Reproduced from table 19.3 in Molecular Biology of the Cell, 4th Edition (2002).

<u>Designation</u>	<u>Tissue</u>	<u>Junction Association</u>	<u>Mutant Phenotype in Mice</u>
Classical Cadherins			
E-cadherin	Epithelia	Adherens junctions	Embryos fail to undergo compaction
N-cadherin	Neurons, heart, skeletal muscle, lens, and fibroblasts	Adherens junctions and chemical synapses	Embryos die from heart defects
P-cadherin	Placenta, epidermis, breast epithelium	Adherens junctions	Abnormal mammary glandular development
VE-cadherin	Endothelial cells	Adherens junctions	Abnormal vascular development
Nonclassical Cadherins			
Desmocollin	Skin	Desmosomes	Unknown
Desmoglein	Skin	Desmosomes	Blistering of skin
T-cadherin	Neurons, muscle	None	Unknown
Fat (Drosophila)	Epithelial and CNS	None	Enlarged imaginal disk and tumors
Protocadherins	Neurons	Chemical synapses	Unknown

The fundamental observation that cells dissociated from whole tissues will aggregate and rearrange following intrinsic affinity relations [13] prompts us to ask how cells aggregate while at the same time retaining the ability to move with respect to one another. That is, in order to rearrange, a cell must provide sufficient adhesive interactions with its neighbors to exert a net force, but it must not adhere so tightly that it cannot move and exchange neighbors. The strength of adhesion of cadherin bonds depends on the level of cadherin expression [8], the half-life of the adhesive bond [65], and the type of cytoskeletal linkage [66]. Cadherin bonds are constantly made and broken, through cytoplasmic internalization and recycling, in a reversible manner during the interaction of cellular surfaces. Consequently, cytoplasmic events such as α - and β -catenin interactions with the cadherin cytoplasmic tail allows for bond strengthening through actin filament binding [64, 67]. On the other hand, the existence of more stable forms of cell-cell contacts – e.g., tight junctions, adherens junctions, and desmosomes –

suggests that the half-life of cadherin bonds, as in the case of adherens junctions, is regulated to produce long-lasting links. The common denominator of stable adhesion contacts seems to be the localization of cadherin receptor links per cell membrane area between two cells.

Cadherin expression serves important functions in terms of balancing cohesion and rearrangement, simultaneously permitting structural changes to occur during development and providing stability of tissues where necessary. A good example of this competition is seen in epithelial sheet formation during development, where tissues such as skin and structures such as tubes evolve in shape and size while maintaining elastic integrity [68, 69]. The best available quantitative description for this process, the Differential Adhesion Hypothesis (DAH), predicts the steady state outcomes of segregation of different populations of cells and shape equilibrium of whole aggregates based on adhesive differences, however, it lacks a mechanism for defining the time-scale by which these outcomes are reached, particularly during cellular rearrangement.

Long-Range Interactions: Cell-ECM Paradigm

Cells do not interact only through the adhesive strength of their cell-cell connections, but use the adhesive properties of biological substrates to generate traction and cellular signaling as well [70]. Extracellular substrates make up a large fraction of the total volume of a tissue and come in several forms, each serving specific functions, e.g., structural stability [71], cellular migration [72], influencing cell shape, and regulating cell survival and proliferation [73]. Most substrates have the ability to self-assemble, as in the case of collagen [74]. Fibronectin, in particular, requires cell surface receptors to start polymerization of its dimeric form into long extended fibrous matrices

[16, 75]. Fig.3 shows a schematic of the two main families of extracellular scaffolds. The proteoglycans (glycosaminoglycan + protein) physically form a continuous gelatinous matrix with the ability to trap water due to Na⁺ ion sequestering and highly negative charge density of their branched conformation [76]. The ability of substrates to fill the interstitial space between cells gives both glycosaminoglycans (GAG's) and proteoglycans their bearing capacity during compressive loads on tissues, which is crucial to the mechanical properties of tendons and ligaments [77, 78].

Beyond the gel-like properties of proteoglycans, fibrous proteins have other important roles in tissue mechanics. Figure B-3 descriptively shows the different types of extracellular proteins bathing the cell-cell interstitial space. Collagen, for example, gives tensile strength to tissues, as is the case in tendons and ligaments and has the additional property of allowing the passage of light, as occurs in the cornea [79]. Collagen is made of a triple helix of α -chains, and during self-assembly, each helix is staggered one on another to provide a high tensile strength [74]. Further tensile strength is achieved through covalently-bound lysine residues on adjacent collagen fibers; this type of cross-linking is seen in the collagen structure of the Achilles' tendon [80].

Other specialized tissues also make use of proteinaceous structures. For example, many tissues rely on elastic properties of proteins in their extracellular matrix to produce mechanical recoil. This is the case in the circulatory and lymphatic systems, where expansion and contraction of vessels is regulated to maintain flow under constant pressure [81, 82]. The matrix of these tissues is elastin, a protein composed of two types of segments: hydrophobic segments providing elastic behavior and alanine-lysine rich

segments where lysine serves as a cross-linking agent to further increase its tensile properties [83].

Because of the importance of matrix mechanical properties to tissue function, various therapeutic approaches have been devised to treat conditions in which function is compromised. For example, after myocardial infarction, the formation of scar tissue leads to cases of ventricular dilation due to impaired elastic properties of scar tissue at the site of infarction. In order to increase heart tissue elasticity, fibroblasts expressing the elastin gene have been seeded onto a mesh that was cultured and transplanted onto infarcted rat hearts *in vivo*. Eight weeks post-implantation, the elastin-treated group exhibited significantly reduced left ventricular volume and increased pressure as compared with controls, demonstrating a quantitative gain-of-function associated with modified scar tissue mechanics [84].

Other matrix proteins are also important to tissue function. Laminins, for example, are mostly concentrated in the basement membrane, at the boundary between the basal part of epithelium and endothelium and the interstitial matrix of tissues. Laminin provides anchorage functions for cells as well as defining cell polarity – thus, abnormal laminin expression in the basal layer leads to defective polarity of epithelial sheets and the disruption of clear boundaries in tissue cytoarchitecture [85]. Laminin is a heterotrimeric glycoprotein arranged in a cruciform shape. The protein is made of heavy and light chains that have functional homology, but have many different types. For example, there are three homologous heavy chains (A, M, and K), and five homologous light chains (B, S, B2, B2t, and Bk1) [86]. The advantage of having isoforms of heavy

and light chains is that the different isoforms have distinct mechanical properties that define functions in cell and tissue anchorage.

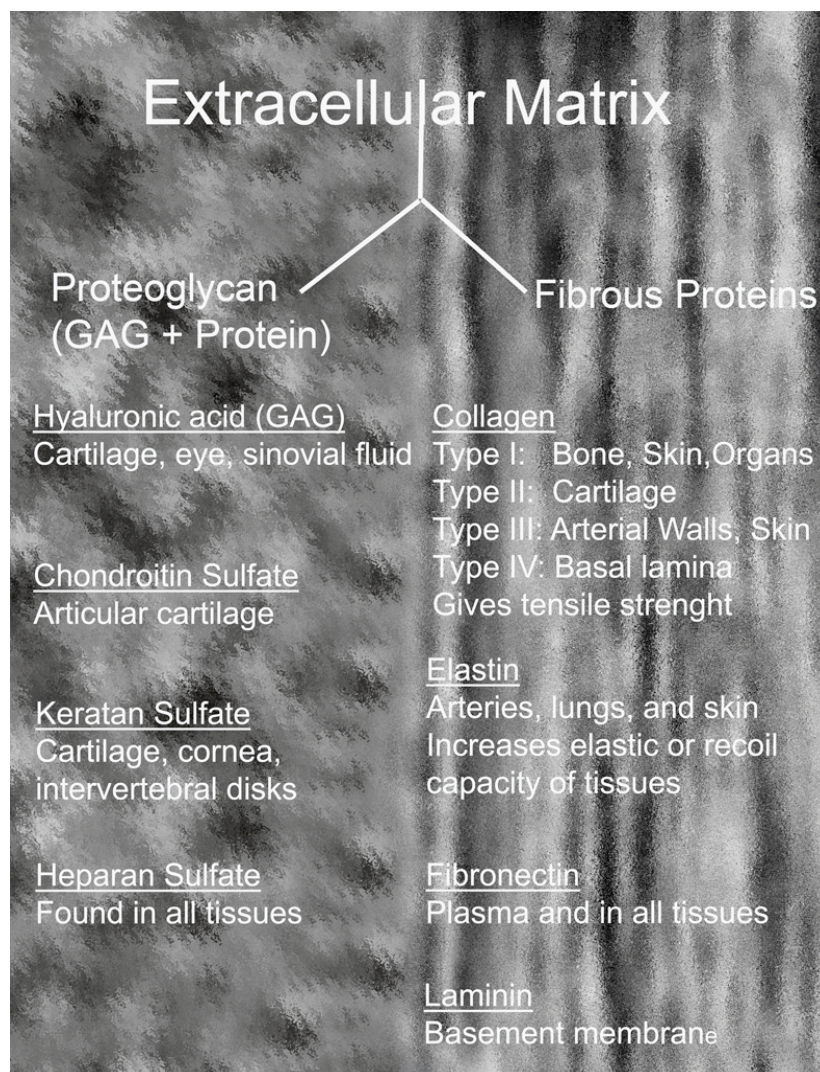


Figure B-3. Diagram describing two major types of ECM proteins. These biological substrates are important since they determine the properties of tissues in terms of tensile and compressive yield stress on biological tissues. For example, the substrates can act as gels trapping large amount of fluid and ions or they can define more fibrous structures that depending on the directionally of their fibers are able to provide important tensile properties to tissues.

Fibronectin: The Basic Unit of a Complex Substrate

The term “fibronectin” evolved as an attempt to unify the functions of the homologous plasma protein cold-insoluble globulin and the Large External Transformation-Sensitive (LETS) protein, secreted during fibroblast activity. In 1975, cold-insoluble globulin and the LETS protein were found to share the same immunochemical properties [87]. Even though the cold-insoluble globulin and the LETS protein have the same biochemical functions, they constitute different protein pools, with the ability to polymerize upon activation with the surface integrin receptor. In the body, fibroblast-secreted fibronectin or LETS is constantly assembled into an insoluble matrix at the cell surface in order for the cell to anchor and carry out important cellular processes. On the other hand, the Hepatocyte-secreted plasma fibronectin or cold-insoluble globulin at an excess concentration of 300 µg/ml in blood [88], has the ability to become either soluble or insoluble depending on the physiological demands of the organism, e.g., during fibrin clot formation [89], or as a chemotactic agent during inflammatory response to injury [90]. This thesis focuses on the effect of soluble fibronectin polymerization on the morphogenesis of biological structures, which is analogous to the polymerization of insoluble fibronectin substrate on the surface of cells.

This reaction requires the interaction of the $\alpha 5 \beta 1$ integrin receptor with the soluble form of fibronectin for polymerization to occur, and it is worthwhile to describe fibronectin and its polymerization in some detail. At the dimer scale, fibronectin is a protein with a total molecular weight of 440,000 Daltons [91]. The dimer is made of two almost homologous large polypeptide fragments of about 60 nm linked through disulfide bridges. Within each fragment, there are several discrete domains that make fibronectin a

very versatile molecule during binding to recognition sites on cell surfaces, bioactive molecules, and insoluble substrates.

Fibronectin is composed of several units and these units deliver specific functions during soluble fibronectin recognition and polymerization. In turn, every unit in the fibronectin dimer is made of repeating secondary structures named type I, type II, and type III [92]. The binding versatility of the soluble fibronectin dimer was characterized through digestion of the fibronectin dimer with proteolytic enzymes such as plasmin, chymotrypsin, and pepsin. The cleaved fragments are defined as “functional fibronectin fragments” because once they are broken into smaller sections they retain their biological activity. An interesting property of protease-digested fibronectin is the ability of its cleaved fragments to retain their original biological activity. This opened the possibility to map the biological activity of the fibronectin moiety. For example, the 29 Kda fragment [93] has been determined to interact with soluble biological molecules and pathogens, e.g., fibrin [94], heparin [95], and *Staphylococcus aureus* [96]. In the same manner, the second larger fragment from the proteolytic digestion of fibronectin with plasmin has important binding sites for active and denatured collagen [97], binding sites for heparin [98], as well as the RGD binding site for cellular recognition through the $\alpha 5 \beta 1$ cell surface receptor [92, 99]. Binding via this receptor is the starting point for the large-scale cellular dynamics presented in this thesis, as will be further elaborated upon in the following section. Figure B-4 is a representation of important domains on the fibronectin dimer. These regions are involved in biological processes during cell recognition and fibronectin matrix formation. Beyond being an ensemble of different domains, another common signature of the fibronectin dimer is the presence of cysteine

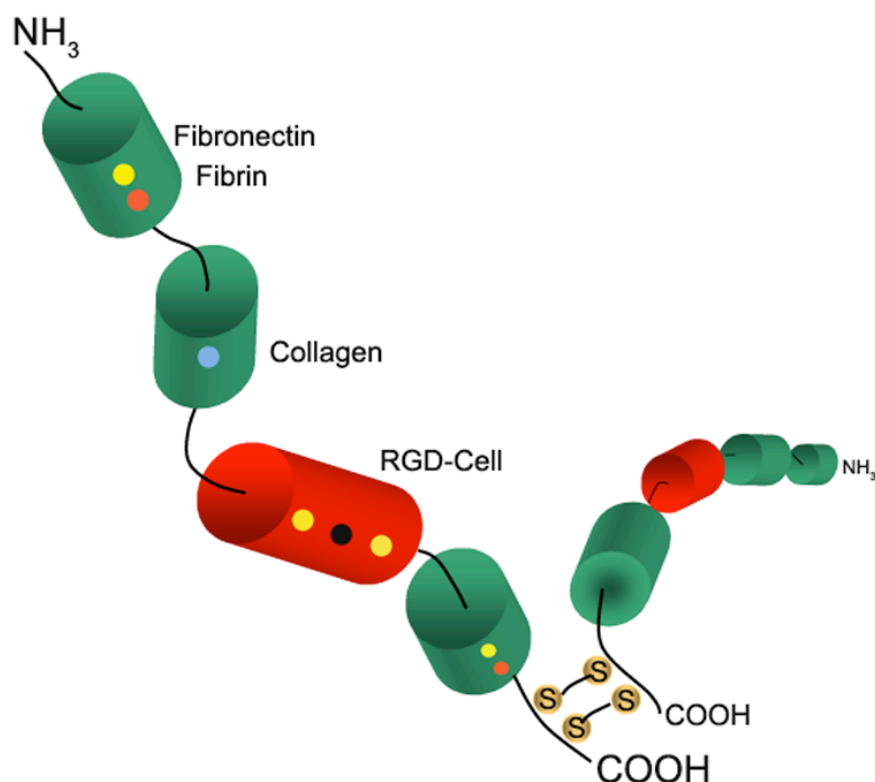


Figure B-4. Soluble form of the fibronectin dimer. The soluble fibronectin molecule consists of two very similar “arms” that are joined with disulfide bonds near the carboxylic end. Here, we are showing the sites that are involved in cell recognition of the dimers, through integrins, and the sites that serve for further polymerization of other fibronectin dimers (yellow) or fibrin (red). Also, there are recognition sites for collagen (blue) and heparin near the carboxylic end (Not shown).

residues connecting these domains. The remaining 23 Kda and 6 Kda fragments near the carboxylic end of the fibronectin molecule have cysteine residues that allow for disulfide bond formation, an important feature that makes each of the fibronectin monomers assemble into its natural dimeric active form [100]. Cysteine residues are common within

the structure of the functional units found in fibronectin, i.e., type I, II, and III domains, which are frequently repeated and assembled to build the larger fragments previously discussed [101]. The existence of cysteine residues throughout the fibronectin molecule increases the reduction-oxidation potential toward making disulfide bridges. This positively influences fiber extension, a required process during insoluble fibronectin matrix formation and deposition [102, 103].

In addition to the biological activity of fibronectin with other substrates and membrane-bound receptors, fibronectin has mechanical properties that allow the coupling of cytoskeletally-generated forces to control fiber directionality and extension during fibronectin polymerization. Seminal work on the physical nature of fibronectin has shown that fibronectin can adopt distinct extended and compacted conformations upon variation of the ionic strength of the protein in solution [104]. Hence at low ionic strength the fibronectin molecule is extended, while at high ionic strength it is more globular [105]. The consequences of fibronectin elasticity are due to its connected modular conformation. For example, the fibronectin modules have differing amounts of cysteine residues that allow disulfide bridging [106]. In addition, the β -sheet conformation of type III domains allows these domains to extend during force-induced stretching by a factor of 5 as compared with the native dimeric form of the fibronectin molecule [107-109]. Thus the essential empirical fact is that fibronectin has an intrinsic structural elasticity that depends on ion concentration differences and force-induced stretching of the fibronectin molecule.

The elastic ability of the fibronectin dimer to positively drive fibrinogenesis [110, 111] has been further examined in in vitro experiments of cells transfected with

fibronectin-YFP and moesin-CFP actin binding protein constructs. These experiments showed that fibronectin stretching property couples with cytoskeletal-generated tension during fibronectin fiber extension. Hence, the mechanical coupling to the cytoskeleton exposes cryptic sites on the fibronectin dimer for fibronectin inter-domain association [112, 113]. Refer to figure B-4 for a clear location of fibronectin-fibronectin interaction sites during fibrillogenesis (yellow dots). Likewise, *in vivo* fibrillogenesis during *Xenopus laevis* gastrulation showed a very complex scenario in which cytoskeletally-generated forces from cells affect the topological rearrangement of fibronectin fibers [114].

The previous account has summarized features of fibronectin that influence its role in ECM formation, in cytoskeletal remodeling and ultimately, in force generation between cells. These effects have important implications for larger scale tissue mechanics during cellular migration and morphogenesis[115] that will be discussed subsequently.

$\alpha 5\beta 1$ -Fibronectin Interactions are Required for Insoluble Fn Matrix Formation

As previously discussed, polymerization of fibronectin requires the interaction with transmembrane proteins of the integrin family. The integrin family of receptors in turn exhibits key levels of activation during integrin-soluble ligand interactions. Functional integrins consist of two non-covalently bound transmembrane heterodimeric glycoprotein subunits α and β . Both of the subunits contribute to the binding of the fibronectin dimer. The α and β subunits contain a large extracellular domain (700-1100 residues), a hydrophobic transmembrane region, and a short tail region (50-70 residues)

with the ability to activate important cytoplasmic pathways [92]. In particular, $\alpha 5 \beta 1$ is the naturally occurring integrin receptor required to initiate the conversion from soluble dimeric fibronectin to the insoluble and extended fibronectin matrix. Figure 5 shows a cartoon of non-covalently bound α and β units. The formation of the $\alpha \beta$ heterodimeric complex is known to require divalent ions to increase the initial interaction of the α and β units [116]. Figure B-5 is a representation of the heterodimeric form of α and β units in the plane of the cell membrane. As the example of the cadherin receptor, the integrin receptor also has an external domain in charge of recognition of soluble proteins, a transmembrane domain to control receptor activation, and cytoplasmic domains to relay information to the inside of the cell.

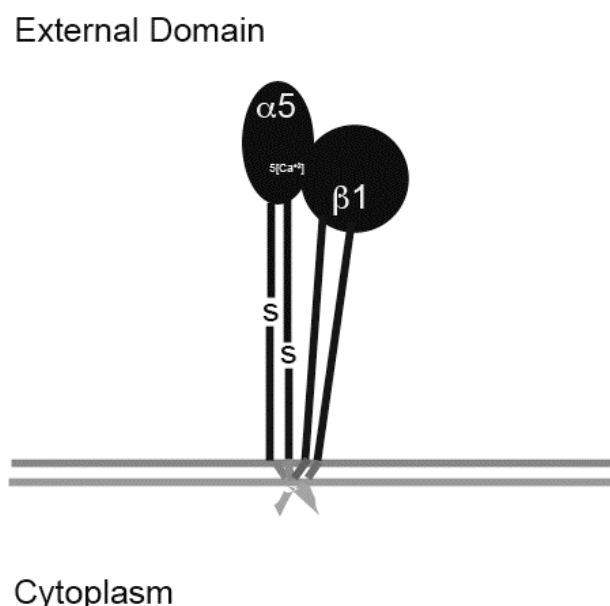


Figure B-5. Heterodimeric form of the integrin receptor. The α and β units are diffusible molecules in the plane of the membrane. Heterodimer $\alpha \beta$ formation is enhanced when divalent cations are present in the interstitial space. This represents the first step of activation. Other forms of activation of the heterodimer toward clustering of pairs of $\alpha \beta$ heterodimers are enhanced

by the concentration of soluble fibronectin. This in turn leads to increased localization of cytoplasmic proteins and activation of important cytoplasmic pathways such as RhoA and Rac1.

The α and β integrin subunits diffuse within the lipid membrane [117], producing fibronectin-independent aggregation of α and β into a heterodimer $\alpha\beta$ [118]. $\alpha\beta$ heterodimers themselves aggregate to form more mature links under the influence of soluble fibronectin dimers, i.e., focal contacts and focal complexes, such that the size of the clustering heterodimers increases the strength and mechanical resistance of a cell on a substrate [119]. Figure B-6 is a representation of clustering dynamics of the $\alpha\beta$ integrin heterodimer on a cell surface. Within the cell, the effect of clustering is to promote the formation of actin filaments that anchor to stable integrin clusters. Connections between the internal cytoskeleton and the extracellular matrix allow for forces to be transmitted that both stabilize cellular structures and produce directed movement of cells on substrates [120].

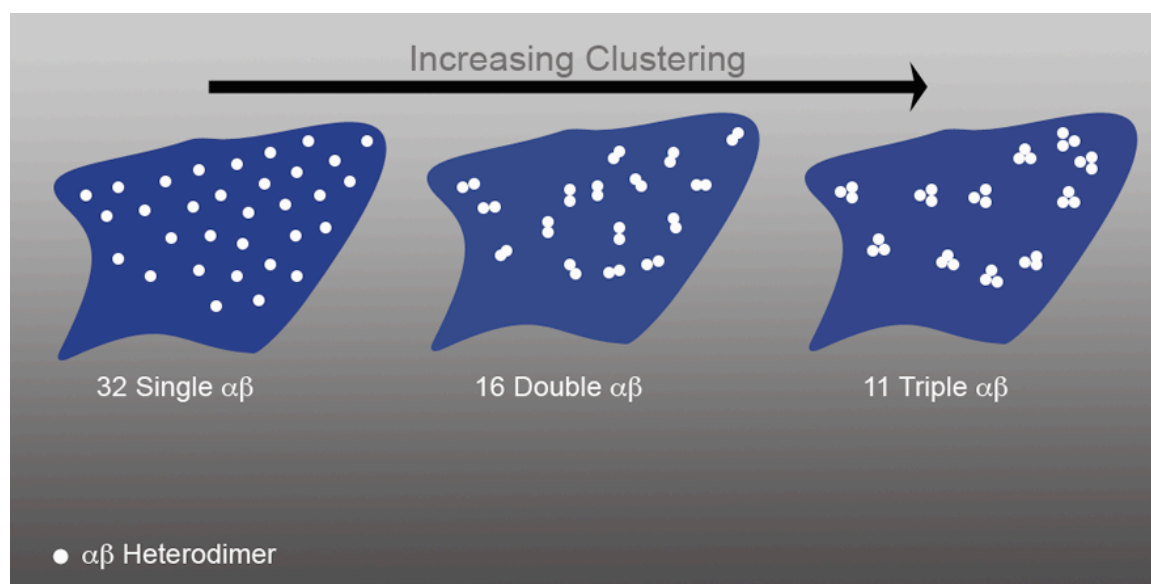


Figure B-6. Integrin heterodimer clustering on planar surfaces. Initial $\alpha\beta$ heterodimers described as white circles, are dispersed across the cell membrane. First, the cytoplasmic protein talin activates the dimers (increasing avidity). Second, the presence of ECM-ligand drives the lateral clustering of individual $\alpha\beta$ heterodimers to form larger clusters. The term valency describes the number of potential clusters made up of a number of $\alpha\beta$ heterodimers. Larger size clusters have been found to correlate with more stable and least likely to break from cytoskeletal-generated forces. While the lower limit of effective cluster size to cause mechanical coupling of the cytoskeleton with the external matrix has been found to be 3 $\alpha\beta$ heterodimers [121], more stable focal complexes range in the 1 to 10- μm range [119]. During active migration, focal contacts in the rear of the cell have higher turnover rates than contacts at the cell front [122]. Hence, the longevity of integrin clustering contributes to migration and multi-cellular structural stability.

The formation of insoluble fibronectin substrate from the soluble form of fibronectin requires that several processes take place at the cell surface. These processes include receptor clustering, priming, activation, and fiber polymerization. First, prior to activation, each subunit diffuses throughout the bilipid membrane, following non-covalent heterodimerization of $\alpha5$ and $\beta1$ units, receptor clustering or valency that increases the avidity of the $\alpha5\beta1$ heterodimer towards soluble fibronectin [123]. Second, priming is a process by which the actual binding and conformation changes of the $\alpha5\beta1$ heterodimer and recognition of the RGD binding site on the fibronectin molecule take place. The priming process has been found to be associated with conformational changes of the cytoplasmic tails of the α and β receptors, which produce bi-directional linkages between the cellular cytoplasm and the external environment [124, 125]. Third,

activation occurs through recognition of the RGD (Arg-Gly-Asp) domain (type III10) and the enhancing sequence (type III9) on the fibronectin molecule. Fourth, activation of the $\alpha 5 \beta 1$ receptors causes bi-directional effects at the extracellular and cytoplasmic compartments of the cell [126-128] leading to fiber polymerization. Within the cell, the cytoplasmic portion of the β subunit binds intracellular anchor proteins, e.g., α -talin, filamin, actinin and paxillin, with affinity to the cytoplasmic tail of α subunit. Binding produces the connection of the intracellular actin cytoskeleton to the external substrate [129]. Also within the cell, actin filament polymerization and clustering of other integrin heterodimers leads to the formation of focal points that positively activate the localization of the cytoplasmic protein focal adhesion kinase, FAK [130]. FAK in turn has the ability to auto-phosphorylate several tyrosine residues, causing activation of downstream pathways that control cellular migration and cytoskeletal dynamics [131]. It is the activation at the cytoplasmic level that enhances the polymerization of the fibronectin matrix, through actin cytoskeletal tension, leading to stretching of polymerized fibronectin and exposure of cryptic sites for fiber extension [110, 132].

Although the biochemical pathways involved during fibronectin polymerization are intricate and highly regulated, the overall dynamics of integrin-fibronectin polymerization follow an orderly and sequential layout from clustering to priming to activation to polymerization that produces stability of focal adhesions between the cytoskeleton and the external matrix. As a consequence of this underlying order, the intricate dynamics of cell-ECM interactions can be organized in terms of receptor expression and the amount of soluble fibronectin in the microenvironment.

The Effect of Integrin Receptor and ECM-ligand Concentration on Cell Migration

The aim of this work is to understand the impact of $\alpha 5 \beta 1$ -fibronectin dynamics on large-scale tissue properties and rearrangement. As previously described, there are several possible levels of control during fibronectin matrix formation, i.e., allosteric activation of the external domains, cytoplasmic cascading effects and bi-directional signaling. Without overshadowing the importance of other factors, in this work we focus on the effect of $\alpha 5 \beta 1$ receptor expression and soluble fibronectin concentration on the mechanical properties and rearrangement dynamics of cell-ECM driven aggregation.

From a dynamic perspective, when cells migrate, they must manifestly exhibit different biomechanical stresses at their leading edge than at their trailing edge. This stress difference permits cells to break contacts at their trailing edge, where the valency is variable and integrin exchange is faster, and to make stationary connection at their leading edge, where the valency increases and integrin exchange is slower [120]. Within the cell, this process is achieved through recycling of broken $\alpha \beta$ heterodimers and actin connections from the receding lamellapodia to the anchored leading edge [121]. It has been found that the optimum migration speed of cells on planar surfaces depends on specific relations between the ECM-ligand and the cell receptor densities [133, 134]. Deviations from this optimum relation cause the cell to decrease its migrating speed in a biphasic manner. For example, if a cell has more than optimum cell-substratum adhesion, the cell will not be able to break the highly adhesive interaction and will become immotile. On the other hand, if the adhesive interaction is lower than optimum, the cell will not have enough traction to generate movement. Furthermore, these migration dynamics have been found to depend on ligand levels, integrin expression, and

integrin-binding affinity during short-term binding. For example, if the cell is optimally migrating at a set value of ligand concentration, an increase in the integrin receptor causes reduction in the migration speed [135].

Recently, the idea that optimal cell migration on planar surfaces is a function of the type of adhesive relation between integrin surface receptors and substrate ligands has led to models of cellular migration in 3D environments. In these models, cellular migration is assessed as a function of substrate stiffness and ECM-ligand/cell surface receptor adhesive relations [136]. Such models predict relations between optimal migration and cell-ECM adhesion strength as well as effects of the mechanical properties of the matrix on cell migration assuming an ECM with fixed properties. On the other hand, as we have described, the ECM is a dynamic material whose composition and mechanical properties are known to depend on cellular metabolism and internal stress states as well as concentrations of cell surface binding sites and soluble fibronectin in the matrix. Thus we emphasize here that the mechanical properties of the ECM are not intrinsic to the ECM, but depend directly on the motion and state of the cell, its surface receptors and the amount of soluble ligand in the microenvironment. In the experimental work that we present here, we investigate how cells rearrange and self-assemble under the combined effects of the cell and ECM (i.e. polymerization of ECM proteins). Even though we don't directly measure the effect of the ECM on the cell (i.e. changes in cytoskeletal state and recycling of cell surface proteins), we consider the inside-out signaling pathway to be an important part of cell-ECM dynamics.

The Effect of Cellular Repulsion on Morphogenesis

Beyond the ability of cells to interact adhesively through cadherin and integrin-ECM interactions, cells respond to chemotropic cues of both attractive and repulsive varieties. Repulsive cues are of two forms: i) electrostatic, and ii) mediated through membrane-bound cell surface receptors.

As previously described, N-CAM has the ability to make homotypic bonds between cells without the requirement of Ca^{2+} to become active [60]. Hence, cell surfaces expressing N-CAM spontaneously adhere, as occurs for example in synaptic neuronal connections and in the formation of neural-glia network architectures [137]. Additionally, N-CAM has the ability to incorporate polymer chains of negatively charged sialic acid moieties, causing electrostatic hindrance between adjacent cell surfaces [63]. This produces repulsion between surfaces, as has been measured under physiological conditions and found to depend on ionic strength and the amount of polysialic acid (PSA) bound to N-CAM [138]. The ability for N-CAM to modulate its attraction into repulsion provides cells with plastic capabilities during tissue remodeling in the nervous system. For example, progenitor cells in the hippocampus express high levels of PSA, which allows for the timely release of precursors from cell clusters to reach maturation in specified niches during neural development. Developmentally, this process is arrested by enzymatic cleavage of PSA from progenitor cells, which stops the regular migration of these cells from their clusters into other regions of the developing brain [139]. Likewise, in vitro measurements of the type and quantity of PSA on N-CAM receptors have shown decreased levels of PSA as embryonic tissue matures [62].

A mechanism that produces cell-cell repulsion that is independent of electrostatic charge occurs through Eph/ephrin interactions. Eph receptors and their corresponding cell surface-bound ligands, the ephrins, are known to modulate both attraction and repulsion during development [140, 141], particularly during the segmentation of the hindbrain [142-144] as evaluated during rhombomere formation, for example in the zebrafish [145, 146]. Eph receptors constitute part of the tyrosine kinase family and contain two subclasses, EphA and EphB, that specifically interact with glycosylphosphatidylinositol (GPI)-membrane-linked EphrinA's and transmembrane EphrinB's ligands [147]. The Eph-ephrin receptor-ligand interaction requires cell-cell proximity or contact [148] to initiate and modulate repulsion through cytoskeletal reorganization [149], active receptor endocytosis [150-152] and metalloprotease cleavage [153, 154].

Differential Adhesion Hypothesis (DAH): from Cell-Cell Interactions to Large-Scale Tissue Assembly

The expression of adhesion membrane proteins on the surface of cells allows for cells to assemble into large-scale structures. The first account of adhesion-related cellular assembly dealt with the aggregation of dissociated sponge tissue [155]. Later, this property was found in amphibian embryonic tissues [13], in which it was shown that fragments of amphibian embryonic tissue would round up, adhere and spread over other tissue in vitro following intrinsic tissue affinities. Tissue affinity was defined as the ability of heterogeneous suspension of dissociated cells to aggregate and adopt the organization of the native tissues [13].

The existence of an “affinity” between cells that could specify cellular positioning led to the formulation of the “Differential Adhesion Hypothesis” (DAH) as a theoretical framework to explain rearrangement phenomena [1]. The DAH states that if two cell populations of types A and B have differences in their number of adhesive receptors such that population A has more adhesive receptors than population B, then the populations would “sort-out” or separate into two different phases, with A being enveloped by B. However, if the adhesive interactions between A and B is greater than the average adhesion of the two types combined, the two populations will remain intermixed. The DAH provides the following theoretical predictions:

- a) The final equilibrium configuration of equally mixed populations of cells is independent of its initial state.
- b) Comparison of equilibrium configurations among tissue types with different adhesive relations obeys a hierarchy of cellular adhesiveness, with more cohesive cells always being enveloped within an aggregate of less cohesive cells. For example, limb bud tissue has the highest measurable surface tension or tissue cohesion. When limb bud tissue is mixed with other embryonic tissues such as pigmented epithelium, heart, liver, and neural epithelium, the limb bud always adopts an internal position with respect to the other embryonic tissue during rearrangement. This property is termed the “transitive relation” among embryonic tissues.
- c) The speed at which any co-aggregation sorts-out is proportional to the difference in cell receptor number between the tissues.

The DAH provides an analogy between liquids and tissues [156]. In this theoretical framework, one can establish a correspondence between the works of adhesion (between unlike phases) or cohesion (between like phases) and the miscibility or immiscibility of phases either of liquid or of tissue types. For example, water has a higher work of cohesion than oil. This difference is directly associated with the type of interaction between their molecules. Simply put, London forces on hydrocarbon molecules are far weaker than hydrogen binding of water molecules, and consequently a mixture of oil and water minimizes free energy by separating into a water phase surrounded by an oil phase, in a manner exactly analogous to that predicted by prediction (b) of the DAH, above. In the presence of a detergent, which increases the adhesion between oil and water, the separated phase gives way to a mixed phase of water and oil. Similarly, the DAH predicts that heterogeneous mixtures of cells expressing different levels of adhesive surface proteins at the cell surface should achieve states of mixing and separation as relative cohesive and adhesive relationships between different cell types are varied.

The DAH predictions agree with experiments provided that cells have the ability to rearrange in response to applied stresses, a property termed tissue liquidity. For cadherin bonds, which are with few exceptions (e.g. stable cadherin links found on epithelial sheet formation during mesenchymal-to-epithelial transitions (MET)) are dynamically associating/dissociating. Hence, cells maintain the ability to rearrange producing persistent tissue liquidity over a range of stresses. As we will show, however, tissue liquidity is not similarly ubiquitous for integrin-ECM bonds, and a goal of the current work is to establish quantitatively the effect of integrin surface receptor and

soluble fibronectin concentrations on tissue liquidity.

The state of liquidity of a tissue can be established by measurements of its gross mechanics when subjected to an external force. For example, it has been shown that centrifugation of embryonic tissues causes different time-dependent responses on aggregates of embryonic tissues depending on their adhesive or cohesive properties. Some tissues deform rapidly and remain deformed until the force is no longer being applied: these tissues are said to behave as viscoelastic-solids. Other types of tissues deform over time and subsequently round up when kept at constant centrifugal force: these tissues are said to behave as viscoelastic-liquids [157].

Cells in aggregates that behave as viscoelastic-solids deform and store energy as a spring when the aggregate is subjected to an external force. While cells in aggregates with viscoelastic-liquid property deform and dissipate energy for comparable magnitudes of external force. The dissipation of forces is related to the type of bond formed with other cells and related to the surface tension of aggregates at equilibrium. For example, it has been experimentally measured that the force required to break a cell-cell cadherin bond is in the pN range[158]. However, the force required to break a cell-ECM bond is in the nN and also increase linearly with the size of the focal adhesion contact [119]. It has been proposed that, analogously to liquids, the ability of cells in aggregates to sort out and to round up when subjected to compressive forces are associated with intrinsic surface tensions of cell aggregates [29].

To summarize, cells are believed to form aggregates in a manner dictated by their adhesive relations. The internal structure of the resulting tissue and its consequent response to external forces also depend on cellular adhesion. For our purposes, we

emphasize an implicit fact involved in this analysis, namely, that it is the ability of cells to move past one other that defines both an aggregate's rearrangement during assembly and its response to external stresses. Aggregates of cells that are locked together and cannot move with respect to one another can neither sort out nor round up.

Experimentally, measuring and tracking how much a cell moves past another poses significant difficulties and, though conceivable in principle, would in practice be problematic, requiring simultaneous tracking of numerous cells within the aggregate in real-time. On the other hand, measurements of stresses and strains on entire aggregates are much more straightforward to acquire, and previous work has demonstrated that such data can be used to obtain quantitative values for surface tensions of tissues [6]. Figure B-7 is a representation of surface tension as an end-point measurement of aggregate cohesivity. Here the initial compressive force is dissipated over time, causing deformation of the aggregate. The final geometry of the aggregate at equilibrium allows for the calculation of the surface tension, through an approximation of the Young-LaPlace equation [6]. Foty et al. demonstrated that, as predicted from phenomenological and less sensitive observations of surface tension [29], embryonic tissues behave as viscoelastic liquids with intrinsic and quantifiable surface tensions. For example, the technique known as Tissue Surface Tensiometry (TST), in which aggregates are compressed between parallel plates, has been applied to embryonic heart and liver chick embryonic tissues, producing measurable and significantly different values of tissue surface tension in vitro. This in turn correlates with cellular rearrangement behaviors, namely to sorting-out and intermixing analogous to cases of miscibility and immiscibility in liquids [7].

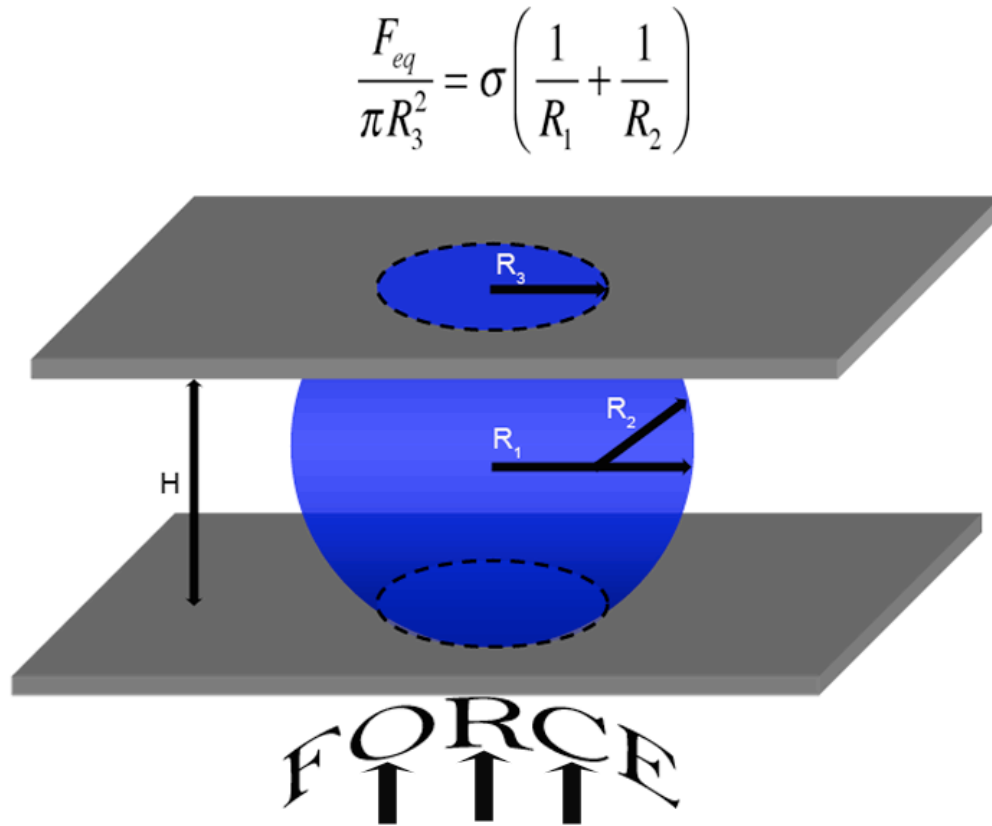


Figure B-7. Effect of compressive forces on aggregate geometry. Aggregates deform when compressive forces act on them. The deformation is calculated with the measurement of the radii of curvature (R_1 and R_2). The value of H is the distance between the plates during aggregate compression and is used to get a better estimate of R_3 . The area of contact with the compressing plate is given simply by πR_3 . The term $F_{eq}/\pi R_3$ is analogous to the pressure term (ΔP) of the Young-LaPlace equation for liquids, which is balanced by the effect of the surface tension term.

In order to determine the relationship between surface tension, and rearrangement of cadherin interactions, mouse fibroblast L-cells have been transfected to express different levels of receptors of the cadherin family. L-cells do not naturally express any form of receptor from the cadherin family, so experiments in which L-cells are

transfected to express particular cadherins can be cleanly performed. Findings from various experiments performed over the last decade are summarized as follows in Table B-2.

Table B- 2. Chronological advances of cadherin-mediated cellular self-assembly.

Year	Cadherin-Based Dynamics
1997	Increases in E- and P- cadherin expression produce corresponding increases in aggregate surface tension and reductions in the invasive phenotype of lung carcinoma cells. Thus cell-cell contact interactions are relevant to cancer metastasis [10].
1998	Dexamethasone, a synthetic glucocorticoid, increases cohesion of human fibrosarcoma cells. Cohesion between human fibrosarcoma cells treated with dexamethason was about 2.5 times the cohesion of untreated cells. This increase was correlated with increasing cadherin expression in treated cell lines [159].
2003	Fibroblast “L-cells” transfected with NCAM, E-, P-, N-, R-, and B-cadherin were assessed in terms of their rearrangement properties during cell mixture combinations. Combinations of cells expressing either different cadherins (e.g., E- versus P-) or the same cadherins (e.g., N- versus N-) were sensitive to receptor number differences during rearrangement, consequently causing “sorting-out” behavior. Heterocadherin interactions of type B- vs. R- showed partial interactions between the two aggregates of B- and R- cadherins. These results showed that sorting out or cellular segregation is driven by differences in cell receptor number and the type of receptor interaction [11]
2005	In the same manner, fibroblast L-cells transfected with P- and N-cadherins were selected to have a different level of expression of each of these receptors at the cell surface. Cell aggregates made from these cell lines had measurable surface tensions. Interestingly, there was a linear relation between the amount of cadherin surface receptor expression and the corresponding measured surface tension [8].
2007	Immortalized mouse pancreatic islets self-assembled to adopt a characteristic “enveloped” morphology. The cell lines in these experiments differed in the number of surface E-cadherin on cells adopting the internal position. Furthermore, transfection of the externally positioned cells with P-cadherin caused weaker cross-adhesive interactions in rearrangement experiments with the cell line expressing E-cadherin [9].

Taken together, these results demonstrate that cadherin-mediated interactions drive rearrangement during tissue self-assembly and contribute to characteristic aggregate mechanical properties. Variables such as receptor number expression and type of cadherin interaction show reproducible effects on tissue rearrangement and mechanical properties that are consistent with the DAH. Notwithstanding these successes of the DAH, the contributions of cell-ECM interactions to cellular self-assembly have not been studied, and in Chapter 4 we demonstrate that variations in integrin surface receptor expression levels and soluble fibronectin concentration produce paradoxical effects on tissue properties and cellular rearrangement that differ qualitatively from existing data in responses to cadherin variation.

DAH Framework on Cell-ECM Contributions to Tissue Mechanics

To a significant extent, *in vivo* embryonic cells are black boxes insofar as one cannot determine with certainty the type of adhesive relationships governing their internal structure or external mechanical characteristics. Cells can interact through cell-cell effects alone, through a mixture of cell-cell and cell-ECM effects, or strictly through cell-ECM effects. Furthermore, these modes of interaction depend on a number of factors including the level of expression of surface receptors, the amount of soluble fibronectin in the cell's microenvironment, and feedback between the cell surface and internal molecular machinery that in turn regulates endocytosis and dynamics of cell surface receptor expression profiles. These complications have led to the development of *in vitro* models focused on the investigation of the influences of cell-ECM interactions on

cellular rearrangement and tissue mechanics. A summary of the findings from these model systems follows in table B-3.

Table B- 3. Chronological advances of the effect of cell-ECM interactions on cellular aggregation.

Year	Cell-ECM Based Dynamics
1962	Limb bud, pigmented epithelium, heart, and liver embryonic chick from both whole-tissue and heterogeneous cell suspension experiments tissues showed “specific” (i.e., similar to in vivo) rearrangement behaviors [28].
1969	Shape change of chick embryonic tissue aggregates subjected to centrifugal forces were correlated to the type of rearrangement observed in tissue fusion or heterogeneous mixture experiments [160].
1972	A heteroculture of heart and liver embryonic cells exhibited a structural transition as a function of time in culture. For short times, the heart tissue tended to envelop liver embryonic tissue, while for longer culture times, heart tissue became enveloped by liver tissue [25].
1978	Analysis of time-dependent responses of embryonic tissues to centrifugal forcing resulted in the finding that tissues behaved as elastic solids over short timescales, but behaved as viscoelastic liquids over longer timescales [29].
1980	Tissue reversal of heart and liver embryonic tissues [25] was found to depend on a protein factor extracted from fibroblast monolayers that affected the physical properties of chick heart embryonic tissue. When heart embryonic cells were re-aggregated either in control media or in media containing the isolated protein factor, the untreated heart tissue always enveloped the heart tissue exposed to the factor [26].
1981	Immunofluorescent histological studies of heart embryonic tissue identified insoluble fibronectin matrix deposition as being the cause for the change in heart tissue properties. Sections of tissue that always adopted an internal position had more insoluble fibronectin in the surrounding matrix than heart embryonic tissue adopting an external position [27].
1984	Rearrangements of heterogeneous mixtures of cells were found to depend on the cells’ ability to form insoluble matrix. Whole embryonic tissue fragments able to deposit fibronectin matrix tended to be enveloped by embryonic tissue lacking this property. Hence as predicted by the DAH, the more cohesive component would adopt an internal position compared with a less cohesive tissue component. However, contrary to the DAH, heterogeneous re-associated

	fragments of the same tissues rearranged with the insoluble-fibronectin producing cells, enveloping the less cohesive cells at equilibrium during regular sorting experiments [161].
1996	Chick embryonic tissues changed their surface tension from a “true,” liquid-like, surface tension over short times in culture to an “apparent,” elastic-solid, tension over longer times in culture. This finding corroborated the results [29] for material properties of embryonic tissues [7].
1998	The mechanical properties of embryonic cells approximate those of ordinary viscoelastic materials. A generalized Kelvin model of viscoelasticity provides the ability to separate the elastic from the viscous responses of tissues under compressive forces. Fitting the force relaxation curve of embryonic tissues provided estimates of relaxation times, elasticity constants, and tissue viscosities of embryonic tissues. An important relation found was that higher tissue cohesion correlated with an increase in the spring and friction constants from the force relaxation curve fit [162].
2003	At matched expression levels of $\alpha 5\beta 1$ integrin and N-Cad in 3D aggregates of Chinese Hamster Ovary (CHO) cells, cell-ECM cohesion was determined to be greater than N-Cad cohesion. These results provided insight into why cohesion of integrin-fibronectin driven aggregation can depend on soluble fibronectin concentration and time in culture [15].
2004	During $\alpha 5\beta 1$ -mediated fibronectin matrix formation, the geometry of the final insoluble fibronectin matrix was found to dictate the degree of cohesion of cellular aggregates. A more extended fibrous fibronectin matrix was observed to deliver more aggregate cohesion than a significantly less fibrous or “punctate” matrix geometry [16].
2005	Surface tension measurements of malignant astrocytoma aggregates showed that this malignant tissue was highly elastic. However, pre-treatment with a trypsin/collagenase cocktail produced liquid-like properties in these aggregates. Significantly, the invasive potential of astrocytoma cells was found to decrease with increasing surface tension, which is in turn correlated with levels of N-Cad expression. Furthermore, in keeping with prior results [159], the surface tension of pre-treated malignant astrocytoma aggregates increased upon treatment with the therapeutic agent dexamethasone in culture conditions [163].
2006	Fibronectin matrix deposition was enhanced on 3D aggregates of a fibrosarcoma cell line, while monolayers of the same cell line failed to polymerize an insoluble fibronectin matrix. The increase in matrix deposition correlates with reduction of Raf-1 expression levels at the transcription level. In the same manner, increased expression of Raf-1 caused the fibrosarcoma aggregates to become less compact. This indicated that there was significant crosstalk between the external microenvironment and the internal transcriptional machinery of the

cell during cellular aggregation [164].

Historically, contributions to our understanding of the role of integrin/fibronectin-mediated cell-ECM interactions on aggregate mechanics and cellular rearrangements have occurred side-by-side with experimental characterizations of cadherin-mediated cell-cell interactions. Figure B-8 is a comparison between the rearrangement dynamics and surface tension relation of embryonic tissues (left panel) and L-cell engineered to express different levels of the cadherin receptor (right panel). The rearrangement behavior at equilibrium is similar for both embryonic tissue and engineered cadherin cell lines. This hints to the possibility that cadherin surface receptor expression and tissue surface tension might be simply proportional in embryonic tissues. However, data are absent at for engineered cell lines at higher levels of cohesion, and consequently effects of integrin receptor expression on cohesion and rearrangement is not known in this parameter range.

Superficially, cell-cell and cell-ECM interactions differ in their effects on mechanics and self-assembly, yet these differences have yet to be adequately explained. Thus there remains a need to clearly define the mechanisms by which ECM regulation affects morphogenesis, and the control network by which the ECM and the cell interact with one another. This thesis will show that integrin-ECM interactions can generate a variety of tissue transitions, including transitions from elastic solids to viscoelastic liquids, not accessible through cell-cell interactions. In particular, cell-ECM interactions produce paradoxical rearrangement behaviors that depend on time and on tissue state in a way that is not explained by any current analytic model.

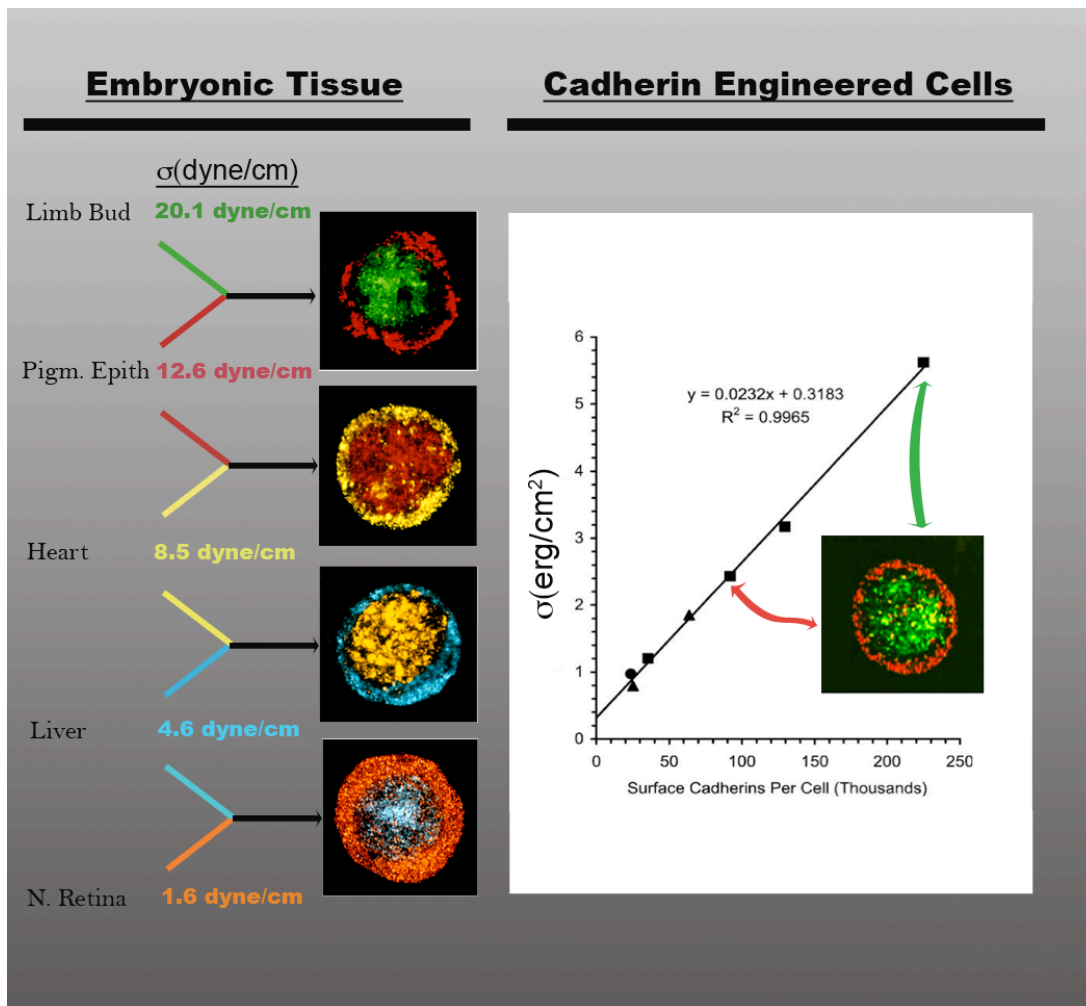


Figure B-8. Comparison between embryonic tissue and cadherin engineered cells. Side-by-side comparison between embryonic tissue suspension and cadherin engineered cells as a function of rearrangement and surface tension values, taken from [7] and [8]. The left panel shows a transitivity relation between envelopment behaviors of cells at equilibrium and their surface tensions - thus embryonic tissues with higher surface tension will always adopt an internal relative position to tissues with lower surface tension. The right panel shows that the same rearrangement behavior appears in L-cells engineered to express different levels of the N-cadherin receptor. Surface tensions here are found to grow linearly with the level of cadherin receptor expression (squares = N-cad, triangles = P-cad, circles = E-cad). The higher surface

tension in engineered cells is about 6 dyne/cm, as compared with Over 12 dyne/cm for embryonic cells.

Tissue Self-Organization Requires Active Substrate Interactions

From an evolutionary perspective, single-celled Protozoan organisms have devised ways to acquire higher-level Metazoan structure such as cellular aggregation and multicellular stability [165]. For example in the case of *Dictyostelium discoideum*, the depletion of its food source triggers cAMP gradients that enhance the streaming of single amoebae leading to aggregation into a sequence of functional structures, e.g., grex, stalk cells, and spore cells that promote the progression of the *Dictyostelium* progeny [166]. This biological example of Protozoa complexity defines two important aspects of cellular aggregation: a) chemically induced amoeba convergence (chemotaxis), b) the effect of cell-substrate interactions aiding slug migration and cell-cell interactions during slug to fruiting body transition.

These mechanisms of control [167-170], as in the case of the basic evolution from single amoeba to fruiting body in the *D. discoideum*, can be viewed as an analogy to the plasticity of embryonic tissue during tissue aggregation and rearrangement. For example, potent factors such as bone morphogenetic protein (BMP), fibroblast growth factor (FGF) [171], and sonic hedgehog (SHH) [172], among others, induce specification of cells during development, as in the case of the initial stage of cAMP inducing single amoebae to converge into a swarm of amoebae [173]. Likewise in more advanced organisms, cell membrane-driven mechanisms lead during development to more complex structure formations such as neural crest migration upon neural tube closure [72], somite formation [174], and sympathetic ganglia formation [175] etc. These crucial processes, we argue,

achieve large-scale morphological formation through mechanisms that at their heart depend on cell-cell and cell-substrate interactions [176-178].

Two-Dimension vs. 3-Dimension Structure in Embryonic Development

A final caveat to the literature on the roles of cell-cell and cell-ECM interactions on structure formation is that embryonic development occurs in a 3-dimensional context, while a plurality of studies describing cellular dynamics during development have been conducted on rigid 2-dimensional substrates. Recently, studies have shown that dimensionality and attendant properties such as cell shape [179], substrate stiffness [180], and type of adhesive interactions (i.e., cell-cell [164] vs. cell-substrate [16]) are significantly different in 2D and 3D environments. As a simple example, recent experimental work using fibroblasts provided evidence for different morphologies and behaviors of cells cultured on planar surfaces or for cells sandwiched between ECM-coated surfaces. When cultured as on a single surface, fibroblasts grow into a broad structure with active lamellipodia and average speeds in the range of $0.61 \pm 0.3 \mu\text{m}/\text{min}$. Adding another ECM-coated surface on the top (dorsal) side of the fibroblast, simulating a more 3-dimensional geometry, changes the cell to a more elongated morphology and consequently the fibroblast reduces its average speed to $0.28 \pm 0.3 \mu\text{m}/\text{min}$ [181]. Complementary work using liver [182] and breast [183] cells likewise demonstrate distinct differences in growth behaviors of cells grown in 2D, in 2D sandwiches, and in full 3D aggregates. Thus it appears that geometry and cell-substrate interactions may play important roles in cellular organization and mechanics.

Cells are also known to exhibit significant haptotactic responses to environmental stiffness. For example, lung endothelial cells grown on micropatterned surfaces of

acrylamide and PDMS, both coated with fibronectin show a pronounced preference to migrate toward stiffer substrates [184]. Likewise, growth-arrested human dermal fibroblasts show migratory preferences on 3-dimensional matrices with variable stiffness. In this case, fibroblasts originally dispersed on a collagen wedge of 0.1 mm with increasing stiffness along the length of the wedge aggregated within 3 days onto the stiffer part of the collagen wedge [185]. In this dissertation, I investigate how properties of 3-dimensional environment affect assembly of both cellular structures and of the ECM itself as a function of cell surface integrin receptor expression.

Even though cellular aggregation seems to be a simple task, tissue specification during aggregation presents a more complex process. This process is marked by the turnover of cellular relations such as cell-cell and cell-substrate interactions, guided to balance and control tissue maturation in the organism. In the formation of the three germinal layers, heart tube evolution in *Drosophila*, and migration of neural crest precursors, the common denominator is the formation of cell-cell and cell-substrate relations controlling cellular aggregation, rearrangement, and signaling events. Thus, this thesis will contribute to the understanding of ECM-driven tissue dynamics as follows:

a) Elucidating the levels of physical control that integrin-fibronectin offers during tissue aggregation, b) Defining the contributions of matrix deposition during cellular rearrangement, and c) Determining contrasting physical roles of the ECM as compared to classical cell-cell interactions.

Chapter 2

Computational Dynamics of Structure and Rearrangement: in silico 3D Cellular Morphogenesis

Computational cell dynamics have opened the possibility to test complex hypotheses. Over the past five decades there has been an attempt to connect micro-scale, molecular, processes to macro-scale mechanisms leading to structure formation in living tissues. In recent years, the field has shown promise to support therapies that could lead to regenerative strategies, potentially even culminating in artificial organ development [1].

As we have described in the Introduction, the connection between micro-scale interactions and morphogenetic features was initiated by a body of research by Townes and Holfreter in the 1950's and was codified in Malcolm Steinberg's "Differential Adhesion Hypothesis" in the 1970's. These studies postulated the physical counterpart of programmed cellular dynamics, namely that the morphogenesis of large-scale structure during development consists of the application of programmed small-scale local interactions of cells via the formation of intermediate-scale structures. The role of these intermediate structures, consisting of aggregates of tens to thousands of cells, has largely been overlooked in studies of tissue formation [2].

Numerous *in silico* approaches have been investigated in the literature [3-5]; the approach that we use here involves the creation of an augmented molecular-dynamics simulation that provides an interface to enable us to study, mechanistically and in detail, how programmed local cellular dynamics lead to the formation of specified physical structures. Examples of structures that follow mechanistic cellular dynamics include pancreatic islets – which have a stereotypical layered organization of α and β cell types – and early neural crest development [6-8]. The fundamental notion in the *in silico* work is

that modulation of adhesive strengths between cell populations leads to rearrangement and cellular self-assembly.

As a first approximation, cellular structure formation can be explained as the result of cells passively following pre-patterned morphogen gradients, as occurs in cases of patterning in *drosophila* due to diffusible morphogens [9] including sonic hedgehog and wingless, causing cells to migrate, reproduce, or apoptose [10]. The theory underlying the formation of pre-pattern structures has been established using reaction diffusion models that demonstrate that heterogeneous and stable patterns can arise from a difference between diffusion rates of an activator and an inhibitor morphogen in an otherwise homogeneous system [11]. Depending on the values of these rates, spots, stripes and other complex patterns can spontaneously and robustly be produced in this manner [12, 13], and cells have been shown to passively position themselves in response to differences in morphogen rates of diffusion [14].

An alternative mechanism for structure formation involves the active participation of cells; this approach has been advocated for example by Forgacs [15] and Murray [2]. The active approach is motivated both by the fact that cells and their internal regulatory mechanisms are the only actors available to control chemical patterning in the first place, and the fact that cellular migration - whether in response to chemical pre-patterns or endogenously - must involve forces between cells or cells on substrates. In our work, we adopt the active approach, in which cells exert forces on one another or on the surrounding ECM via variations in adhesive interactions.

As we have described in the introduction, adhesive interactions between cells is directly associated with the expression of membrane receptors [16] of the cadherin and

integrin families. Cadherins produce direct cell-cell adhesion and, more indirectly, cause activation of key intracellular pathways regulating actin dynamics [17], cell growth, and differentiation [18]. Integrin surface receptors control interactions between cells and the ECM [19], as well as mediating the polymerization of the ECM itself [20, 21]. Thus cadherins produce short-range interaction forces between cells in contact, while integrins produce longer-range interactions through the extended matrix. The latter interactions, through the ECM, have been found to convey more binding energy than the former, cell-cell, interactions [22], and the interplay between these two kinds of interactions has been shown to affect structure formation during embryonic development [23-25].

In the following chapter, we simulate the generation of complex structures governed by membrane-bound receptors connecting cells, analogous to cells connected through springs. The force between cells is Hookean and its strain response is viscoelastic. Furthermore, we simulate range of interaction in our model as the biological counterpart of short or long-range interactions described in the section “Biological Aspect of Cellular Binding” in the main background of this thesis.

We examine the organization of cells in 3D geometries, recreating *in vivo* scenarios during cellular aggregation and rearrangement. The current chapter in 3D patterning is published work in the Journal of Biophysics.

Abstract

We describe a model that simulates spherical cells of different types that can migrate and interact either attractively or repulsively. We find that both expected morphologies and previously unreported patterns spontaneously self-assemble. Among the newly discovered patterns are segmented states of alternating discs, and an “onion” state, in which cells form multilayer round-aggregates of two cell types. We show that these unique states result from cellular attraction that increases with distance (e.g. as membranes stretch viscoelastically), and would not be seen in traditional, e.g. molecular, potentials that diminish with distance. Most of the states found computationally have been observed in vitro, and it remains to be established what role these self-assembled states may play in in vivo morphogenesis.

Introduction

The formal study of biological pattern formation dates at least to Turing [11], who proposed that a competition between reaction and diffusion of chemical agents leads to a variety of spatially and temporally varying patterns. Turing's proposition has been explored in numerous applications [2, 26] including in patterns of importance for development [27-31], camouflage [32], mate choice [33, 34], and evolutionary diversity [35].

In Turing's approach to biological morphogenesis, chemical patterns are established through a reaction-diffusion mechanism of chemotropic or chemotrophic agents, and cells are considered to be mere passive constituents that are laid down in response to chemical pre-patterns. Malcolm Steinberg proposed an alternative approach [36], the "Differential Adhesion Hypothesis" (DAH), which postulates that biomechanics between cells plays an active role in biological pattern formation [15]. In this scenario, adhesion or cohesion relations and consequent migration between cells lead to morphogenesis – e.g. in an aggregate of two types of cells, those cells that adhere more strongly would tend to migrate to the interior of developing biological structures, and cells that adhere less strongly would migrate to the exterior (cf. Fig. 3(d)). The DAH has been confirmed using a variety of cell types [22, 37-39], and its role during developmental morphogenesis has been extensively studied in numerous animal models, beginning perhaps with the work of Edelman [40].

In recent years, evidence has emerged demonstrating that morphogenesis is regulated by active cellular repulsion as well as attraction [41], for example, during the development of zebrafish rhombomeres [42], in *Drosophila* embryogenesis [43], in

vertebrate hindbrain segmentation [44], in retinal mapping [45, 46], and elsewhere. At least two mechanisms for cellular repulsion are documented in the literature. First, incorporation of sialic acid in cell surface receptors generates repulsion through electrostatic interactions between nearby acid pairs [47], and second, Eph receptors and their corresponding membrane-bound ligands are known to modulate both attraction and repulsion during development [44, 48]. These constitute two subclasses of receptors from the tyrosine kinase family, EphA and EphB, that specifically interact with GPI-membrane linked EphrinA and transmembrane EphrinB ligands [49]. Hence the receptor and ligand interaction, Eph-Ephrin, requires cell-cell proximity to initiate and modulate repulsion [50, 51], analogously to cellular attraction that occurs through stable cadherin links or integrin-fibronectin focal points.

To our knowledge, no theoretical analysis or inventory of 3D morphologies that form due to direct cellular attractive and repulsive interactions has appeared previously in the literature. In this chapter, we present an *in silico* study intended to fill this void by investigating what structures self-assemble when two types of cells are allowed to interact attractively or repulsively. As we will show, it is straightforward to simulate cellular self-assembly using established computational techniques, and we find that both obvious and unexpected morphologies of cells emerge spontaneously.

Model Description

Algorithmically, our approach resembles dissipative particle-dynamics simulations, in which spherical particles interact or migrate according to prescribed rules. Cells differ from inert particles in a number of ways, for example effects of reproduction and differentiation have been discussed previously [52], and other cell-specific dynamical

features have also been discussed in the literature [53-57]. For a review of these approaches, as well as a modeling approach that includes nonspherical cell geometries, see ref. [58]. In the work described here, to facilitate rapid exploration of parameter space we model only spherical cells, and we define idealized forces between interacting cells. We do not include intracellular behaviors associated with cytoskeletal anisotropies, nor do we consider history-dependent forces, transport of surface-binding proteins or non-spherical cell shapes. Thus these results are not applicable to cells with complex shapes (e.g. neurons or glia), or to cells whose dynamics are strongly influenced by interior structures (e.g. platelets or myocytes). The results presented here may be germane to nearly spherical cells that move slowly compared with timescales of making and breaking of bonds – e.g. cells early in development, or undifferentiated neoplastic cells. Despite these limitations, a variety of nontrivial morphologies form spontaneously, several of which do not seem to have previously been reported or analyzed.

The model that we use is described in the Appendix (see also refs [52] & [59]), and in brief contains both mechanical responses to compression and prescribed attractive or repulsive behaviors as are produced by membrane-bound proteins such as cadherins, integrins, and Eph receptors and ephrin ligands. To simulate cellular responses to compression, we prescribe that cells compress according to a “Voigt” model, like damped springs [60, 61], producing an outwardly directed normal force as sketched in figure 2-1(a). Cells can attract one another in one of two ways: they can cohere through membrane-bound molecules (e.g. cadherins), or they can exert forces intermediated by the extra-cellular matrix, or ECM (via integrin binding) [21, 53, 62, 63].

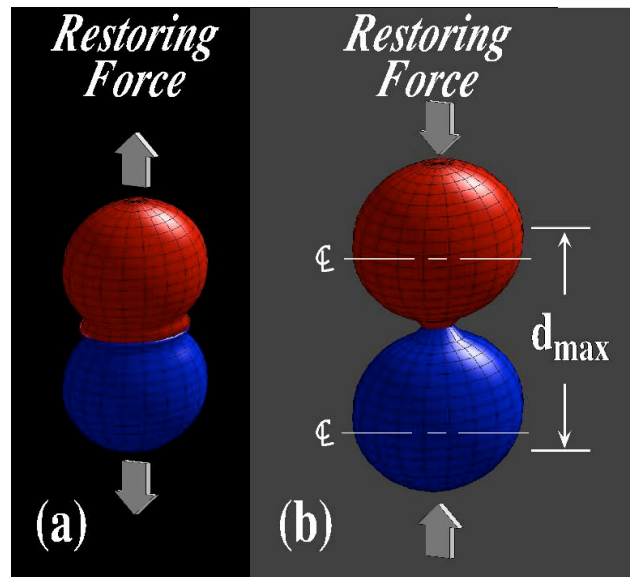


Figure 2-1. Schematics of interactions between cells. (a) Caricature of two cells being compressed together, illustrating the outward restoring force described in text. (b) Caricature of cells responding to being pulled apart by exerting an attractive restoring force. As suggested by the scale indication to the right, cells within a maximum separation between cell centers, d_{\max} interact; cells further apart than this distance move freely.

As sketched in figure 2-1(b), we model cell-cell attraction by allowing cells that are within a distance, d_{\max} , of one another to attract, again as damped springs. This attraction is intended to model membrane tension of two cells connected to one another either directly or through the ECM [64-66]. A cell that is pulled further than d_{\max} is assumed to break free and to feel no further force from its neighbor [67, 68]; likewise once cells begin to compress one another, their attraction vanishes. Beyond these prescribed interactions between cells, we include randomized cellular motion and viscous damping due to a surrounding fluid or ECM in standard ways: randomized motion is simulated as an integrated random walk [69], and viscosity is included by reducing every cell's velocity by a fixed fraction each computational timestep. Finally, in view of the

existence of distinct attractive and repulsive cellular cues [44, 47, 70, 71], we permit cells to either attract or repel one another, and for this purpose we consider two cell types that can interact either homotypically (between like cells) or heterotypically (between unlike cells) with different attractive or repulsive strengths.

In the following simulations, we show results using attractive interactions using a Voigt relation, which increases in strength with distance. In the attractive Voigt form, the force of interaction goes as $k \cdot (r-d)$, where r is the separation between the cell centers, d is the cell diameter, and k is a constant that is negative for attractive interactions. As for repulsive interactions, we use a force that diminishes with distance following the κ/r^2 relation. The repulsive κ/r^2 form is biomechanically reasonable in that one expects repulsive forces to diminish with separation. The parameters k and κ have different units: dimensionally, $\kappa = k \cdot L^3$, where L is a characteristic length. In our simulations, L is of order of the diameter of a cell, D , which we set to unity so that the interaction strengths κ and k will have comparable units.

We remark that Young's moduli for cells in living tissue range from hundreds to millions of kilopascals [72] depending on tissue type and environment; hence a dimensional simulation applicable across relevant scales would be problematic. Consequently, our simulations are strain based rather than stress based: that is, we provide dimensionless computations from which the fractional deformation of a cell defines its elastic response. To convert our results to dimensional units - i.e. to estimate stress based data - one would need to multiply the strain by the Young's modulus for the cells of interest. As examples, strains in our simulations are of order 10%, so that corresponding stresses would be of order 10 Pa for brain tissue and 1 kPa for muscle, and

corresponding forces on a single cell (for cell surface area of order 10^{-6} cm^2) would range from 10^{-4} dyne (1 nN) to 10^{-2} dyne (100 nN).

The formulation that we use is surely not definitive, and one can include any number of possible complications, however to lowest order, our approach of using a Voigt model for attraction and an inverse r^2 repulsive model seems to span the range of plausible inter-cell interactions mediated by membrane-bound factors [73] in 3D morphologies. In the following section, we detail transitions in cellular morphology that occur as homo- and hetero-typic strengths are altered, as in the case of in vitro experiments in which cadherin or integrin expression levels are varied [39] as described in figure 2-2.

Phase Diagram

In this section, we present a phase diagram obtained using a damped spring model for the attractive interaction, and repulsive interactions that decrease with increasing distance. For the attractive and repulsive interactions, we allow cells to interact up to a maximum distance between their centers of $d_{\text{max}} = 3$ cell diameters. This is not an unphysiological distance, as cells deform considerably during development [54], and interactions between cells over larger distances than this are seen in both vertebrates [74] and more primitive life-forms [75].

Simulations have also been performed using up to 1000 cells, however as we will describe, many of the morphologies seen are essentially spherical in shape, and spherical structures are unstable at high cell numbers – that is, larger aggregates tend to break apart into smaller clusters. This is simply a consequence of finite surface tension, and is the identical effect to that which produces water droplets of limited size. To avoid long

transient calculations as these ‘droplets’ form, we perform most of our calculations using only 250 cells, however we have confirmed in separate simulations that non-spherical structures (especially discotic states described below) persist at larger cell numbers.

As we have mentioned, the simulation permits interactions at a distance, through the extracellular matrix (ECM), which influences cell motion both passively (i.e. through viscous effects [60]) and actively (e.g. through contractile forces exerted by the cytoskeleton via integrins on the cell membrane [2], or through repulsive sialic-acid or ephrin mediated interactions). Figure 2-2 displays equilibrium structures that self-assemble from initially heterogeneous mixtures of cells as a function of homotypic and heterotypic interaction strengths between cells. Following a counter-clockwise direction, in quadrant I we find random states, as one would expect from cells that all repel one another. In quadrant II, we find two new and unexpected morphologies. At weak heterotypic attraction, a stable 3-layered structure resembling an “onion” forms, as shown in the upper-left inset. The onion contains a small inner core of red cells inside a larger envelope of blue cells, which is itself covered with a final mantle of red cells. Increasing the homotypic repulsive strength causes the onion structure to transition into a less spherical discotic structure at the expense of increasing intercalation of red and blue cell types held through weak heterotypic interactions.

In quadrant III, we find morphologies that one would anticipate from the DAH, including the hemi-clusters shown appear due to a stronger homotypic than heterotypic attraction, which causes like cells to prefer proximity to one another within mixed aggregates. Lastly, quadrant IV shows the formation of like-clusters as a result of heterotypic

repulsion and homotypic attraction. Spatially, the inter-cluster distances are proportional to the strength of the heterotypic repulsion, analogous to magnets with like polarity.

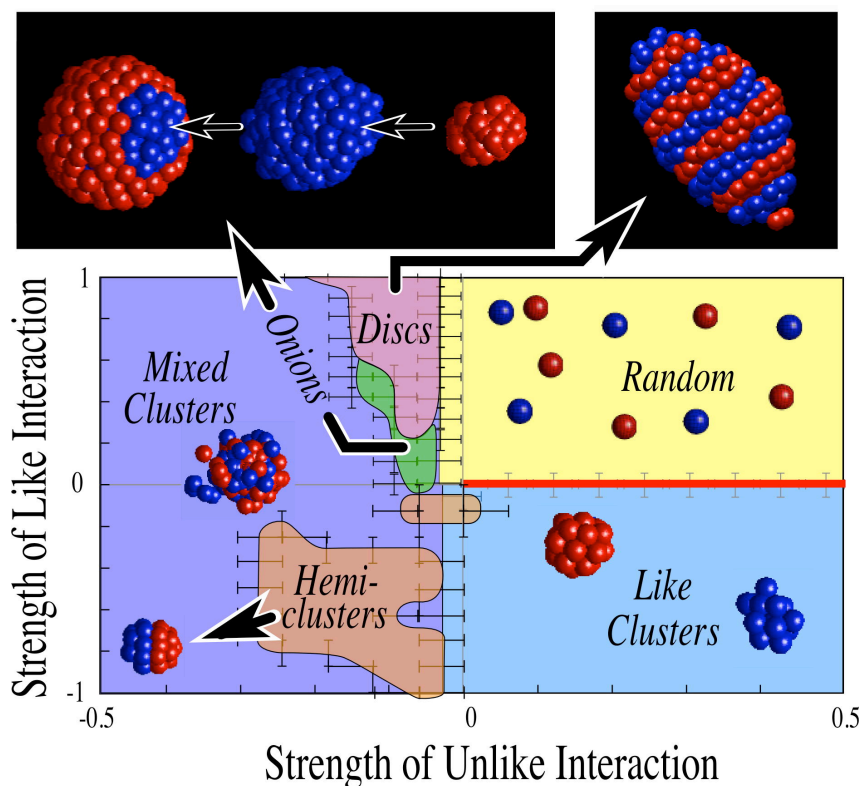


Figure 2-2. Phase diagram for Hookean attraction and inverse r^2 repulsion. Enlarged view at top left shows the onion structure. This self-assembled structure has a layered organization, as shown in expanded views on the upper left. This and the discotic state, shown at top right, are previously unreported structures.

Discussion

We have shown through direct simulation that interactions between cells in a simplified computational model can generate several distinct self-assembled morphologies. In figure 2-3, we show comparisons between these simulated morphologies (upper insets) and similar states (main panels) found through in vitro

experiments in which different cell types exhibiting different cadherin or integrin expression levels are mixed in co-cultures using established techniques [38]. In figure 2-3(a-d) we show respectively: separated homoclusters, joined hemiclusters, a mixed cluster, and an enveloped cluster. These morphologies follow strictly attractive relations as predicted by the DAH. These structures have been previously reported, for example in ref [77].

Our simulations have also revealed two additional structures. First, as shown in figure 2-3(e), we find that an alternating segmented morphology, which we have referred to as ‘discs,’ appear robustly and reproducibly in simulations. Such structures abound in studies of both vertebrate and invertebrate development; we will have more to say about this shortly. We are unaware of in vitro cell culture experiments that have produced such structures i.e. repeating discs of a characteristic size, however a search of our laboratory’s record, involving numerous experiments using a variety of cell types, revealed several examples of alternating segments. In the main panel of figure 2-3(e), we show such an example of a potential discotic state seen in a co-culture of immortalized mouse insulinoma and glucagonoma cell suspensions. It seems likely to us that other such examples may be forthcoming now that they have been theoretically predicted. On the other hand, we have not been able to identify from existing in vitro experiments a second structure that appears robustly in our simulations, the onion structure, shown in figure 2-3(f).

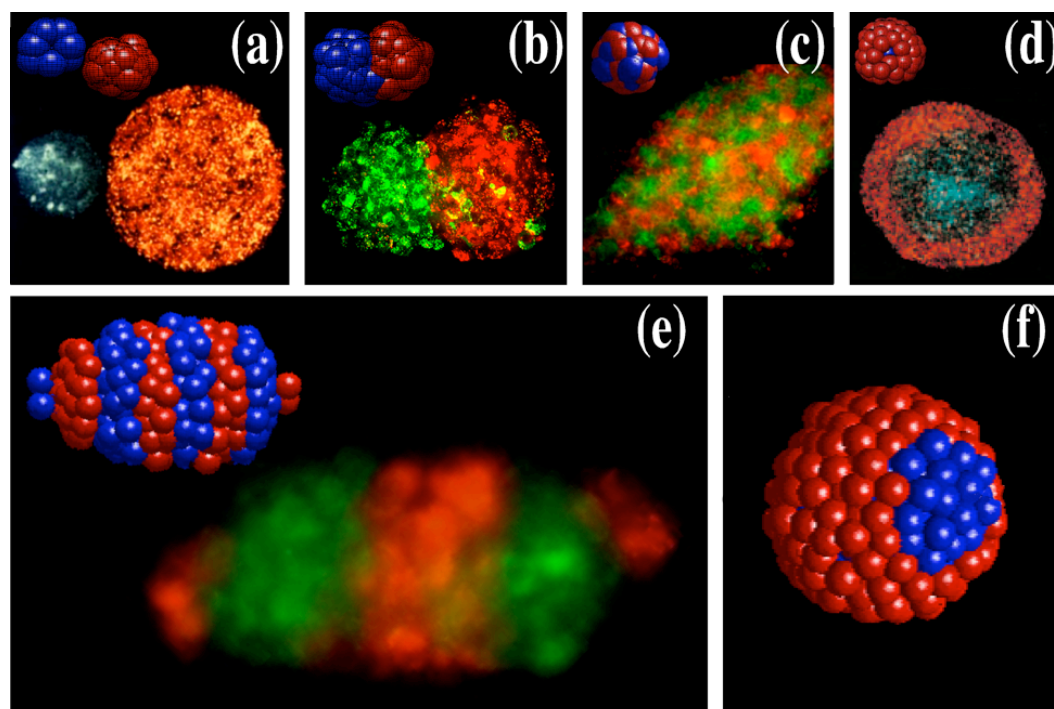


Figure 2-3. Comparison in vitro and in silico cell organization patterns. (a) Homoclusters: green cells are embryonic chick limb bud mesenchyme; orange cells are embryonic chick neural retina. (b) Originally non-cohesive L cells transfected with B-cadherin (green) and R-cadherin (red) – reprinted with permission from ref.[39]. (c) Mixed cluster: green cells are invasive prostate cancer cells; red cells are carcinoma-associated fibroblasts. (d) Orange cells are embryonic neural retina, and blue cells are embryonic chick liver cells – reprinted with permission from Foty et al., (1996) Dev. 122: 1611-20. (e) Alternating segments: green cells are MIN6 mouse insulinoma cells; red cells are mouse alpha-TC glucagonoma cells. Experimental details described in Foty et al., (2005) Dev. Biol. 278: 255-63. (f) Simulated onion state has not yet been reported experimentally to our knowledge.

In closing, the philosophy of this study has been that morphogenesis is regulated both by passive responses of cells to genetically prescribed chemical gradients and by active interactions between cells as mediated by membrane proteins such as adhesion

molecules. The discotic state (figure 2-2, upper right inset) is a case in point: examples are seen in numerous segmented structures, e.g. in rhombomeres, and arguably in annelid segments and even in the *Drosophila* syncytium. Careful experimental investigations indicate that alternating segmentation in rhombomeres may be strongly influenced by active cellular interactions [42-44, 78]. However, it is well documented in *Drosophila* that alternating segmentation appears under tightly regulated genetic control [79, 80], and where in any event segmentation appears before cell boundaries have even formed. Thus examples of both mechanical and chemical patterning paradigms are readily found.

This suggests several open questions. First, it remains to be seen how these two patterning influences interact. Our simulations demonstrate that mechanical interactions alone can spontaneously generate a few specific building blocks. This being the case, it is difficult to hold the view that evolution could have proceeded without at some point sampling these building blocks. This leaves it unclear which structures may be produced by chemical pre-patterns and genetically established despite the tendency of cells to self-assemble into these building blocks, and which may have been constructed as evolution capitalized on this tendency.

Second, our simulations are considerably simplified, neglecting important effects including shape changes due to cytoskeletal forcing, feedback between external stresses and internal cellular functions, and even precise conservation of cellular volumes as agglomerates are compressed. Certainly many of these shortcomings can be improved through embellishments to the spherical cell model that we have presented (see esp. Ref. [58]), and it would be important to establish whether the structures predicted in our simplified simulations are reproduced in more detailed and complicated models.

Third, the simulations described in this section only used two components, while complex organ systems contain many more cell types, and even the earliest developmental processes progress from a three-part layer of endoderm, mesoderm and ectoderm cells. Thus it is desirable to investigate what self-assembled morphologies appear using more cell types.

Finally, our simulations have exclusively been under steady conditions, whereas in vitro development exhibits extensive temporal control over protein expression affecting everything from small-scale growth and migration to larger scale entire organ size and shape. Evidently considerable in silico work remains ahead to understand how structures emerge, grow, and change during normal development.

Acknowledgement

We thank Kristen Bennett for experimental results using insulinoma and glucagonoma cells.

Appendix: Model Details

In this appendix, we describe the simulation used in this section. We first summarize the mechanical interactions between simulated cells, and we then define the boundary and initial conditions and the integration approach used.

The mechanical system

The flowchart for the in silico model is shown in figure 2-4. As summarized in the text, we use a Voigt model, in which a cell of unit mass displaced from an equilibrium position (typically defined to be when cells are first placed in contact) from its j neighbors by a distance Δx_j , feels a restoring force,

$$F_i = -\sum k \cdot \Delta x_j - \eta_{\text{cytoplasm}} \cdot \dot{V}_i,$$

where k is a Hooke constant, and v_i is the velocity of the i -th cell. $\eta_{\text{cytoplasm}}$ is a viscosity representing the cytoplasmic resistance to strain. Including viscoelasticity into the model allows cells to have time dependent stress-strain relations and energy dissipation as the cellular interactions mature over time due to viscous damping.

The signs of forces are chosen so that the restoring force is negative (attractive) when the cells are pulled apart, and positive (repulsive) when cells are compressed together. Since negative forces represent attractive interactions mediated by cadherins (for short ranges) or integrin-ECM interactions (for longer ranges), while positive forces represent hydrostatic responses of cells to being compressed, there is no reason for the Hooke constant to be the same for each alternative, and indeed in the simulation they take on different values. Explicitly, when cell surfaces overlap, they repel with one constant, k_0 , intended to represent their response to compression; when they are separated up to a distance, d_{max} , they attract or repel with a different constant intended to represent forces due to cadherins and integrins as described in the body of this section; and beyond d_{max} , cells are assumed to break free from one another. The simulation can include any number of cell types, but in the present simulation we consider only two cell types, denoted A or B, so that cadherin or integrin mediated forces is defined by a homotypic interaction strength, k_{1AA} or k_{1BB} between like A-A cells or B-B cells respectively, or by a heterotypic strength, k_{1AB} , between unlike cells.

Computational details

Cells have initial positions (x_i, y_i, z_i) , taken initially to be random within a computational domain of fixed volume, “Domain Size”. Reflective boundary conditions are used to contain cells within the computational domain, and to allow cells to rearrange, Domain

Size is scaled with the number of cells used (typically 250, although we have confirmed that similar patterns obtain using particle numbers up to 1000). The simulations are highly damped to represent the low Reynolds' number environment surrounding cells, so even if by chance two cells are initially placed nearly on top of one another, the cells move slowly apart to accommodate the large initial compressive forces without numerical artifacts. All cells wander stochastically as described elsewhere [52, 59], to avoid persistent metastable states.

We simulate the velocity of the cells using Euler integration. Since the cellular environment is highly dissipative, there is no need for a time-reversible integration method; nevertheless we have performed separate comparison simulations using Verlet integration, which revealed no noticeable differences in outcomes. Explicitly, the force obtained in A1 is used to update the velocity and position of the i -th cell according to:

$$\vec{v}_i(t + \Delta t) \rightarrow \vec{v}_i(t) + \frac{1 - \eta_{\text{fluid}}}{m} \vec{F}_i(t) \Delta t + \vec{f}_i(t) \quad [\text{A2}]$$

$$\vec{x}_i(t + \Delta t) \rightarrow \vec{x}_i(t) + \vec{v}_i(t) \Delta t + \vec{F}_i(t) \frac{\Delta t}{2m} \quad [\text{A3}]$$

where the cell mass, m , is taken to be unity, $\eta_{\text{fluid}} = 0.5$ produces exponential damping to represent the viscosity of the interstitial fluid or matrix, $\vec{f}_i(t)$ is a random vector producing migration and is uniformly distributed up to a maximum radius 0.01, and the timestep $\Delta t = 0.5$ (smaller timesteps were investigated, and produced no noticeable difference in the final states shown).

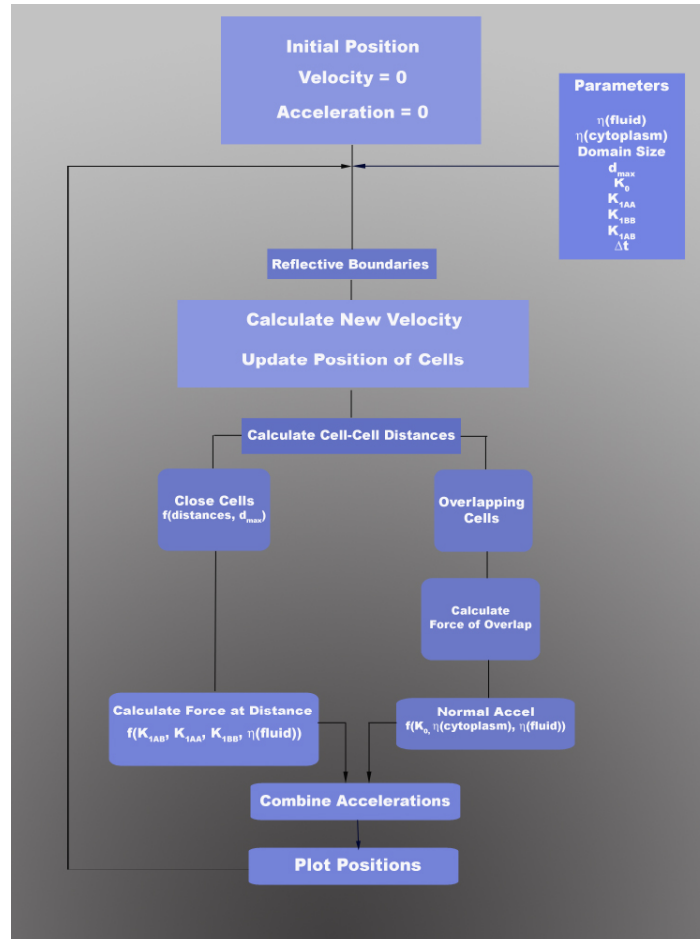


Figure 2-4. Flow chart of in silico model. Beginning with cells randomly distributed with zero velocity and acceleration, cells move and interact under the influence of parameters defining viscosities (η_{fluid} & $\eta_{\text{cytoplasm}}$), interaction strengths (k_{IAB} , k_{IAB} , k_{IAB} & k_0), and computational features such as the size of the computational domain and timestep (Δt). Cells that are close to one another (i.e. within d_{max}) are attracted or repelled with prescribed heterotypic (k_{IAB} , k_{IAB}) or heterotypic (k_{IAB}) interaction strengths, and cells that overlap are repelled hydrostatically with a different strength (k_0).

Chapter 2 Bibliography

1. Jakab, K., et al., Tissue engineering by self-assembly of cells printed into topologically defined structures. *Tissue Eng Part A*, 2008. **14**(3): p. 413-21.
2. Murray, J.D., *Mathematical Biology*. Third Edition ed. Spatial Models and Biomedical Applications. Vol. II: Springer.
3. Graner, F. and J.A. Glazier, Simulation of biological cell sorting using a two-dimensional extended Potts model. *Phys Rev Lett*, 1992. **69**(13): p. 2013-2016.
4. Mombach, J.C., et al., Quantitative comparison between differential adhesion models and cell sorting in the presence and absence of fluctuations. *Phys Rev Lett*, 1995. **75**(11): p. 2244-2247.
5. Glazier, J.A., et al., Coordinated action of N-CAM, N-cadherin, EphA4, and ephrinB2 translates genetic prepatterns into structure during somitogenesis in chick. *Curr Top Dev Biol*, 2008. **81**: p. 205-47.
6. Cirulli, V., et al., Expression and function of alpha(v)beta(3) and alpha(v)beta(5) integrins in the developing pancreas: roles in the adhesion and migration of putative endocrine progenitor cells. *J Cell Biol*, 2000. **150**(6): p. 1445-60.
7. Esni, F., et al., Neural cell adhesion molecule (N-CAM) is required for cell type segregation and normal ultrastructure in pancreatic islets. *J Cell Biol*, 1999. **144**(2): p. 325-37.
8. Monier-Gavelle, F. and J.L. Duband, Cross talk between adhesion molecules: control of N-cadherin activity by intracellular signals elicited by beta1 and beta3 integrins in migrating neural crest cells. *J Cell Biol*, 1997. **137**(7): p. 1663-81.
9. Pribyl, M., C.B. Muratov, and S.Y. Shvartsman, Transitions in the model of epithelial patterning. *Dev Dyn*, 2003. **226**(1): p. 155-9.
10. Tabata, T. and Y. Takei, Morphogens, their identification and regulation. *Development*, 2004. **131**(4): p. 703-12.
11. Turing, A.M., The chemical basis of morphogenesis. 1953. *Bull Math Biol*, 1990. **52**(1-2): p. 153-97; discussion 119-52.
12. Nakamasu, A., et al., Interactions between zebrafish pigment cells responsible for the generation of Turing patterns. *Proc Natl Acad Sci U S A*, 2009. **106**(21): p. 8429-34.
13. Kondo, S., M. Iwashita, and M. Yamaguchi, How animals get their skin patterns: fish pigment pattern as a live Turing wave. *Int J Dev Biol*, 2009. **53**(5-6): p. 851-6.
14. Wolpert, L., Positional information and pattern formation. *Philos Trans R Soc Lond B Biol Sci*, 1981. **295**(1078): p. 441-50.
15. Forgacs, G.a.N., S.A., *Biological Physics of the Developing Embryo*: Cambridge.
16. Steinberg, M.S. and M. Takeichi, Experimental specification of cell sorting, tissue spreading, and specific spatial patterning by quantitative differences in cadherin expression. *Proc Natl Acad Sci U S A*, 1994. **91**(1): p. 206-9.
17. Zandy, N.L. and A.M. Pendergast, Abl tyrosine kinases modulate cadherin-dependent adhesion upstream and downstream of Rho family GTPases. *Cell Cycle*, 2008. **7**(4): p. 444-8.
18. Chen, C.L. and H.C. Chen, Functional suppression of E-cadherin by protein kinase Cdelta. *J Cell Sci*, 2009. **122**(Pt 4): p. 513-23.

19. Hynes, R.O., Integrins: versatility, modulation, and signaling in cell adhesion. *Cell*, 1992. **69**(1): p. 11-25.
20. Schwarzbauer, J.E. and J.L. Sechler, Fibronectin fibrillogenesis: a paradigm for extracellular matrix assembly. *Curr Opin Cell Biol*, 1999. **11**(5): p. 622-7.
21. Robinson, E.E., R.A. Foty, and S.A. Corbett, Fibronectin matrix assembly regulates alpha5beta1-mediated cell cohesion. *Mol Biol Cell*, 2004. **15**(3): p. 973-81.
22. Robinson, E.E., et al., Alpha5beta1 integrin mediates strong tissue cohesion. *J Cell Sci*, 2003. **116**(Pt 2): p. 377-86.
23. Steinberg, M.S., Does differential adhesion govern self-assembly processes in histogenesis? Equilibrium configurations and the emergence of a hierarchy among populations of embryonic cells. *J Exp Zool*, 1970. **173**(4): p. 395-433.
24. Davis, G.S., H.M. Phillips, and M.S. Steinberg, Germ-layer surface tensions and "tissue affinities" in *Rana pipiens* gastrulae: quantitative measurements. *Dev Biol*, 1997. **192**(2): p. 630-44.
25. Schoetz, E.M., et al., Quantitative differences in tissue surface tension influence zebrafish germlayer positioning HFSP, 2008. **2**(1): p. 1-56.
26. Ball, P., *The Self-Made Tapestry*. 1999, UK: Oxford U. Press, .
27. Aegerter-Wilmsen, T., et al., Model for the regulation of size in the wing imaginal disc of *Drosophila*. *Mech Dev*, 2007. **124**(4): p. 318-26.
28. Nellen, D., et al., Direct and long-range action of a DPP morphogen gradient. *Cell*, 1996. **85**(3): p. 357-68.
29. Wolpert, L., *Principles of Development* 1998: Oxford University Press.
30. Reeves, G.T., et al., Computational analysis of EGFR inhibition by Argos. *Dev Biol*, 2005. **284**(2): p. 523-35.
31. Neumann, C.J. and S.M. Cohen, Long-range action of Wingless organizes the dorsal-ventral axis of the *Drosophila* wing. *Development*, 1997. **124**(4): p. 871-80.
32. Parichy, D.M., Evolution of danio pigment pattern development. *Heredity*, 2006. **97**(3): p. 200-10.
33. Endler, J., Predation, light intensity and courtship behavior in *Poecilia reticulata* (Pisces: Poeciliidae)". *Anim. Behav*, 1987(35): p. 1376-85.
34. Houde, A., *Sex, Color and Mate Choices in Guppies*. 1997, Princeton Princeton U. Press.
35. Couldridge, V. and G. Alexander, Color patterns and species recognition in four closely related species of Lake Malawi cichlid. *Behav. Ecol.*, 2002(13): p. 64-9.
36. Steinberg, M.S., Reconstruction of tissues by dissociated cells. Some morphogenetic tissue movements and the sorting out of embryonic cells may have a common explanation. *Science*, 1963. **141**: p. 401-8.
37. Foty, R.A., et al., Liquid properties of embryonic tissues: Measurement of interfacial tensions. *Phys Rev Lett*, 1994. **72**(14): p. 2298-2301.
38. Foty, R.A., et al., Surface tensions of embryonic tissues predict their mutual envelopment behavior. *Development*, 1996. **122**(5): p. 1611-20.
39. Duguay, D., R.A. Foty, and M.S. Steinberg, Cadherin-mediated cell adhesion and tissue segregation: qualitative and quantitative determinants. *Dev Biol*, 2003. **253**(2): p. 309-23.

40. Edelman, G.M., Cell adhesion and morphogenesis: the regulator hypothesis. *Proc Natl Acad Sci U S A*, 1984. **81**(5): p. 1460-4.
41. Wilkinson, D.G., How attraction turns to repulsion. *Nat Cell Biol*, 2003. **5**(10): p. 851-3.
42. Cooke, J.E., H.A. Kemp, and C.B. Moens, EphA4 is required for cell adhesion and rhombomere-boundary formation in the zebrafish. *Curr Biol*, 2005. **15**(6): p. 536-42.
43. Yoshikawa, S., et al., Wnt-mediated axon guidance via the Drosophila Derailed receptor. *Nature*, 2003. **422**(6932): p. 583-8.
44. Xu, Q., et al., In vivo cell sorting in complementary segmental domains mediated by Eph receptors and ephrins. *Nature*, 1999. **399**(6733): p. 267-71.
45. Nakamoto, M., et al., Topographically specific effects of ELF-1 on retinal axon guidance in vitro and retinal axon mapping in vivo. *Cell*, 1996. **86**(5): p. 755-66.
46. Chan, J., et al., Morphogenesis of prechordal plate and notochord requires intact Eph/ephrin B signaling. *Dev Biol*, 2001. **234**(2): p. 470-82.
47. Johnson, C.P., et al., Direct evidence that neural cell adhesion molecule (NCAM) polysialylation increases intermembrane repulsion and abrogates adhesion. *J Biol Chem*, 2005. **280**(1): p. 137-45.
48. Kullander, K. and R. Klein, Mechanisms and functions of Eph and ephrin signalling. *Nat Rev Mol Cell Biol*, 2002. **3**(7): p. 475-86.
49. Unified nomenclature for Eph family receptors and their ligands, the ephrins. Eph Nomenclature Committee. *Cell*, 1997. **90**(3): p. 403-4.
50. Shao, H., et al., Characterization of B61, the ligand for the Eck receptor protein-tyrosine kinase. *J Biol Chem*, 1995. **270**(10): p. 5636-41.
51. Stein, E., et al., Eph receptors discriminate specific ligand oligomers to determine alternative signaling complexes, attachment, and assembly responses. *Genes Dev*, 1998. **12**(5): p. 667-78.
52. Shinbrot, T., Simulated morphogenesis of developmental folds due to proliferative pressure. *J Theor Biol*, 2006. **242**(3): p. 764-73.
53. Gracheva, M.E. and H.G. Othmer, A continuum model of motility in ameboid cells. *Bull Math Biol*, 2004. **66**(1): p. 167-93.
54. Munro, E.M. and G.M. Odell, Polarized basolateral cell motility underlies invagination and convergent extension of the ascidian notochord. *Development*, 2002. **129**(1): p. 13-24.
55. Levine, H., W.J. Rappel, and I. Cohen, Self-organization in systems of self-propelled particles. *Phys Rev E Stat Nonlin Soft Matter Phys*, 2001. **63**(1 Pt 2): p. 017101.
56. Merks, R.M.H. and J.A. Glazier, A cell-centered approach to developmental biology. *Physica A*, 2005(352): p. 113-30.
57. Rejniak, K.A., An immersed boundary framework for modelling the growth of individual cells: an application to the early tumour development. *J Theor Biol*, 2007. **247**(1): p. 186-204.
58. Palsson, E., A three-dimensional model of cell movement in multicellular systems *Future Gen. Comp. Sys.* , 2001(17): p. 835-52.
59. Caicedo-Carvajal, C.E. and T. Shinbrot, In silico zebrafish pattern formation. *Dev Biol*, 2008. **315**(2): p. 397-403.

60. Koay, E.J., A.C. Shieh, and K.A. Athanasiou, Creep indentation of single cells. *J Biomech Eng*, 2003. **125**(3): p. 334-41.
61. Walton, O.R. Numerical simulations of inelastic frictional particle-particle interactions ed. M. Roco, Stoneham: Butterworth-Heinemann.
62. Lauffenburger, D.A. and A.F. Horwitz, Cell migration: a physically integrated molecular process. *Cell*, 1996. **84**(3): p. 359-69.
63. Adams, J.C. and F.M. Watt, Regulation of development and differentiation by the extracellular matrix. *Development*, 1993. **117**(4): p. 1183-98.
64. Pedersen, J.A. and M.A. Swartz, Mechanobiology in the third dimension. *Ann Biomed Eng*, 2005. **33**(11): p. 1469-90.
65. Janmey, P.A. and D.A. Weitz, Dealing with mechanics: mechanisms of force transduction in cells. *Trends Biochem Sci*, 2004. **29**(7): p. 364-70.
66. Zhu, C., G. Bao, and N. Wang, Cell mechanics: mechanical response, cell adhesion, and molecular deformation. *Annu Rev Biomed Eng*, 2000. **2**: p. 189-226.
67. Zhu, C., et al., Measuring receptor/ligand interaction at the single-bond level: experimental and interpretative issues. *Ann Biomed Eng*, 2002. **30**(3): p. 305-14.
68. Evans, E., D. Berk, and A. Leung, Detachment of agglutinin-bonded red blood cells. I. Forces to rupture molecular-point attachments. *Biophys J*, 1991. **59**(4): p. 838-48.
69. Maskery, S.M., H.M. Buettner, and T. Shinbrot, Growth cone pathfinding: a competition between deterministic and stochastic events. *BMC Neurosci*, 2004. **5**: p. 22.
70. Maskery, S.M. and T. Shinbrot, Deterministic and stochastic elements of axonal guidance. *Annu Rev Biomed Eng*, 2005(7): p. 187-221.
71. Mellitzer, G., Q. Xu, and D.G. Wilkinson, Eph receptors and ephrins restrict cell intermingling and communication. *Nature*, 1999. **400**(6739): p. 77-81.
72. Wells, R.G., The role of matrix stiffness in regulating cell behavior. *Hepatology*, 2008. **47**(4): p. 1394-400.
73. Simson, R., et al., Membrane bending modulus and adhesion energy of wild-type and mutant cells of *Dictyostelium* lacking talin or cortexillins. *Biophys J*, 1998. **74**(1): p. 514-22.
74. Maderspacher, F. and C. Nusslein-Volhard, Formation of the adult pigment pattern in zebrafish requires leopard and obelix dependent cell interactions. *Development*, 2003. **130**(15): p. 3447-57.
75. Huber, O. and M. Sumper, Algal-CAMs: isoforms of a cell adhesion molecule in embryos of the alga *Volvox* with homology to *Drosophila* fasciclin I. *EMBO J*, 1994. **13**(18): p. 4212-22.
76. Wolpert, L., Cell boundaries: knowing who to mix with and what to shout or whisper. *Development*, 2003. **130**(19): p. 4497-500.
77. Foty, R.A. and M.S. Steinberg, Cadherin-mediated cell-cell adhesion and tissue segregation in relation to malignancy. *Int J Dev Biol*, 2004. **48**(5-6): p. 397-409.
78. Trainor, P.A. and R. Krumlauf, Patterning the cranial neural crest: hindbrain segmentation and Hox gene plasticity. *Nat Rev Neurosci*, 2000. **1**(2): p. 116-24.

79. Nusslein-Volhard, C. and E. Wieschaus, Mutations affecting segment number and polarity in *Drosophila*. *Nature*, 1980. **287**(5785): p. 795-801.
80. Shvartsman, S.Y., C.B. Muratov, and D.A. Lauffenburger, Modeling and computational analysis of EGF receptor-mediated cell communication in *Drosophila* oogenesis. *Development*, 2002. **129**(11): p. 2577-89.

Chapter 3

Interplay Between $\alpha 5\beta 1$ Receptor Expression and Soluble Fibronectin Concentration Influences Tissue Visco-elasticity and Rearrangement

Abstract

Tissue organization during embryonic development and wound healing depends on the ability of cells on the one hand to exchange adhesive bonds during active rearrangement and on the other to become fixed in place as tissue homeostasis is reached. Cells achieve these contradictory tasks by regulating either cell-cell adhesive bonds, mediated by cadherins, or cell-extracellular matrix (ECM) connections, regulated by integrins and soluble fibronectin. Cell-cell interactions are well studied; cell-ECM interactions less so. In this chapter we present experimental findings that elucidate the role of integrin receptors and soluble fibronectin on tissue biomechanical properties. As has been documented with cadherin-mediated interactions, we find that aggregate cohesion increases up to a critical value with integrin receptor expression. At higher receptor expressions, we find that aggregate cohesion actually decreases, which we attribute the tight binding of cells to the ECM that prevents them from rearranging into a dense aggregate. Likewise we find paradoxical changes in aggregate size over time and other aggregate properties that appear when soluble fibronectin (a key ECM ingredient) is depleted by an overabundance of cells in an aggregate. Finally, we discuss potential implications of complex cell-ECM dynamics for applications in development and healing.

Introduction

The expression and function of various cell surface adhesion systems, such as cadherins and integrins, impart measurable biophysical properties to cellular aggregates [1-3]. One such property, tissue surface tension, has previously been shown to correlate strongly with tissue cohesion and segregation [1].

Cellular aggregation has been widely studied, with a biophysical origin that can be traced to the 1950's with the studies of Townes and Holtfreter, who explored the aggregation properties of amphibian embryonic tissue. These early experiments showed that cells dissociated from whole tissues would re-aggregate and rearrange to adopt their original positions within the embryo. Townes and Holtfreter also showed that fragments of embryonic tissues would “round up” (form spherical aggregates) and “sort out” (encapsulate other tissues) in vitro, following intrinsic tissue “affinities,” i.e. strengths of binding between specific cell types [4]. Affinity between fragments of embryonic tissue was determined to be a property of single cells dissociated from whole tissues. The existence of an affinity between individual cells that could specify cellular positioning in an aggregate led to the formulation of the Differential Adhesion Hypothesis (DAH) as a theoretical framework to explain cellular rearrangement and cohesive phenomena during aggregation and tissue self-assembly [5]. The DAH predicts that heterogeneous mixtures of cells expressing different levels of adhesive proteins at the cell surface can, through aggregation and rearrangement, achieve states of miscibility (mixing), or immiscibility (separation) [6-9].

Adhesion between cells is known to control the gross mechanics of a tissue. It has been shown, for example, that embryonic tissue fragments subjected to external centrifugal forces respond differently depending on their intercellular adhesive relations

[10]. On the one hand, some cellular aggregates deform upon application of a compressive force and remain deformed once the force is removed: such aggregates are termed viscoelastic-solids (see figure 3-3, following). On the other hand, other cellular aggregates deform under comparable compressive forces but return to a spherical droplet shape once released: cells in these aggregates can slide past one another, and the aggregate is termed a viscoelastic-liquid. It has been proposed that the ability of cells in aggregates to rearrange and round up at equilibrium when subjected to compressive forces is associated with an intrinsic surface tension analogous to that of liquid surface tension. [11, 12].

Historically, embryonic tissues have been the original models for the study of rearrangement, aggregation, and response of tissues to external forces. Early experiments allowed only for measurements of bulk mechanical properties as a function of the site of tissue dissection. For example, pigmented epithelium fragments were found to envelop heart fragments under standard tissue culture conditions. Similarly, dissociated pigmented epithelium and heart cells were observed to segregate, or “sort-out”, from each other, adopting similar relative positions as are found in vivo [7]. Subsequent experiments revealed that the times at which tissues are dissected and the amount of time over which tissues are incubated markedly influence this sorting behavior. For example, embryonic heart tissue cultured for 1.5 days always envelopes liver tissue cultured for 2.5 days, however when these tissues were both incubated for 2.5 days, a phase-reversal takes place, so that embryonic liver tissue now envelops heart tissue [13]. This phase-reversal suggests that some change in tissue mechanical properties must occur as time evolves. Other work on a variety of embryonic systems has further illuminated

connections between tissue viscoelasticity and site of origin and time in culture [11, 12, 14].

Understanding these complicated effects has been hampered by the fact that it is difficult to determine with certainty details about cellular adhesive relations governing a tissue's mechanical properties. Cells can interact through cell-cell effects alone, through a combination of cell-cell and cell-extracellular matrix (ECM) effects, or strictly through cell-ECM effects. Effects of direct, cell-cell interactions on tissue mechanics are comparatively well documented: for the most part, tissues expressing cadherins (which mediate cell-cell adhesion) exhibit viscoelastic-liquid behavior, and measurements have shown that in this case tissue surface tension is linearly related to levels of cadherin receptor expression [1]. Biomechanical effects of cell-ECM interactions are considerably less clear, however.

In particular, the formation of an ECM from fibronectin requires the polymerization by cell surface receptors of soluble fibronectin dimers into an extended insoluble matrix [15]. This process spans length-scales from nanometer-scale receptor clustering to receptor-ligand interactions to micrometer-scale fibronectin polymerization and deposition [16-23]. Moreover, the biochemical pathways regulating fibronectin polymerization are intricate and provide several levels of control during this process [19, 24], and as a consequence multiple timescales are also involved in cell-ECM interactions.

The time-dependence of tissue responses to cell-ECM interactions is a logical consequence of the polymerization of soluble fibronectin into an insoluble matrix, which is governed by interaction with cellular integrin receptors. Functional integrins consist of two non-covalently bound transmembrane heterodimeric glycoprotein subunits α and β .

The α and β subunits contain a large extracellular domain (700-1100 residues), a hydrophobic transmembrane region, and a short tail region (50-70 residues) with the ability to activate important cytoplasmic pathways [25]. Importantly, the $\alpha 5 \beta 1$ heterodimer both binds to the ECM and mediates the polymerization of soluble fibronectin (sFn) into insoluble fibronectin matrix [26]. The integrin-mediated formation of the ECM provides a mechanism for tissue cohesion that is quite distinct from aggregation based on cadherin interactions, which obey largely history independent bond formation and breaking dynamics [27, 28]. Accordingly, integrin-mediated and cadherin-mediated adhesion operate through different mechanisms and with different time scales that may influence their roles during embryonic development and other biological processes such as wound healing and malignant invasion [1, 29].

In the in vitro model that follows, we will analyze the role of cell-ECM contributions to tissue mechanical properties by exploring: a) the interplay between $\alpha 5 \beta 1$ - surface receptor expression and soluble fibronectin concentration, b) the role of these biological parameters in defining tissue transitions from viscoelastic-liquid to viscoelastic solids and, c) the interplay between integrin and cadherin-based adhesion systems on mechanical properties and cell rearrangement. Through this work, we seek to improve the quantitative understanding of complex behaviors of cellular aggregation and organization.

Results

Characterization of integrin receptor level expression and fibronectin matrix assembly

As described in the Methods section, we fully characterized four CHO- $\alpha 5\beta 1$ clones that express different levels of the $\alpha 5\beta 1$ integrin surface expression. Figure 3-1 is a FACS plot showing four stable levels of the $\alpha 5$ subunit of the $\alpha\beta$ heterodimer after transfection and selection with G418 antibiotic of CHO-B2 cells. In figure 1, from left to right, CHO-P3 or P3 signal has no signal since these cells were transfected, as negative control, with a plasmid lacking the $\alpha 5$ construct. To the right are cells expressing the $\alpha 5$ subunit of the $\alpha 5\beta 1$ integrin heterodimer. In increasing order, $\alpha 5(L)$, $\alpha 5(M)$, $\alpha 5(H)$, and $\alpha 5(HH)$ or low, mid, high, and highest are representative expression levels of the $\alpha 5\beta 1$ integrin heterodimer. Figure 3-2 is a FACS plot of stable CHO cell lines with dual expression of $\alpha 5\beta 1$ and N-cadherin receptors. Figure 3-2(a) shows the relative signal expression at two levels of the $\alpha 5$ subunit, figure 3-2(b) shows matched $\alpha 5$ expression signals of CHO- $\alpha 5\beta 1$ /Ncad cells to those of figure 3-2(a). Lastly, figure 3-2(c) shows the N-cadherin (N-cad) expression from the CHO- $\alpha 5\beta 1$ /Ncad cell line. We compared the N-cad level of expression of this cell line to the CHO-N-cad cell line (red solid line), which has already been characterized in our laboratory [2].

As a unified nomenclature, we will refer to these groups of CHO cell line clones as $\alpha 5\beta 1(L)$, $\alpha 5\beta 1(M)$, $\alpha 5\beta 1(H)$, and $\alpha 5\beta 1(HH)$ for the integrin expression group. As for the dual expression group, we will refer to these clones as $\alpha 5\beta 1(M)/N\text{-cad}$ and $\alpha 5\beta 1(HH)/N\text{-cad}$ in the remainder of this chapter.

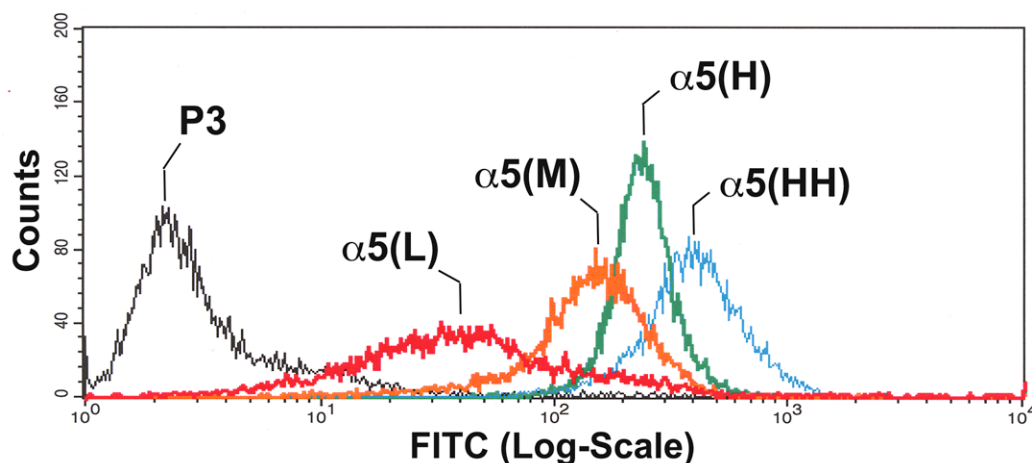


Figure 3-1. Analysis by flow cytometry of $\alpha 5\beta 1$ expression. The relative levels of $\alpha 5\beta 1$ surface receptor expression after transfection and selection for positive clones, e.g. $\alpha 5\beta 1$ - (Low(L), Mid(M), High(H) and Highest(HH), were compared with those of the parent cell line transfected with an empty vector control, P3. Four distinct populations expressing different levels of integrin receptor were expanded and used for subsequent experiments.

Since the interaction of the $\alpha 5\beta 1$ receptor and soluble fibronectin causes the polymerization of fibronectin dimers into insoluble fibronectin fibers, we assessed the formation of insoluble fibronectin matrix of CHO cells seeded on plates at different receptor expression and soluble fibronectin concentrations. Figure 3-3 is a composite of the insoluble fibronectin signal from the cells seeded on glass coverslips after immunostaining. For example, as expected the signal increases as the concentration of soluble fibronectin increases, with thicker and longer insoluble fibronectin fibers when cells are seeded with 300- $\mu\text{g/ml}$ soluble fibronectin. Also, we find that qualitatively the insoluble fibronectin signal increases with increasing $\alpha 5\beta 1$ integrin receptor expression.

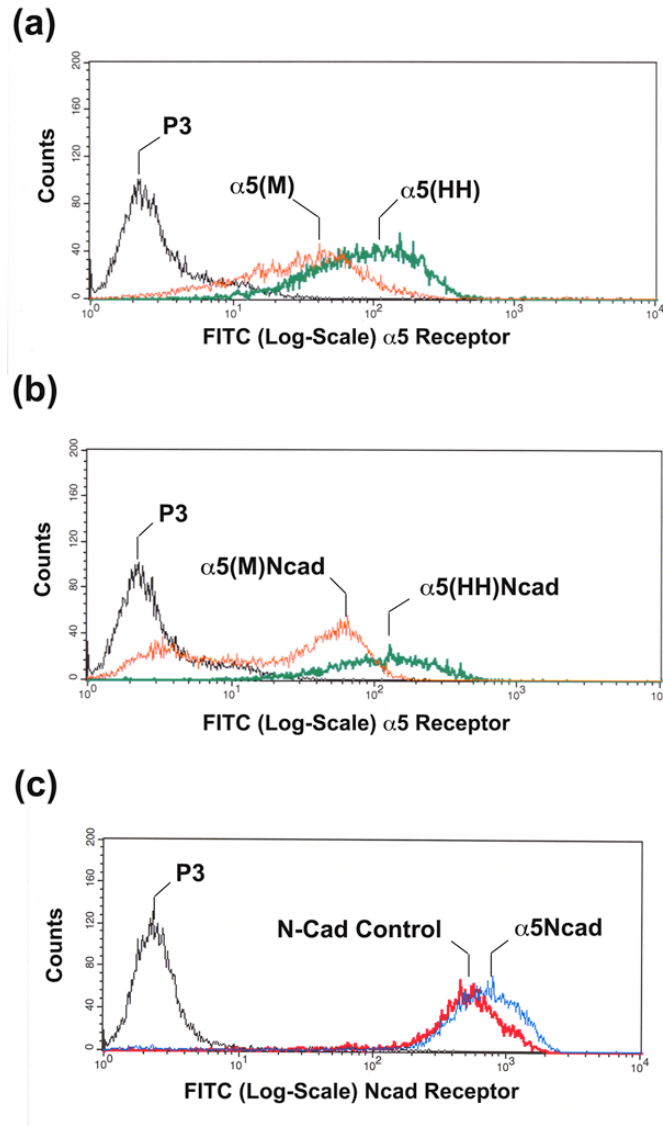


Figure 3-2. Analysis by flow cytometry of dual $\alpha 5\beta 1$ and N-cad receptor expression. Figure 3-2(a) are representative levels of expression of CHO- $\alpha 5\beta 1$ cells lines, and figure 3-2(b) has matched levels of the integrin surface receptor expression of CHO- $\alpha 5\beta 1$ /Ncad cell line to those of CHO- $\alpha 5\beta 1$. Figure 3-2(c) has the signal of the N-cad expression (solid blue line) in the CHO- $\alpha 5\beta 1$ /N-cad cell line. The solid red line represents a signal from CHO-N-cad for comparative purposes.

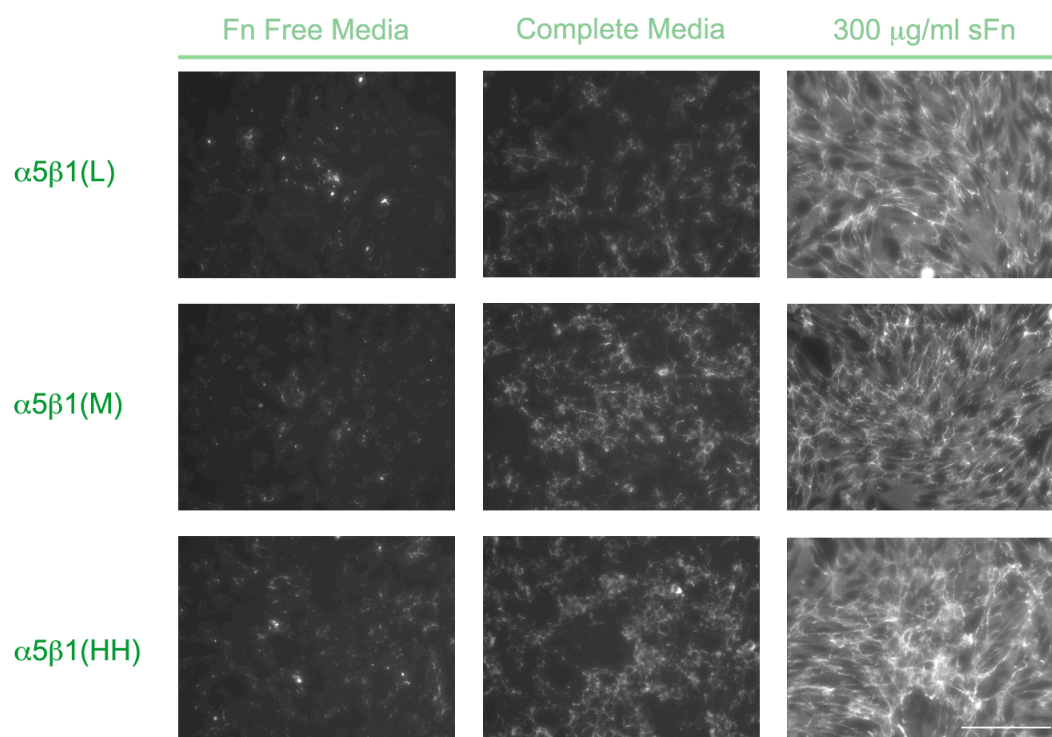


Figure 3-3. Fibronectin matrix assembly on glass coverslips after 24 hours. Cell lines expressing different levels $\alpha 5\beta 1$ receptor were plated at a density of 5×10^5 cell/ml in Fn-free media, complete media (endogenously containing 30- μ g/ml soluble fibronectin (sFn)), and media supplemented with 300- μ g/ml sFn respectively. Here, the fibrous and extended insoluble fibronectin matrix, as indicated by the white fibrous matrix, qualitatively correlates with sFn concentration from fibronectin free media up to 300- μ g/ml sFn and integrin expression from $\alpha 5\beta 1$ (L) to $\alpha 5\beta 1$ (HH). Scale Bar 100 μ m.

The interplay between $\alpha 5\beta 1$ receptor density and soluble fibronectin concentration promotes changes in tissue mechanical properties.

The ability of cells to move relative to one another within an aggregate is termed “tissue liquidity” [12]. As with other liquid systems, a tissue with high liquidity exhibits a measurable surface tension that is load independent. On the other hand, some tissues have low liquidity, and produce surface tensions that depend on load history. If a liquid-like aggregate is compressed once, producing a surface tension σ_1 , and then a second time with larger force, yielding a tension σ_2 , one expects to obtain ratios of $\sigma_2/\sigma_1 \approx 1$. Such a tissue is termed a ‘viscoelastic-liquid’. This is distinct from a tissue (in which cells cannot continuously rearrange) that produces ratios of $\sigma_2/\sigma_1 > 1$: these tissues are termed “viscoelastic-solids”. A viscoelastic-solid will spring back almost immediately upon release of a compressive force, while a viscoelastic-liquid will regain its original spherical shape but only some time after the compressive force is released. These behaviors are illustrated in figure 3-4 below, where we display a comparison between different types of aggregate responses to repeated loads. These plots are from two different fractions of aggregates of CHO cells expressing the $\alpha 5\beta 1(M)$ receptor compressed within the same range of forces. Although prepared identically, the two exemplar aggregates shown produce both qualitatively and quantitatively different responses to imposed loads. For example, the ratios of F_2/F_1 and σ_2/σ_1 were 1.5 (+/- 0.07) and 1.0 (+/- 0.02) for $\alpha 5\beta 1(M)$ viscoelastic-liquid aggregates ($n = 10$) and 1.5 (+/- 0.02) and 1.0 (+/- 0.1) for $\alpha 5\beta 1(M)$ viscoelastic-solid aggregates ($n = 6$).

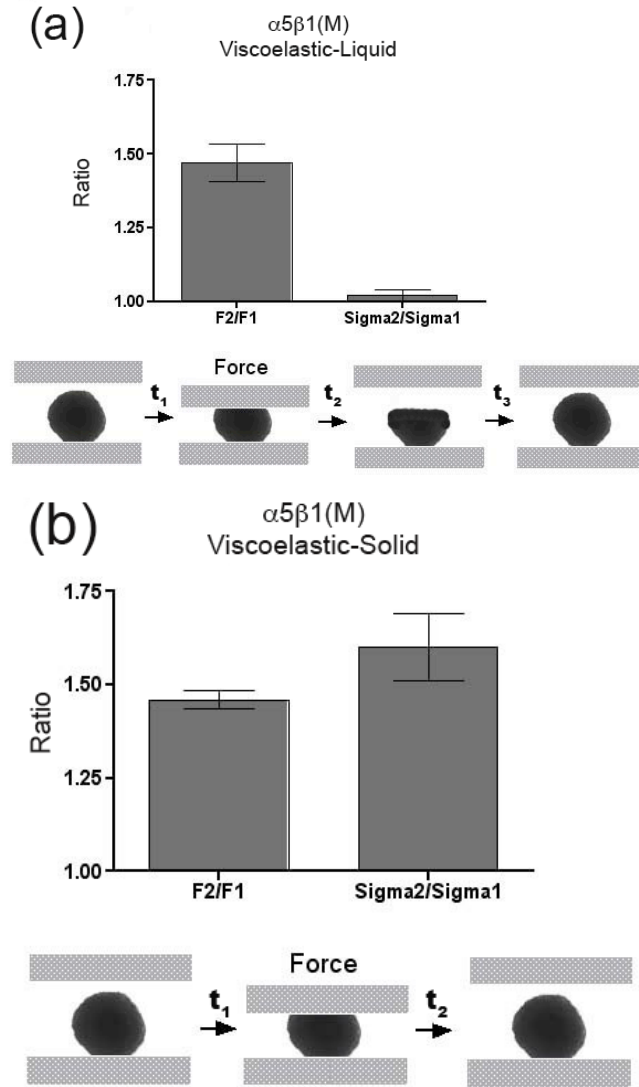


Figure 3-4. Responses of CHO-a5b1(M) cell aggregates to a compressive force reflect mechanical properties. Two possible material properties arise as a consequence of compression. These properties are intrinsic to the type of interactions between cells in the aggregates. In figure 3-4(a), cells in an aggregate are held comparatively loosely through $\alpha 5\beta 1$ -fibronectin adhesive links ($n = 10$). The bottom insert is a representation of these dynamics, which require more transition time ($t_2 + t_3$) to gain the original shape upon removal of the compressive force. These aggregates behave as viscoelastic-liquids and their surface tension or tissue cohesion is independent of the applied force (upper part of panel), a common feature of tissue liquidity [37]. The initial compressive force applied is F_1 ; a second force is F_2 ; corresponding surface tensions

are σ_1 and σ_2 . In contrast, figure 3-4(b) depicts cells that are tightly bound to one other and are unable to dissipate compressive forces ($n = 6$). Such aggregates regain their shape instantaneously upon removal of compressive load and less transition time (t_2) to regain their initial shape. These aggregates behave as viscoelastic-solids and their surface tension is proportional to the magnitude of the force applied (top of panel).

As described in the methods, one validation of our experimental system is the comparison of the ratios of compressive forces to the ratio of surface tensions (σ 's). As in the case of simple liquids, the surface tension should not depend on the compressive force history. For example, figure 3-4(a) shows the comparison between force ratio F_2/F_1 and σ_2/σ_1 of CHO- $\alpha 5\beta 1$ (M) cell aggregates. Here, 62% of the total data set of 16 aggregates behaves as a viscoelastic-liquid, as evidenced by a significant difference between the force ratio and the surface tension ratio. This difference is a suitable metric for the presence of a liquid-like aggregate because in such aggregates, the surface tension is nearly constant (i.e. $\sigma_1/\sigma_2 \approx 1$) despite significant differences in imposed force (i.e. when $F_2/F_1 \neq 1$). The bottom insert is a representation of the time-dependent dynamics of these aggregates. Aggregates behaving as viscoelastic-liquids take some time to regain their equilibrium shape after compressive loads are removed from the aggregates. By contrast, figure 3-4(b) shows that 38% of CHO- $\alpha 5\beta 1$ (M) behaves also as viscoelastic-solids. This is apparent from the dependence of surface tension on initial compressive forces: the ratio of surface tensions, σ_1/σ_2 , here increases with ratio of compressive force, F_2/F_1 . The bottom insert shows a sequence of snapshots showing that these aggregates promptly spring-back to recover their original shape upon removal of the compressive load.

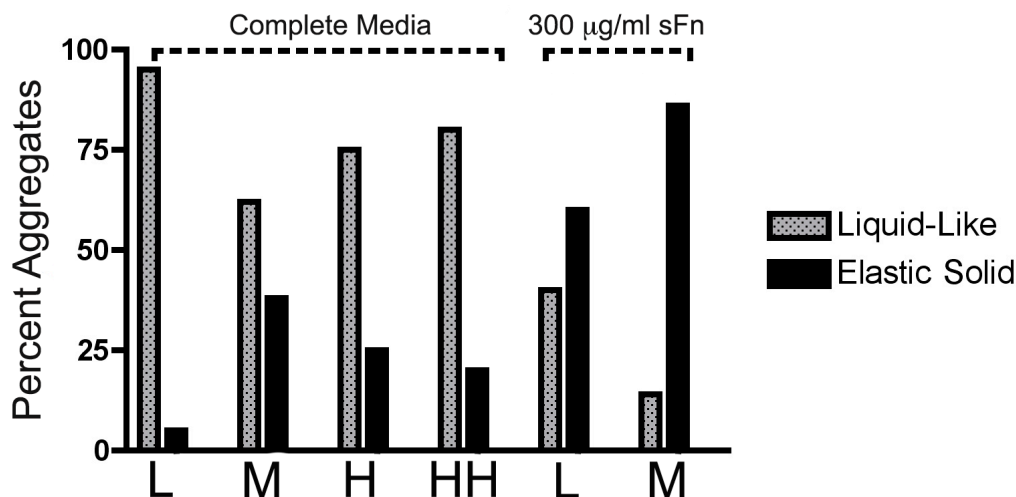


Figure 3- 5. Viscoelastic properties of aggregates. As mentioned in figure 4, cells held through $\alpha 5\beta 1$ -fibronectin adhesive relations have two types of materials properties, e.g. viscoelastic-liquid or liquid-like or viscoelastic-solid or elastic solid (I will use these terms interchangeably for the remaining of the chapter). Here, L, M, H, and HH represent CHO- $\alpha 5\beta 1$ (L, M, H, and HH) integrin expression respectively. Using the comparison between ratio of force and ratio of surface tension, we plot the percent of aggregates with liquid-like properties (light gray bars) and aggregates with elastic solid properties (dark bars). These percentages are calculated from the total number of compressed aggregates (Data Set). Aggregates at each level of integrin expression were either incubated in complete media or media supplemented with 300- $\mu\text{g/ml}$ sFn.

It has been documented that embryonic tissues change their tissue properties over time [13, 36], a behavior that is seen also in CHO- $\alpha 5\beta 1$ aggregates, which increase their cohesion as a function of time [2]. Here we show that these changes in aggregate properties are achieved through changes in soluble fibronectin and integrin receptor expression. Figure 3-5 displays the relative fractions of viscoelastic-liquid and viscoelastic-solid aggregates in data sets of 16-20 aggregates, as a function of $\alpha 5\beta 1$

receptor expression and soluble fibronectin concentration. The gray bars show the fraction that behave as viscoelastic-liquid, while the dark bars represent the fraction of aggregates that behave as viscoelastic-solid. We see a clear transition in the liquid-like to elastic-solid percentages when soluble fibronectin is increased. For example, 95% of aggregates of CHO- $\alpha 5\beta 1$ (L) incubated in standard tissue culture media display viscoelastic-liquid behavior, however, when aggregates of the same clone were incubated in the presence of 300- $\mu\text{g/ml}$ sFn, only 40% displayed liquid behavior. Thus tissue properties depend both on $\alpha 5\beta 1$ expression and on soluble fibronectin concentration.

Scrutiny of figure 3-5 reveals a surprisingly complex dependence of aggregate mechanical properties on $\alpha 5\beta 1$ receptor expression at constant sFn concentration. Qualitatively, from examining the data obtained in complete media we observe an apparent biphasic transition of the viscoelastic-liquid fraction as $\alpha 5\beta 1$ expression is increased. From CHO- $\alpha 5\beta 1$ (L) to CHO- $\alpha 5\beta 1$ (M) the fraction of aggregates that behave as viscoelastic-liquids decreases from 95% to 62%, however, from CHO- $\alpha 5\beta 1$ (M) to CHO- $\alpha 5\beta 1$ (H) and CHO- $\alpha 5\beta 1$ (HH) this fraction increases from 62% to 75% and 80% respectively. This finding indicates that $\alpha 5\beta 1$ -fibronectin interactions produce unexpected and non-trivial changes in aggregate mechanical responses and, presumably, the internal aggregate structures that lead to these responses.

This biphasic shift between liquid and solid behaviors is reflected in another property, namely the relationship between aggregate volume and surface tension. For liquid systems, these two parameters are independent. That is, a small aggregate will produce the same surface tension as a large aggregate: this is a simple representation of the applicability of the Young-LaPlace surface tension relation to simple fluids. In

contrast, elastic solids demonstrate a direct relationship between size and surface tension: in turn this is a result from linear elasticity theory.

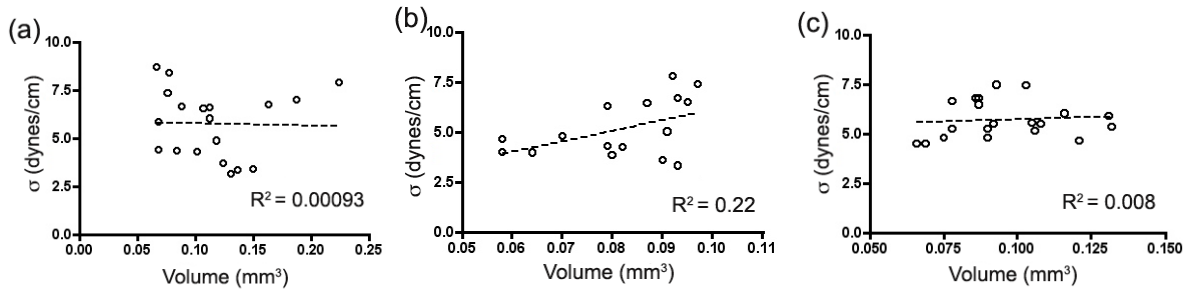


Figure 3-6. Plots of aggregate surface tension vs. aggregate volume. For a true liquid, there should not exist any relation between surface tension and volume. These plots are for aggregates identified as being liquid-like by the method described in Figure 5 (i.e. $\sigma_1/\sigma_2 \approx 1$ despite $F_2/F_1 \neq 1$) using aggregates with (a) CHO- $\alpha 5\beta 1$ (L), (a) CHO- $\alpha 5\beta 1$ (H), and (a) CHO- $\alpha 5\beta 1$ (HH) from data sets, each containing 16 to 20 aggregates. The independence of surface tension on volume, as well as applied load, is a secondary test that helps us discriminate between samples that have true liquid-like properties from those that have more mixed biophysical properties i.e., transitions to viscoelastic-solid like properties.

Figure 3-6 shows a comparison between aggregate volume inferred from cross-sectional area measurements of snapshots (cf. lower panels, figure 3-4) and measured surface tensions, using aggregates selected to behave in liquid-like manners (as evaluated using the method described in figure 3-5) from cell lines CHO- $\alpha 5\beta 1$ (L, H and HH). The surface tension for viscoelastic liquid aggregates is observed to be independent of aggregate volume, as can be inferred from the twin facts that the correlation coefficients of the data shown are very small - indicating that tension is not correlated with volume - and that any correlation that does exist produces a low or zero slope - indicating that tension does not change significantly with volume in any case.

Apparently, as shown in figure 3-5, the fraction of aggregates that behave in a liquid-like manner diminishes and then grows in a biphasic manner as integrin expression is changed from low to moderate to high to very high levels. Notwithstanding the change in this fraction, as shown in figure 3-6, some aggregates retain liquid-like properties over all integrin expression levels tested. In the remaining sections, we will develop methodologies to further explore the implications of these unexpected relations of $\alpha 5\beta 1$ receptor expression on material properties of cell aggregates.

Increasing $\alpha 5\beta 1$ surface receptor affects surface tension in a biphasic manner.

In this section, we investigate the role of $\alpha 5\beta 1$ surface receptor differences and sFn concentrations on aggregate surface tension. As described in the Methods section, we generated aggregates of CHO- $\alpha 5\beta 1$ (L, M, H, and HH) integrin receptor expression in standard tissue culture conditions, and with 300- $\mu\text{g}/\text{ml}$ sFn. It is known that CHO cells secrete small amounts of endogenous fibronectin [41], and since sFn concentrations are expected from figure 3-5 to affect aggregate properties, we assayed the amount of sFn secreted from our cells. For this purpose, we carried out ELISA measurements of the cumulative amount of CHO cells fibronectin secretion over 3 days from 30 hanging drops (10 μl each) at a cell seeding density of 2.5×10^6 cells/ml in fibronectin-depleted media. We found that the cumulative amount of fibronectin secreted over 3 days was below 1 $\mu\text{g}/\text{ml}$ (data not shown). Thus, endogenous levels of CHO cells fibronectin do not contribute significantly to tissue cohesion. This allows us to compare the cohesion of the aggregates as a function of variable $\alpha 5\beta 1$ receptor expression, as shown in table 3-1.

For each aggregate with known integrin receptor expression, we performed double compressions and calculated their corresponding surface tensions (σ). As explained in figure 3-4, tissue liquidity is confirmed through comparison of the ratios of force to the ratios of sigma. As shown in table 3-1, tissue surface tension increases from 5.7 ± 0.3 to 10.4 ± 0.7 dynes/cm for CHO- $\alpha 5\beta 1$ (L) and CHO- $\alpha 5\beta 1$ (M), but a further increase in $\alpha 5\beta 1$ expression to CHO- $\alpha 5\beta 1$ (H) and CHO- $\alpha 5\beta 1$ (HH) results in a paradoxical drop in surface tension to 5.5 ± 0.3 dynes/cm and 5.6 ± 0.16 dynes/cm respectively. These more quantitative data confirm the unexpected trend shown in figure 3-5.

Figure 3-7 is a visual representation of table 3-1, where we plot the surface tension versus $\alpha 5\beta 1$ expression. Beside each datum, we include the percent of aggregates that behave as viscoelastic-liquids, revealing an inverse-relationship between this percent and the measured surface tension. For example, 95% percent of CHO- $\alpha 5\beta 1$ (L) aggregates ($n = 20$) are liquid-like and have an average surface tension of 5.7 ± 0.3 dynes/cm, while only 60% of CHO- $\alpha 5\beta 1$ (M) aggregates ($n = 15$) are liquid-like and have an average surface tension of 10.4 ± 0.7 dynes/cm. However, a subtle increase in number of aggregates with liquid-like properties occurs at CHO- $\alpha 5\beta 1$ (H) and CHO- $\alpha 5\beta 1$ (HH), which exhibit 75% ($n = 16$) and 80% ($n = 20$) liquid-like behaviors with surface tensions of 5.5 ± 0.3 and 5.6 ± 0.2 dynes/cm respectively.

Table 3-1. Aggregate surface tension measurements as a function of $\alpha 5\beta 1$ receptor density.

σ_1 and σ_2 represent the respective surface tensions for first and second compressions, and $\sigma_{1,2}$ is the average of σ_1 and σ_2 . We also validated the simple liquid nature of these aggregates by comparing the ratio of surface tension (σ_2/σ_1) to the ratio of applied forces (F_2/F_1). These

aggregates behave as simple liquids, since $F2/F1$ is very significantly different from σ_2/σ_1 (***) indicates that $p < 0.05$).

$\alpha 5\beta 1$ Receptor Expression	σ_1 (dynes/cm)	σ_2 (dynes/cm)	σ_2 and σ_1	$\sigma_{1,2}$ (dynes/cm)	σ_2/σ_1	F2/F1	σ_2/σ_1 vs. F2/F1 ($p < 0.05$)
$\alpha 5\beta 1$ (L)	5.5 +/- 0.4	5.8 +/- 0.4	P = 0.4	5.7 +/- 0.3	1.1 +/- 0.03	1.5 +/- 0.03	***
$\alpha 5\beta 1$ (M)	10.4 +/- 1.0	10.6 +/- 1.0	P = 0.8	10.4 +/- 0.7	1.0 +/- 0.02	1.5 +/- 0.06	***
$\alpha 5\beta 1$ (H)	5.3 +/- 0.4	5.8 +/- 0.4	P = 0.2	5.5 +/- 0.3	1.1 +/- 0.03	1.5 +/- 0.02	***
$\alpha 5\beta 1$ (HH)	5.4 +/- 0.2	5.7 +/- 0.2	P = 0.3	5.6 +/- 0.16	1.1 +/- 0.02	1.5 +/- 0.01	***

From these data, we can define two states of aggregate properties: a high surface tension state corresponding to aggregates with high tissue cohesion and high fraction of aggregates with viscoelastic-solid properties, and low surface tension state corresponding to a high fraction of aggregates with viscoelastic-liquid properties. This behavior is to be distinguished from cadherin-mediated cohesion, which is known to increase linearly with cadherin receptor expression [1]. These results reveal that whether measured in terms of fraction of liquid-like aggregates or surface tension, there is a biphasic transition of aggregates from viscoelastic-liquid to viscoelastic-solid back to viscoelastic-liquid as $\alpha 5\beta 1$ receptor density is increased.

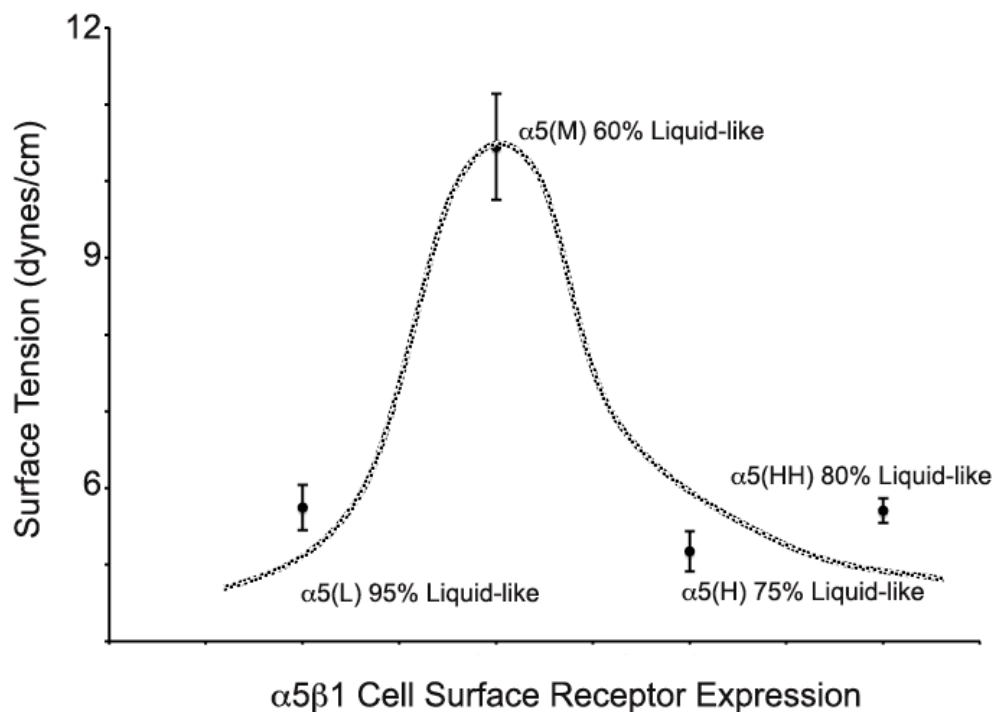


Figure 3-7. Biphasic behavior of tissue surface tension. Plot of data from table 3-1, showing values of surface tension versus unscaled levels of $\alpha 5\beta 1$ receptor expression. The hatched line is not quantitative, but is included to aid the eye. This graph shows the “biphasic” nature of $\alpha 5\beta 1$ -fibronectin cell adhesive interactions. Surface tension initially increases with $\alpha 5\beta 1$ receptor expression to a maximum level, but then abruptly decreases with continued increases in the integrin expression. The graph also includes the percent of aggregates with liquid-like properties as the integrin receptor expression is varied.

$\alpha 5\beta 1$ expression and soluble fibronectin concentration influence aggregate compaction

The dimeric form of soluble fibronectin interacts with the $\alpha 5\beta 1$ integrin receptor to initiate fibronectin matrix formation [26]. This step initiates a series of events, consisting of focal adhesion formation and cytoskeletal coupling, that ultimately lead to fibronectin fiber extension and matrix deposition [42]. Little is known about the effect of

integrin $\alpha 5 \beta 1$ receptor profile on the aggregation properties of cells. As shown in table 3-1 and figure 3-5, aggregate properties depend in a biphasic way on integrin receptor expression. In this section, we examine the kinetics of how matrix deposition occurs during the formation of our aggregates.

In our in vitro system, a 10- μ l hanging drop at a cell seeding density of 2.5×10^6 cells/ml contains 25,000 cells. During the formation of an aggregate, the volume occupied by cells and matrix can be evaluated by visual inspection, revealing that aggregates typically ‘compact’, or reduce the cross-sectional area of the visible aggregate. Evaluating the compaction of aggregates over time thus provides a way of evaluating how cohesion between cells and the ECM cause an overall aggregate contraction and affect aggregate mechanical properties. This method is chiefly qualitative, but it provides an easily obtainable view into the kinetics underlying the effects of cellular adhesion on aggregate assembly [43].

Resulting plots of aggregate cross-sectional area (‘compaction’) over time are shown in figure 3-8 for the four cell lines previously described. In panel (a), we show that compaction of our 25,000-cell aggregates decreases monotonically over time. The compaction profiles displayed have three characteristic features: a) the compaction at day 2 is much lower for aggregates $\alpha 5 \beta 1$ (L and M) than for $\alpha 5 \beta 1$ (H and HH), with approximately a 2-fold difference in compaction between the two groups, b) by day 3, all aggregates have compacted to comparable values, and c) thereafter, compactions profiles level off for all cell lines, reaching similar aggregate size in all cases.

To unveil kinetics effects, we compare these results with a second set of experiments using 50,000-cell aggregates. This set of experiments was chosen to

determine whether the higher cell number - in the same medium as before - might deplete the available sFn over time. These results, shown in panel (b) of figure 3-8, reveal that all cell lines compact similarly on days 2 and 3, however on day 4, the $\alpha 5\beta 1(\text{HH})$ preparation increases its compaction, and on day 5, both $\alpha 5\beta 1(\text{H})$ and $\alpha 5\beta 1(\text{HH})$ aggregates grow or de-compact. These results are consistent with the hypothesis that higher integrin expression results in increased consumption of available sFn, causing the highest expressing cell lines to deplete the available sFn, producing aggregates that first shrink and then grow.

We can examine this behavior through a visual comparison between aggregates over time and after 5 days, as shown in figure 3-9. In this figure, we display a comparison between two representative cases of these unexpected dynamics using $\alpha 5\beta 1(\text{M})$ and $\alpha 5\beta 1(\text{HH})$ groups in 25,000 and 50,000 cell aggregates. Figure 3-9(a) shows that $\alpha 5\beta 1(\text{M})$ aggregates compact monotonically for both aggregate cell numbers tested, whereas figure 3-9(b) demonstrates that aggregate cell number has a dramatic effect on the time-dependent compaction dynamics of the $\alpha 5\beta 1(\text{HH})$ clone. Thus the $\alpha 5\beta 1(\text{HH})$ 50,000 cell aggregates de-compact over time, whereas the 25,000 cell aggregates stay compacted, even though the surface integrin receptor expression per cell is held fixed. In light of these results, we set out to determine whether depletion of sFn in the aggregate microenvironment is specifically responsible for the changes in surface area seen.

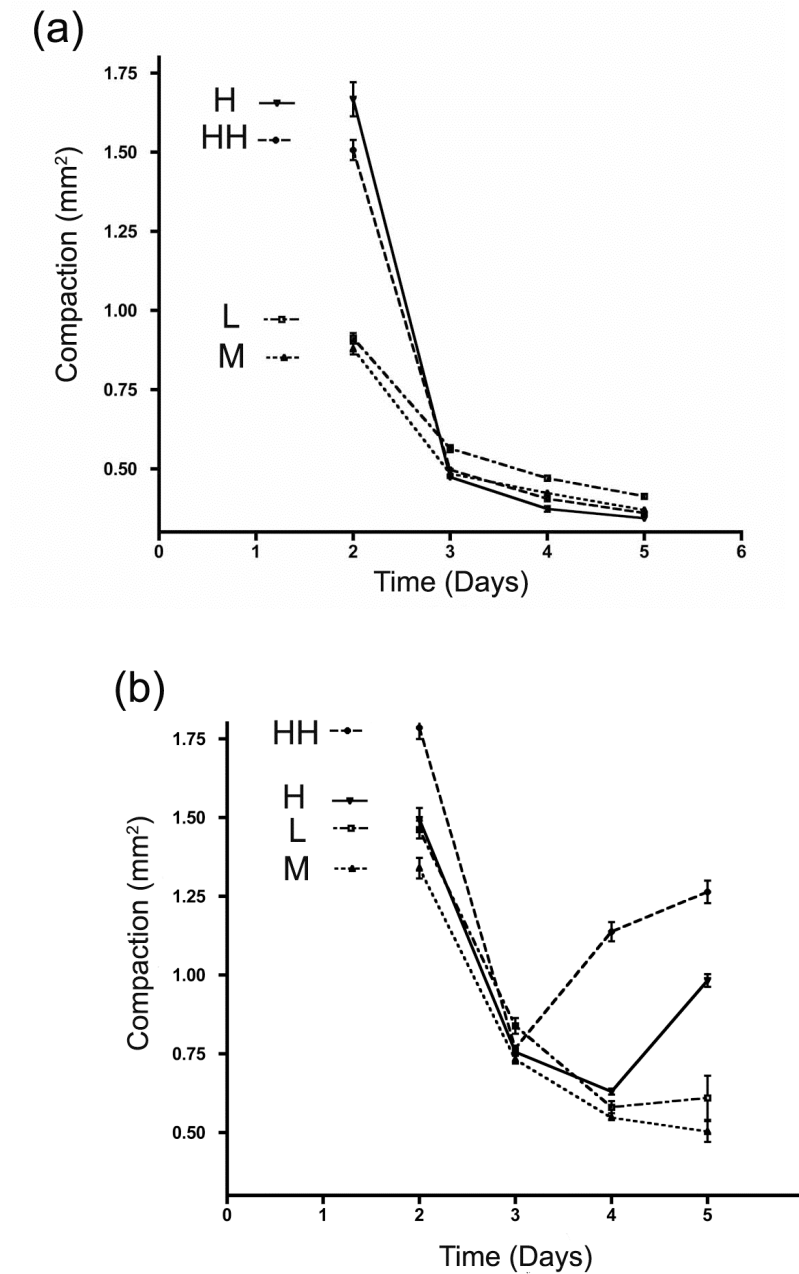


Figure 3-8. Aggregation assays as a function of initial cell seeding density and constant tissue culture media. Here, aggregates at a cell seeding density of 25,000 (Figure 3-8(a)) and 50,000 (Figure 3-8(b)) for the same $\alpha 5\beta 1$ integrin expression. Measurements were initiated on day 2 and repeated daily up to day 5. Each data point represents 10 aggregates per time point for each level of integrin receptor expression.

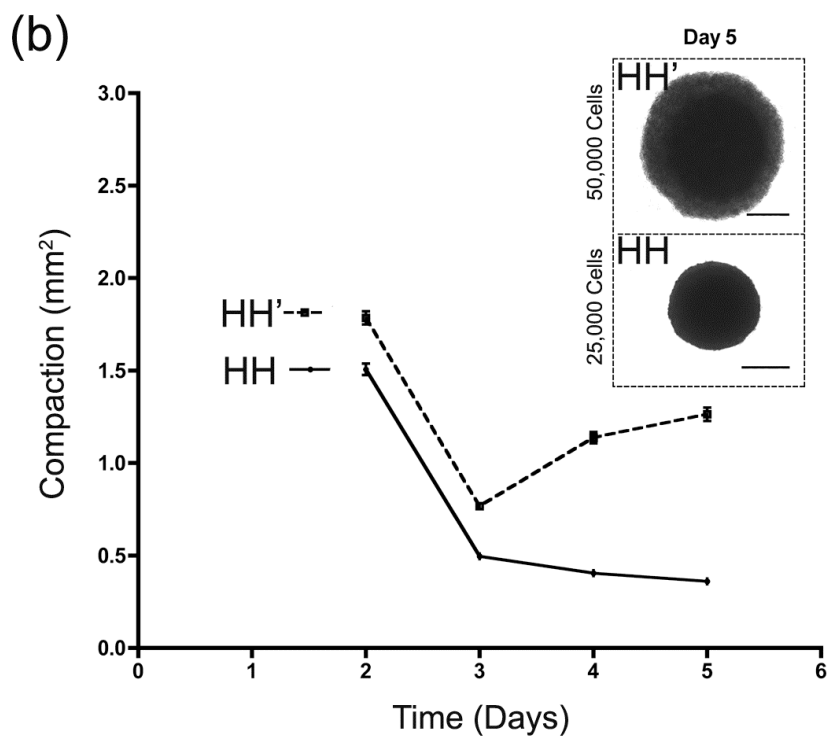
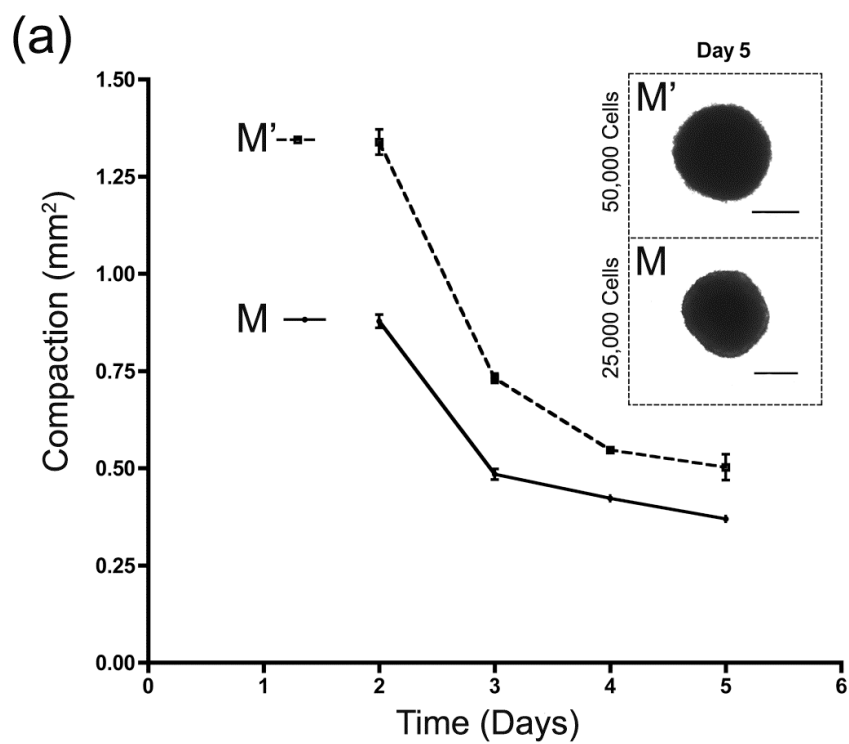


Figure 3-9. Cell aggregation as a function of cell seeding density and $\alpha 5\beta 1$ receptor expression. Cell aggregation profiles of approximately 25,000 or 50,000 cells as a function of two integrin surface receptor expression, $\alpha 5\beta 1$ (M) and $\alpha 5\beta 1$ (HH). Panel (a) shows $\alpha 5\beta 1$ (M) receptor expression. Both curves have the same dynamics of change in aggregation. Panel (b) shows the response of $\alpha 5\beta 1$ (HH) aggregates at the same cell seeding density and tissue culture conditions as panel (a). The 50,000 cell aggregates exhibit re-enlargement (dotted line) whereas the 25,000 cell aggregates do not (solid line). The insets are microphotographs taken at day 5. Each picture represents the average size at day 5. Scale bar is 0.4 mm.

The effect of $\alpha 5\beta 1$ integrin receptor expression on sFn concentration and insoluble Fn matrix

The $\alpha 5\beta 1$ integrin receptor requires the dimeric form of soluble fibronectin to initiate fibronectin fiber extension and matrix formation [42]. The polymerization process of soluble Fn dimers into an extended matrix of fibers is the result of positive factors such as fibronectin dimer elastic properties [44]. The ability to stretch allows fibronectin dimers to exposure “cryptic” polymerization sites that enhance fibronectin fiber extension [15]. The kinetics of active fibronectin polymerization depend on the sFn concentration and the rate of sFn utilization, and we therefore measured these parameters as a function of $\alpha 5\beta 1$ receptor expression, following the same cell seeding densities of our TST measurements (approximately 25,000 cells per aggregate).

To this end, we measured the concentration of sFn over time (days), as cells aggregated as hanging drops in tissue culture medium with 30- μ g/ml sFn. (Refer to Methods). We measured the amount of soluble fibronectin at days 3, 4, and 5. We

reiterate that the sFn concentration at each time-point is the result of the metabolic activity of cell surface $\alpha 5\beta 1$ receptors, thus, we expect to see a decline in available sFn as time evolves and as receptor expression increases.

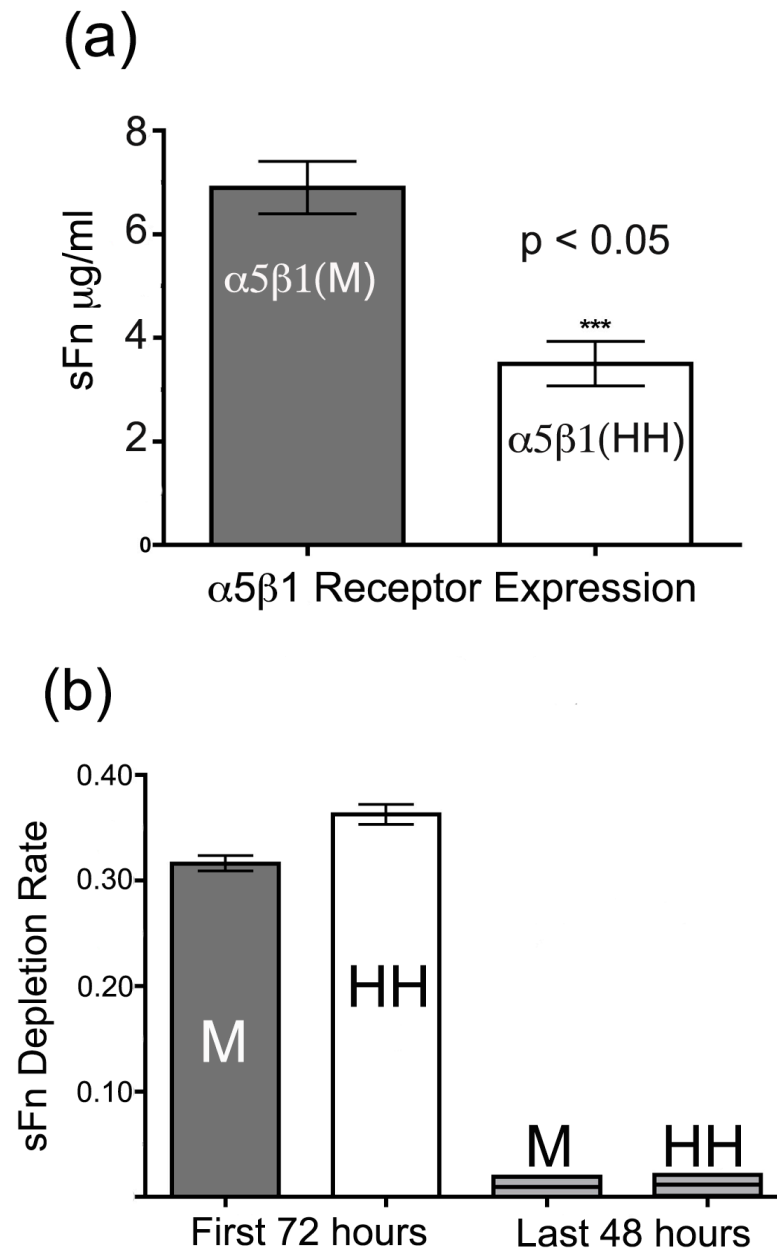


Figure 3- 10. sFn concentration and rate of sFn utilization during aggregation of CHO- $\alpha 5\beta 1$ (M and HH). Panel (a) shows the effect of $\alpha 5\beta 1$ receptor expression (25,000-cell aggregate) utilization after 3 days of cell aggregation in hanging drop. Differences in $\alpha 5\beta 1$ receptor expression cause significant changes to sFn concentrations in the microenvironment of aggregating cells. Panel (b) shows a biphasic consumption rate of soluble fibronectin depletion. The depletion rate for the first 72 hours is again presented on the left. The sFn rate of utilization on the last 2 days of cell culture is presented on the right side. Clearly, the rate of depletion slows during the last 48 hours and no longer correlates with the level of $\alpha 5\beta 1$ receptor expression.

In figure 3-10 (a-b) we compared the effect of $\alpha 5\beta 1$ expression (from M to HH) on sFn concentration and rates of sFn utilization. Panel (a) is a comparison of the average sFn concentration between 3 and 5 days. As shown in figure 3-10(a), the CHO- $\alpha 5\beta 1$ (M) preparation has twice the sFn concentration ($P = 0.0005$) of the CHO- $\alpha 5\beta 1$ (HH) preparation. In panel (b) we compared, for the same levels of integrin expression, the rate of sFn utilization ($\mu\text{g/ml}\cdot\text{hr}$) between $\alpha 5\beta 1$ (M) and $\alpha 5\beta 1$ (HH) levels of integrin expression. The rate of soluble sFn utilization has two time-scales: for the first 72 hours, there is high rate of sFn utilization of these cells, which correlates with aggregate compaction as seen in figure 3-8(a). For the last 48 hours, the rate of sFn utilization drops and its concentration does not change, which also correlates with smaller changes in aggregate compaction after 3 days in figure 3-8(a). We found that cells with $\alpha 5\beta 1$ (HH) level of expression utilize more sFn, with a value of $0.36 \pm 0.01 \mu\text{g/ml}\cdot\text{hr}$ when compared to the rate of utilization of $\alpha 5\beta 1$ (M), with a sFn rate of $0.30 \pm 0.01 \mu\text{g/ml}\cdot\text{hr}$. Therefore, we expect these aggregates to have marked differences in the insoluble matrix. We next demonstrate that differences in insoluble fibronectin matrix do exist by comparing immunostained fresh tissue sections of CHO- $\alpha 5\beta 1$ (M and HH)

aggregates.

Figure 3-11 depicts immunostained frozen sections of aggregates containing 25,000 cells of $\alpha 5\beta 1$ (M) and $\alpha 5\beta 1$ (HH) surface receptor expression. Fibronectin matrix is stained green and nuclei are stained blue (see Methods). In panel (a) we see CHO- $\alpha 5\beta 1$ (M) aggregates, in which the fibronectin matrix is dense and in close association with cell nuclei. Tissue sections of CHO- $\alpha 5\beta 1$ (HH) aggregates also appear to contain a fibrous matrix, but the matrix does not seem to be either as dense or as closely associated with cells (Panel (b)). This indicates that CHO- $\alpha 5\beta 1$ (HH) cells produce a sparser matrix than CHO- $\alpha 5\beta 1$ (M) cells, despite the increased consumption of sFn (cf. figure 3-10(a)) by the former cells. This is consistent with the hypothesis that the more rapid sFn polymerization kinetics of CHO- $\alpha 5\beta 1$ (HH) cells lead to the localized depletion of sFn, which interferes with the creation of a global, interconnected ECM.

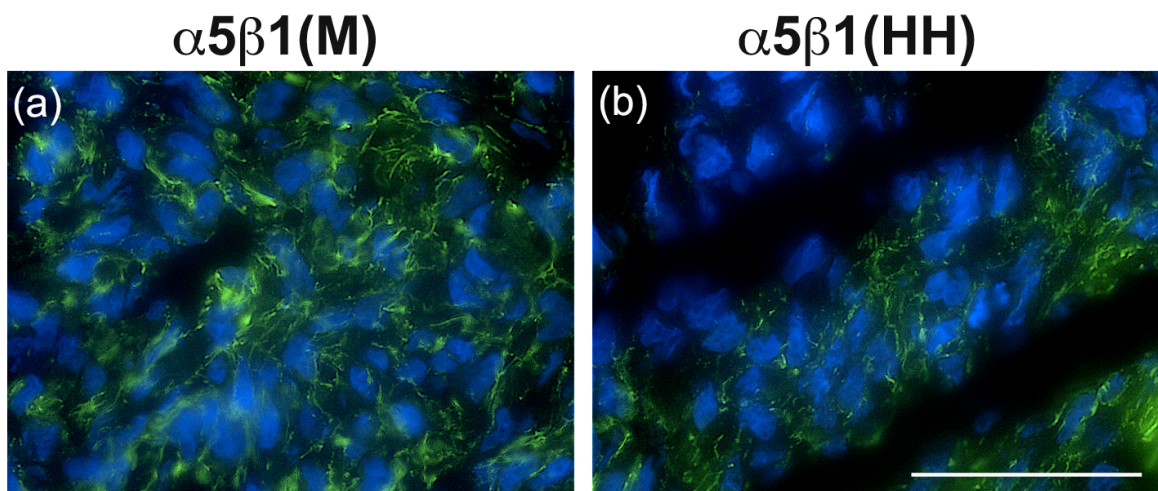


Figure 3-11. Fresh tissue aggregate immunostaining. Representative immunostained tissue sections from whole 25,000-cell aggregates as a function of $\alpha 5\beta 1$ (M and HH) receptor expression. These aggregates were cut on a cryostat at day 3 following regular hanging drop

methods. Each tissue section is 5- μm thick. The green signal identifies the insoluble matrix holding cells together and the blue signal identifies the cell nuclei. The scale-bar is 50- μm . Exemplars shown are typical of $\alpha 5\beta 1(\text{M})$ and $\alpha 5\beta 1(\text{HH})$ sections (2 pairs of sections from different slides were compared in the course of this work); variation in actual Fn connectivity occurs from sample to sample. However, the relative qualitative differences are maintained.

The effect of N-cadherin on $\alpha 5\beta 1$ -Fibronectin interactions

The effects of cell-ECM and cell-cell interactions are typically measured independently. However it is expected that these systems would interact during development, cancer dynamics, and tissue regeneration. Notably, during epithelial to mesenchymal transitions (EMT), the expression of N-cad on the cell surface marks the transition to a more motile cellular state, and possible interactions between cadherin-based and integrin-based adhesion mechanisms that may affect cellular motility are therefore of considerable interest.

To test the combined effect of N-cad and $\alpha 5\beta 1$ integrin receptor on tissue cohesion, we generated CHO cell lines that expressed both $\alpha 5\beta 1$ and N-cadherin as described in figure 3-2. We selected CHO- $\alpha 5\beta 1$ /N-cad clones that matched $\alpha 5\beta 1$ levels seen in $\alpha 5\beta 1(\text{M})$ and $\alpha 5\beta 1(\text{HH})$ cell lines. We determined the level of N-cad expression in these CHO- $\alpha 5\beta 1$ /N-cad cell lines (cf. Figure 3-2(c)) to confirm that the level of N-cad expression is independent of $\alpha 5\beta 1$ expression.

We then measured tissue surface tensions as previously described for CHO- $\alpha 5\beta 1(\text{M})$ /N-cad and CHO- $\alpha 5\beta 1(\text{HH})$ /N-cad. Figure 3-12 depicts the relation between aggregate volume (mm^3) and surface tension (σ) for $\alpha 5\beta 1(\text{M})$ /N-cad aggregates (figure

3-12(a)) and $\alpha 5\beta 1$ (HH)/N-cad aggregates (figure 3-12(b)). As described for $\alpha 5\beta 1$ (L, H, and HH) aggregates, the surface tension values of $\alpha 5\beta 1$ (M)/N-cad and $\alpha 5\beta 1$ (HH)/N-cad do not depend on aggregate volume. This suggest that these aggregates have liquid-like properties [37], as we have described previously.

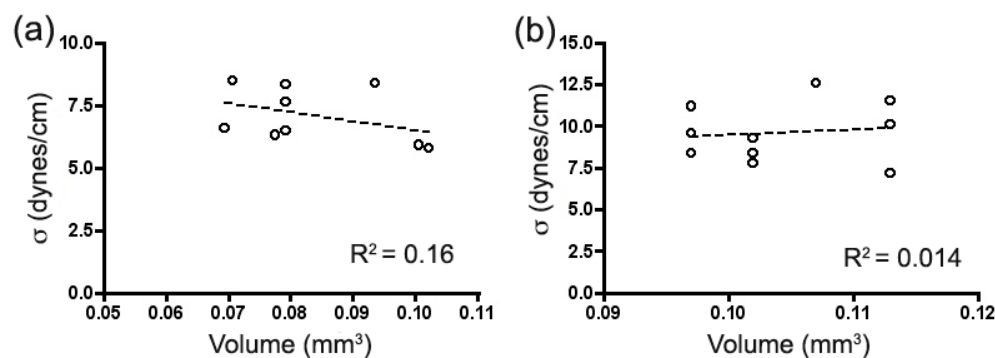


Figure 3-12. Plots of aggregate surface tension vs. aggregate volume. These plots of surface tension vs. aggregate volume shows a low coefficient of correlation (R^2) between surface tension and volume for aggregates expressing both $\alpha 5\beta 1$ and N-cad receptors. The surface tension data shown are the result of 10 double compressions for each cell line expressing $\alpha 5\beta 1$ (M)/N-cad (panel (a)) and $\alpha 5\beta 1$ (HH)/N-cad (panel (b)).

Table 3-2 shows surface tension measurements after double compressions on 10 aggregates from each $\alpha 5\beta 1$ /Ncad receptor expression. We find that these aggregates behave as simple liquids both by the comparisons shown in figure 3-12 and by the statistically significant difference between the ratio of sigma (σ_2/σ_1) and the ratio of force F_2/F_1 ($p < 0.0001$). Thus N-cadherin expression appears to engender changes in aggregate mechanical properties compared to $\alpha 5\beta 1$ integrin alone.

Table 3- 2. Aggregate surface tension measurements as a function of $\alpha 5\beta 1$ receptor and N-cad expression. Surface tension values measured after double-compressions of single aggregates of $\alpha 5\beta 1$ (M or HH)/N-cad. σ_1 and σ_2 represent the respective surface tensions from each compression, and $\sigma_{1,2}$ is the average. We use $\sigma_{1,2}$ to make comparisons of surface tension values of $\alpha 5\beta 1$ (M)/N-cad and $\alpha 5\beta 1$ (HH)/N-cad. We validate the simple liquid nature of these aggregates by comparing the ratio of surface tension (σ_2/σ_1) to the ratio of force applied (F_2/F_1). These aggregates behave as viscoelastic liquids since the ratio of force is significantly different from the ratio of sigma σ_2/σ_1 ($p < 0.0001$).

Dual $\alpha 5\beta 1$ /N-cad Receptor Expression	σ_1 (dynes/cm)	σ_2 (dynes/cm)	$\sigma_{1,2}$ (dynes/cm)	σ_2/σ_1	F2/F1	σ_2/σ_1 vs. F2/F1 ($p < 0.0001$)
$\alpha 5\beta 1$ (M)/N-cad	7.0 +/- 0.5	8.0 +/- 0.4	7.4 +/- 0.4	1.16 +/- 0.06	1.5 +/- 0.04	***
$\alpha 5\beta 1$ (HH)/N-cad	9.5 +/- 0.6	9.7 +/- 0.5	9.6 +/- 0.4	1.0 +/- 0.05	1.5 +/- 0.02	***

For example, the frequency of aggregates with viscoelastic-solid properties was only 10% for aggregates co-expressing $\alpha 5\beta 1$ integrin and N-cadherin receptors for comparable levels of integrin expression. We observed that the incidence of viscoelastic-liquid aggregates increases when N-cad is present in this cells lines, as $\alpha 5\beta 1$ (M) and $\alpha 5\beta 1$ (HH) are compared to $\alpha 5\beta 1$ (M)/N-cad and $\alpha 5\beta 1$ (HH)/N-cad respectively, as shown on table 3-3. Additionally, there are significant changes in the values of tissue surface tension. At $\alpha 5\beta 1$ (HH) receptor expression, N-cad increases the cohesion without reducing the fraction of liquid-like aggregates (% liquidity) of the $\alpha 5\beta 1$ (HH)/N-cad data set. As for the $\alpha 5\beta 1$ (M)/N-cad cells, N-cad increased the percent liquidity of these aggregates as compared with the $\alpha 5\beta 1$ (M) aggregates. We will elaborate more about these trends on the discussion section.

Table 3- 3. Surface tension values and percent liquidity. This comparative table allows us to see an interesting trend. N-cad-mediated adhesion; N-cad increases the fraction of aggregates with liquid-like properties in the presence of $\alpha 5\beta 1$ -fibronectin adhesive interactions.

Type of Adhesive System	$\sigma_{1,2}$ (dynes/cm)	% Liquidity
$\alpha 5\beta 1$ (M)	10.4 +/- 0.7	62%
$\alpha 5\beta 1$ (M)/N-cad	7.4 +/- 0.4	90%
$\alpha 5\beta 1$ (HH)	5.6 +/- 0.16	85%
$\alpha 5\beta 1$ (HH)/N-cad	9.6 +/- 0.4	90%

These data demonstrate that N-cad contributes to tissue mechanical properties and the following conclusions are made:

- N-cadherin increases the liquid-like properties of aggregates that interact through $\alpha 5\beta 1$ -fibronectin. For example, $\alpha 5\beta 1$ (M) aggregates have transitional properties between those of viscoelastic-liquid and viscoelastic solid. Adding N-cad into the cell surface of $\alpha 5\beta 1$ (M) cells decreases the likelihood of producing viscoelastic-solid aggregates.
- N-cad has different effects depending on the properties of cell-ECM interactions. For $\alpha 5\beta 1$ (M), N-cad lowers the value of surface tension from $(10.4 \pm 0.7$ to 7.4 ± 0.4 dynes/cm). For “softer” aggregates of $\alpha 5\beta 1$ (HH), the same level of N-cad increases the surface tension from 5.6 ± 0.2 to 9.6 ± 0.4 dynes/cm without changing causing transition to viscoelastic-solid properties. (Compare surface tension and percent liquidity between $\alpha 5\beta 1$ (HH)/N-cad and $\alpha 5\beta 1$ (M) aggregates.

The influence of $\alpha 5\beta 1$ and $\alpha 5\beta 1/Ncad$ on cell rearrangement

Embryonic tissues governed by cadherin-mediated adhesion are documented to rearrange according to their relative surface tension values such that populations of cells with higher surface tension always become enveloped by ones with lower surface tension. This rearrangement behavior follows strict tissue transitivity rules and has been experimentally verified on cells lines engineered to express different levels of cadherins [1, 29]. Here we ask whether differences in the $\alpha 5\beta 1$ receptor expression also result in segregation of cell populations by surface tension. We mixed $\alpha 5\beta 1(M)$ and $\alpha 5\beta 1(HH)$ cell lines at a 1:1 ratio and then examined the effect of sFn concentration. (See Methods for detailed description). In figure 16(a) we display a characteristic aggregate obtained from cells maintained in standard tissue culture conditions. The cell populations do not segregate from one another and remain intermixed after 3 days in hanging drop. However, the cells do compact into a sheet-like structure. Although sheet-like structure formation has been previously described for engineered CHO-cells [43], formation of sheets for fully functional $\alpha 5\beta 1$ receptor is a new observation to this work. Panel (b) shows an aggregate obtained using the same ratio of cells in media supplemented with sFn at a concentration of 100-mg/ml. At higher sFn levels, the cells remain intermixed, however their overall volume decreases for the same time in hanging drop as compared with panel (a) (note the differences in scale bars).

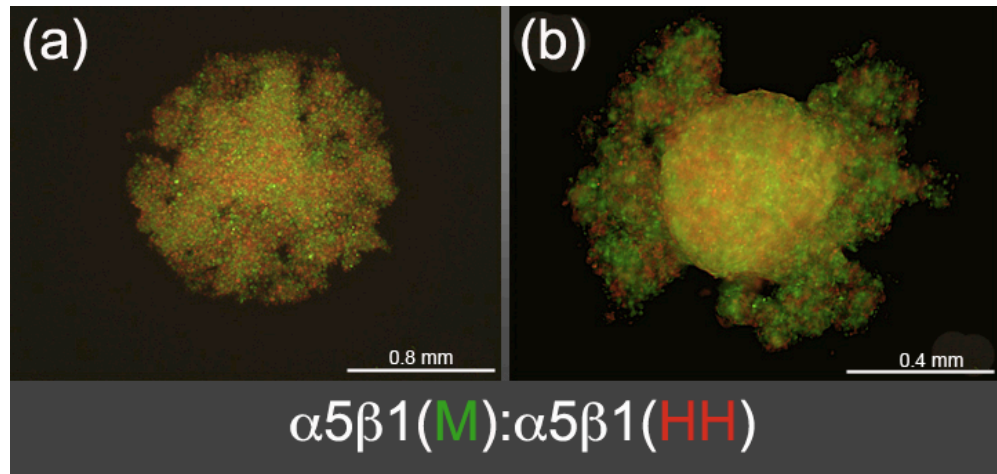


Figure 3-13. Lack of rearrangement of cells expressing different levels of $\alpha 5\beta 1$ integrin receptor. $\alpha 5\beta 1(M)$ and $\alpha 5\beta 1(HH)$ have surface tension values of 10.4 ± 0.7 and 5.6 ± 0.2 dynes/cm respectively. If these surface tensions were cadherin-mediated they would drive cellular segregation as documented previously in the literature. $\alpha 5\beta 1(M)$ and $\alpha 5\beta 1(HH)$ cells are labeled with green and red-intercalating dyes respectively. Cells in a 1:1 ratio are mixed (a) in standard tissue culture conditions or (b) with the addition of 100- μ g/ml soluble fibronectin. Changes occur in cellular compaction rather than degree of segregation. Note that scale-bars are 0.8 and 0.4 mm respectively.

Evidently, cells expressing different levels of $\alpha 5\beta 1$ integrin, and so producing significantly different surface tension values, did not sort out as they would for cadherin-mediated adhesion. We therefore tested whether $\alpha 5\beta 1$ integrin could confer sorting behavior when different levels of $\alpha 5\beta 1$ expression levels are mixed with the parent cell line (P3). This experiment is germane because CHO-P3 cells lack the $\alpha 5$ integrin receptor, and do not bind to the ECM as do CHO- $\alpha 5\beta 1$ cells, thus the inclusion of CHO-P3 cells allows for the presence of two independent cell types that interact differently with the ECM (described further shortly). Figure 3-14 shows the different rearrangement

behaviors of $\alpha 5\beta 1$ (M and HH) cells mixed with CHO-P3. We followed the same conditions as the rearrangement experiment described in figure 3-13. The cells were resuspended in standard tissue culture media, 30-mg/ml and 100-mg/ml sFn in culture media. The top panel shows the rearrangement behavior of CHO- $\alpha 5\beta 1$ (M)(red):CHO-P3(green) cells. Here mixed aggregates exhibited the formation of small clusters of red CHO- $\alpha 5\beta 1$ (M) cells within a field of green CHO-P3 cells. This clustering seems to increase as the amount of soluble fibronectin in the media increases from top left to top right. The bottom panel represents rearrangement of mixtures of CHO- $\alpha 5\beta 1$ (HH)(red):CHO-P3(green) cells. At low soluble fibronectin concentration, the $\alpha 5\beta 1$ (HH)(red) population appears to adopt an external position (peripheral segregation) with respect to the P3 population(green). This configuration is also seen in mixtures of $\alpha 5\beta 1$ (H and L):CHO-P3 cells (Data not shown) and represents a surprising finding in our in vitro system. As the concentration of fibronectin increases to 30 and 100 μ g/ml, we now see a reversal of the original pattern of segregation. Now $\alpha 5\beta 1$ (HH) cells occupy a more central location and the P3 population surrounds them. We also found at higher levels of soluble fibronectin that patterns were quite dynamic with formation of interconnected clusters and other structures shown in figure 3-15.

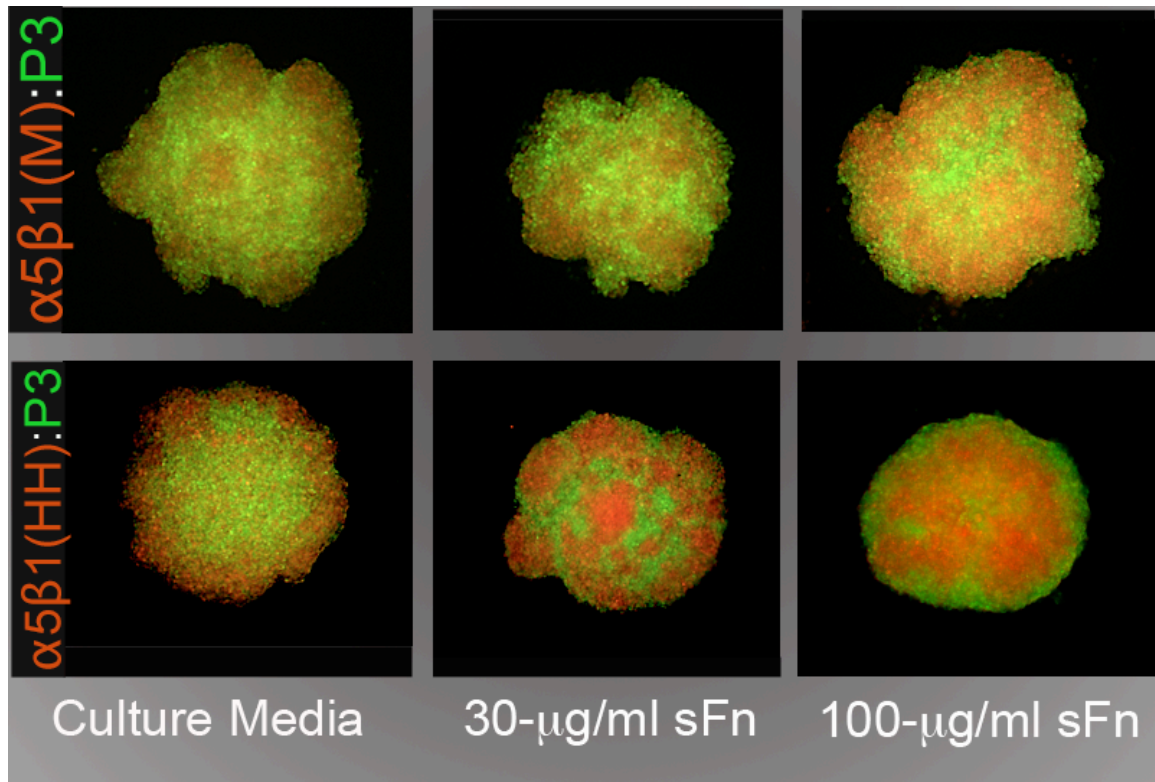


Figure 3- 14. Rearrangement dynamics of $\alpha 5\beta 1$ cells and its parent cell line, P3(green).

Culture conditions were the same as data presented in figure 13. Left to right: standard tissue culture media, 30 μ g/ml, and 100 μ g/ml. Each photomicrograph is representative of a set of 10 hanging drops. Rearrangement of $\alpha 5\beta 1$ cells (red) and CHO-P3(green) labeled with a membrane intercalating dye. For full description refer to Method section.

We conclude that fibronectin-driven rearrangement requires tissue liquidity (as for cadherins) but lower heterotypic adhesive relationships. For example, mixing two populations of cells with the ability to make a matrix would increase both their cohesive and cross-adhesive strengths since these properties are driven by a common feature: the ability to form a fibronectin matrix. However, reducing the adhesive relations by mixing with CHO-P3 (cells unable to make a matrix in the presence of sFn) allows for the rearrangement of cell populations with viscoelastic-liquid properties.

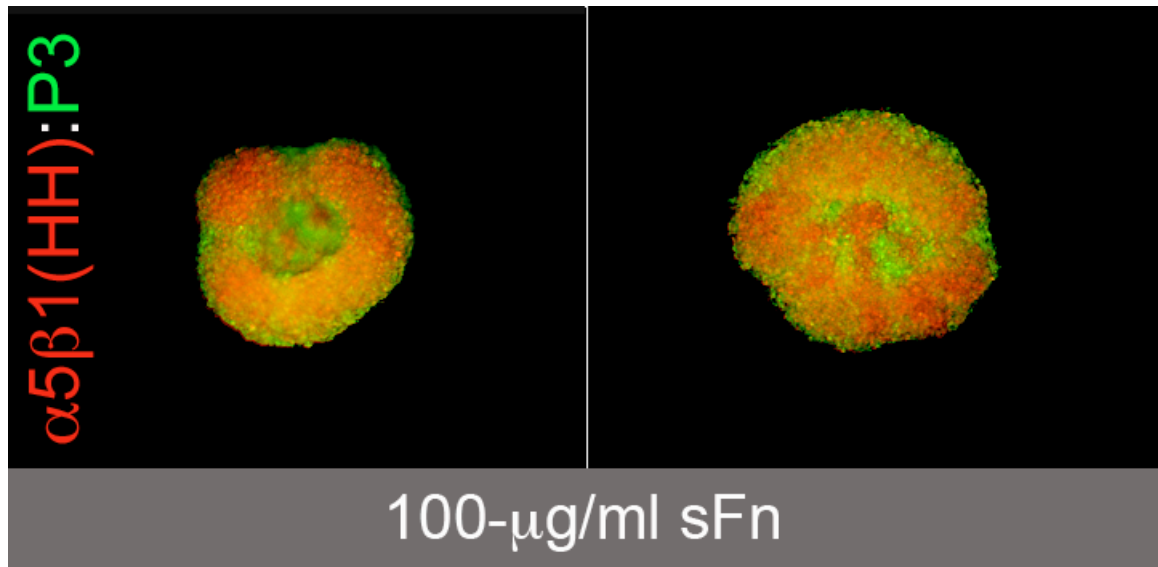


Figure 3- 15. Exotic rearrangement dynamics of $\alpha 5\beta 1(\text{HH})$. Most rearrangement at day 3 for lower concentration of sFn seldom gives different structures. One could get in a set of 10 aggregates the same final rearrangement as the case of rearrangements in regular culture media. However, we found that at high soluble fibronectin $\geq 100\text{-mg/ml}$ structures differ considerably, both in terms of rearrangement and final aggregate structure. Here is a mixture of $\alpha 5\beta 1(\text{HH})(\text{red}):P3(\text{green})$ interacting at an initial sFn concentration of $100\text{-}\mu\text{g/ml}$.

We demonstrated that co-expressing N-cad and $\alpha 5\beta 1$ -integrin affects cohesion and enhances tissue liquidity. Therefore, we next assess the rearrangement behavior of CHO- $\alpha 5\beta 1(\text{M}$ and $\text{HH})/\text{Ncad}$ in heterogeneous mixtures with CHO-P3.

Cells expressing dual $\alpha 5\beta 1$ and N-cad showed different rearrangement dynamics than $\alpha 5\beta 1$ cells in heterogeneous mixtures with CHO-P3. Bottom panel, in standard tissue culture medium, $\alpha 5\beta 1(\text{HH})/\text{N-cad}$ cells adopt a more internal position compared to cells expressing a similar amount of $\alpha 5\beta 1$ integrin receptor but no N-cad (Compare figures 14 and 16). This represents a new morphogenetic transition, from peripherally segregating $\alpha 5\beta 1(\text{HH})$ cells to internally segregating $\alpha 5\beta 1(\text{HH})/\text{N-cad}$ cells, that appears

to depend on the interplay between $\alpha 5\beta 1$ and N-cad. Further Increase of soluble fibronectin causes these cells to internalize and form metastable cohesive clusters.

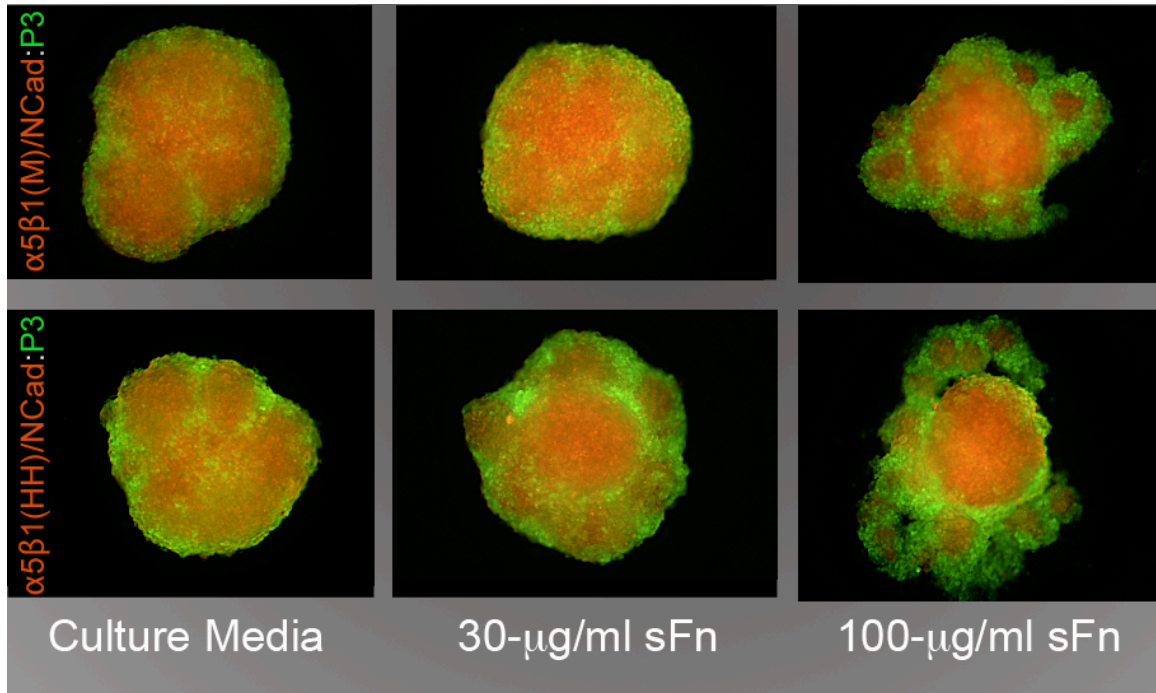


Figure 3- 16. Rearrangement dynamics of $\alpha 5\beta 1$ /N-cad cells with CHO-P3 cells. For this rearrangement assay, we follow the same conditions as in figure 14. Top panel $\alpha 5\beta 1$ (M)/N-cad(red):P3(green). Bottom panel $\alpha 5\beta 1$ (HH)/N-cad(red):P3(green). We incubate these cell suspension at increasing sFn concentration.

As the sFn increases to 100- μ g/ml soluble fibronectin, $\alpha 5\beta 1$ -clusters dislodged from the main continuous CHO-P3 population. This suggests a relative reduction of cross-adhesion due to an increase in aggregate cohesion within the $\alpha 5\beta 1$ /Ncad population. Top panel, we have the interaction of $\alpha 5\beta 1$ (M)/N-cad and CHO-P3 heterogeneous mixtures. The interesting feature about the rearrangement dynamic at regular tissue culture is the internalization of $\alpha 5\beta 1$ (M)/N-cad cells relative to CHO-P3. This is a surprising fact because, comparison of the dynamics on this figure with the dynamics of $\alpha 5\beta 1$ (M):CHO-

P3 in figure 3-14 reveals another important difference between cadherin-mediated and integrin-mediated adhesion. We show here that the internal segregation of $\alpha 5\beta 1(M)/N$ -cad and intermixing of $\alpha 5\beta 1(M)$, for the same culture conditions, correlate with tissue liquidity on the integrin expressing cells (Table 3). Thus, in our in vitro system N-cad has the potential to cause change in already prescribed cell-ECM adhesive relations. This further impacts tissue mechanical properties and cellular rearrangement.

Discussion

Cellular aggregation and segregation are features that define the ability of populations of cells to form multi-layered structures. Many morphogenetic processes require interaction between different cell types, particularly during the compartmentalization of the embryonic layers and subsequent organogenesis. Adhesion receptors on cell surfaces play a crucial role in the force generation and structure formation during cellular assembly. The activity and number of these receptors are in turn regulated by cell-cell and cell-substrate adhesion.

Cadherins are well studied and have been demonstrated to confer both the ability to regulate tissue cohesion and to drive rearrangement simply by varying receptor density between groups of cells. On the other hand, cell-ECM interactions are defined principally from the perspective of effects on the migration of cells seeded on planar surfaces. Studies of cell migration have elucidated important behaviors such as focal adhesion dynamics, clustering of membrane receptors, and cell-substrate relations governed by focal adhesions, among other complex effects on single cells, however these studies lack data on the assembly of multi-cellular aggregates. Given that cells generally express both cadherin and integrins, in this chapter we have investigated whether $\alpha 5\beta 1$

integrin could also provide a mechanism whereby differences in expression patterns could drive cell rearrangement and change tissue properties. Our work has been both qualitative - revealing microstructures involved in cellular aggregation dominated by cell-ECM interactions - and quantitative - using a variety of biochemical assays as well as tissue cohesion measurements to quantify of receptor-mediated adhesive interactions under controlled conditions. Our findings are as follows.

Interplay between integrin receptor density and soluble fibronectin concentration influence tissue mechanical properties

We found first that $\alpha 5\beta 1$ -fibronectin adhesions confer a range of surface tensions that depend in a non-trivial way on the level of $\alpha 5\beta 1$ -expression and soluble fibronectin (sFn) concentration. For example, as $\alpha 5\beta 1$ expression is increased from low to moderate levels, surface tension increases from 5.5 dynes/cm to 10.4 dynes/cm, but further increase in $\alpha 5\beta 1$ -receptor expression paradoxically causes a drop in surface tension to back to about 5 dynes/cm for high and very high $\alpha 5\beta 1$ levels. Likewise, we found what we have termed a biphasic transition from viscoelastic-liquid to viscoelastic-solid behavior in cell-aggregates such that more aggregates behave as viscoelastic-solids for moderate $\alpha 5\beta 1$ expression than for either higher or lower expression values.

Additionally, our measurements show that the amount of sFn - and the history of its presence - affects the mechanical properties of cellular aggregates. For example, we have demonstrated that aggregates can initially diminish in volume, but then enlarge over time as sFn is depleted from the microenvironment. Correspondingly, we found that cellular rearrangement is significantly affected by sFn concentrations, leading to qualitative changes in structures that assemble from in vitro aggregates.

Previous studies have documented that embryonic tissues can change physical properties depending on their embryonic stage of development, the history of culture conditions, and the level of exogenous fibronectin [12, 13, 36, 45, 46]. In our in vitro system, we have defined specific biomechanical endpoints that correlate with $\alpha 5\beta 1$ receptor expression and soluble fibronectin concentration, thus empirically associating the effect of cell-mediated fibronectin deposition with bulk cell-aggregate material properties.

The behaviors that we report have not to our knowledge previously been described and signal a distinction between integrin-mediated and cadherin-mediated adhesion. It is well documented first that increasing surface cadherin expression produces a linear and monotonic increase in surface tension [1] and second that $\alpha 5\beta 1$ -fibronectin adhesive interactions confer, on a molecule to molecule basis, stronger cohesion than cadherin-mediated interactions [2]. It is therefore surprising that both integrin expression and soluble fibronectin concentration affect tissue properties and assembly in the complex ways that we have described. We propose that these complex behaviors may affect the ability of cells to re-arrange and establish specific spatial relationships during development and wound healing.

Structure formation is affected by soluble fibronectin concentration history

To further explore the mechanism underlying the biphasic response of aggregate rheology on ECM properties and history, we extended our experimental design to include very high $\alpha 5\beta 1$ -receptor expression, changes in sFn levels, and variations in cell population numbers. In these experiments, we found that $\alpha 5\beta 1$ (HH) cells deplete more

sFn from their environment than cells expressing lower levels of the $\alpha 5 \beta 1$ -receptor. We also determined that the rate of depletion of sFn correlates with the change in volume of cell aggregates over time. For fast utilization of sFn, we observed substantial changes in aggregate volume over time. However, as aggregate volume plateaued, the rate of sFn consumption was greatly reduced after 3 days in hanging drop.

Our results showed that increasing $\alpha 5 \beta 1$ -receptor expression increases the consumption of available soluble fibronectin in the microenvironment, and so we would expect quantitative differences of the insoluble fibronectin matrix to appear as a function of integrin receptor expression. However, immunostaining of tissue sections at very high levels of $\alpha 5 \beta 1$ expression revealed a less robust matrix, in which cells appeared less connected with one another. We have proposed that these matrix properties correlate with a drop of cohesion of CHO- $\alpha 5 \beta 1$ (HH) aggregates provoked by sFn depletion in the cellular microenvironment.

This idea is not entirely new; for example the role of sFn limitations on turnover in the insoluble fibronectin matrix has been previously described on cell monolayers [47, 48]. It has also been shown that a fibronectin matrix with longer fibers and high connectivity produces higher aggregate cohesion, and that a shorter or more punctate fibronectin matrix promotes the formation of sheets of cells rather than round aggregates [43]. Our data indicate that sFn may be a limiting factor in cellular assembly as it is used up during active fibronectin fiber polymerization [42, 49], a result that may have implications for prior findings as well.

Interplay between N-cadherin and $\alpha 5\beta 1$ -fibronectin interactions on aggregate mechanical properties

The expression of N-cadherin and a loss of E-cadherin have been found to mark the transition from epithelial to mesenchymal phenotypes and to correlate with cancer metastasis [50, 51]. For this and other reasons, it is of interest to understand cadherin interactions with integrin adhesion mechanisms. In a final series of experiments, we therefore compared aggregate mechanical properties as specified by integrin–Fn interactions alone with cadherin-based interactions. These experiments showed that aggregates expressing both modes of interaction tended to a more liquid phenotype, accompanied by a small decrease in surface tension. This surprising result suggests that there may be interplay between integrin- and cadherin-mediated dynamics; since both are present during development, this interplay may be of practical significance.

By contrast, $\alpha 5\beta 1$ (HH) and $\alpha 5\beta 1$ (HH)/N-cad aggregates showed an increase in surface tension from 5.5 dynes/cm to 9.6 dynes/cm. However, the increase in cohesion occurred without a change in the viscoelastic properties of the aggregates as described in table 3-3. These results suggest that N-cad, when co-expressed with $\alpha 5\beta 1$ integrin may play a dual role, depending on the level of $\alpha 5$ being expressed. On the one-hand, N-cad expression can have an additive effect when $\alpha 5\beta 1$ is expressed at high levels; on the other hand, N-cad expression can produce a phase transition from elastic to liquid behavior when $\alpha 5\beta 1$ is co-expressed at lower levels. The ability of N-cad to produce transitions to viscoelastic-liquid behavior may be due to the ability of these bonds to maintain viscoelastic-liquid properties over a range of increasing cadherin receptor

expression [2]. Even though we are able to describe the effect of N-cad on $\alpha 5 \beta 1$ -fibronectin on the mechanical properties and rearrangement behaviors, these findings require further study with other form of the cadherin receptor such as P- and E- cadherin. For example, our results do not answer questions about cytoplasmic effects such as activation of key pathways controlling cytoskeletal rearrangement. This supports previous observations from the literature that expression of dual adhesive systems can produce increases in cohesion without causing abrupt changes in aggregate mechanical and rearrangement properties [9, 36].

The effect of integrin alone and integrin-cadherin adhesion on cellular rearrangement

As previously discussed, including N-cad-based interactions give rise to changes in tissue surface tension and liquidity. Tissue liquidity is the bulk property of cohering cells to rearrange as cell-cell bonds are dynamically formed and broken. Therefore, tissue liquidity has a direct correlation with the ability of cells to sort-out or segregate at equilibrium according to differences in tissue cohesion [9, 36, 38, 52, 53]. In our work, we have uncovered three properties of $\alpha 5 \beta 1$ -fibronectin mediated adhesion on cellular rearrangement. i) Differences in $\alpha 5 \beta 1$ -receptor expression do not appear to drive cell sorting, as do cadherin-based differences. Increasing the concentration of soluble fibronectin does not enhance segregation but, as expected, decreases the overall volume of the tissue-aggregate. ii) Heterogeneous mixtures of cells that are unable to make a matrix with CHO- $\alpha 5 \beta 1$ cells cause segregation as long as the CHO- $\alpha 5 \beta 1$ cells express integrins at levels that in isolation produce have viscoelastic-liquid properties. iii) Co-expression of N-cad at high and mid levels of $\alpha 5 \beta 1$ expression cause sorting behaviors

analogous to rearrangement seen in embryonic cell mixtures, and in mixtures of cells with differences in cadherin expression [1, 36].

Aggregates of cells are held together by both cell-ECM and cell-cell bonds. For cell-cell bonds, the Differential Adhesion Hypothesis (DAH) predicts that a cell population with more bonds will adopt an internal position relative to a cell population with fewer bonds [7]. On the contrary, we have shown that unexpected rearrangement behaviors are seen when cells are held through $\alpha 5\beta 1$ -fibronectin adhesive bonds. For example, $\alpha 5\beta 1$ -aggregates with viscoelastic-liquid properties adopt an external position relative to the control CHO-P3, defined as peripheral sorting. This represents a different form of segregation, when compared to internal sorting of heterogeneous mixtures of embryonic tissues and cadherin expressing cells [29, 36]. Peripheral sorting has been observed in mixtures of cardiac mesenchymal cells (Mes) and myocytes (My), cellular precursors of chick embryonic heart tissue. According to Armstrong et al., Mes with the ability to ensemble a matrix sorts to the surface following higher concentration of the soluble fibronectin. As Mes starts to make the insoluble fibronectin matrix, it excludes the myocyte population towards the interior of the aggregate [54]. By comparison, in our in vitro system we found that peripheral sorting requires tissue liquidity and low heterotypic adhesive relations. However, increasing soluble fibronectin concentration or expressing N-cad at low soluble fibronectin concentration produces a transition from the peripheral sorting to internal sorting as observed in equilibrium configurations of embryonic cell mixtures.

In conclusion, we have measured the mechanical properties of aggregates held through cell-ECM and cell-ECM/cell-cell interactions. We have determined that the

biphasic nature of $\alpha 5 \beta 1$ -Fn interactions appears to be the result of a kinetic balance between the level of integrin expression at the cell surface and the available soluble fibronectin in the microenvironment. This balance affects the degree of aggregation of these cells and the resulting mechanical properties of these aggregates. Additionally, we have found that both expected and unexpected morphologies are produced by the rearrangement dynamics of integrin-mediated cell suspensions. As for the expected morphologies, N-cad expression causes the known internal sorting, as postulated by the DAH. However, unexpected morphologies such as peripheral sorting of cohesive populations are also seen with cell-ECM interactions. We have determined that these morphologies, originally described in embryonic heart cell mixtures, depend on specific integrin receptor expression as well as sFn concentration.

This work describes mechanical and rearrangement behaviors that are potentially found during wound healing, development, and stroma-epithelial boundary dynamics during cancer states. Future work requires the scrutiny and differentiation of effector cytoplasmic pathways controlling cytoskeletal rearrangement during cell-ECM and cell-cell. In particular, it would be of interest to correlate the different tissue properties and rearrangement behaviors as the result of receptor-mediated adhesion and highly regulated cytoskeletal dynamics.

Methods

Complete Media

All cell lines were maintained at 37°C and 95% air/ 5% CO₂. The media used for these cells consisted of Dulbecco's Modified Eagle's Medium (High Glucose, 1x Gibco (Invitrogen™), supplemented with 10% fetal calf serum [30] (Hyclone Logan, Utah), 1mM sodium pyruvate (1%), 0.1 mM MEM non-essential amino acids (1%), and 100µg/ml streptomycin sulfate (1%). Note: for every hanging drop aggregation experiment, the required volume of complete media was made fresh following the same proportions of reagents previously described or supplemented with rat plasma fibronectin for higher initial soluble fibronectin concentrations.

Complete Squeezing Media

This is the standard media for aggregate compression experiments. This media is made with CO₂ Independent Media 1x Gibco, Invitrogen™, 10% Fetal Calf Serum (Hyclone Logan, Utah), and 1% 100µg/ml streptomycin sulfate. Prior to use in the TST chamber, vials of 50-ml conical tubes of complete squeezing media were put at 37° C overnight for degassing.

Chinese Hamster Ovary Cells (CHO-B2)

This is a cell line that has a particular profile of expression of adhesion molecules. For Example, it expresses the β 1 integrin subunit in ample quantities. But, it has null

expression of the $\alpha 5$ subunit [31]. Additionally, it has neglectable levels of N-cadherin receptor expression that allow these cells to form sheets [2]. This cell line is easily transfected and represents a good model for the assessment of the effect of the $\alpha 5\beta 1$ receptor on cell-ECM dynamics. In principle, we control the level of expression of the $\alpha 5\beta 1$ integrin heterodimer receptor through the transfection of the $\alpha 5$ construct.

Electroporation of CHO-B2: Generation of CHO-P3 and CHO- $\alpha 5\beta 1$ Cell lines

In order to generate cell lines that express different levels of expression of the human $\alpha 5$ integrin receptor, the CHO-B2 (null for $\alpha 5$ expression) was transfected by electroporation with a construct containing the $\alpha 5$ insert and resistance vector to G418 according to previous work in our laboratory [2]. Cells were transfected at 200 volts and 960 μ F in a 0.4 cm electroporation cuvette using a Biorad Gene Pulser II apparatus. After electroporation, cells were left in ice for 10 minutes and then plated and grown to confluency in selection media (complete media supplemented with either 800 μ g/ml and 400 μ g/ml of G418). The empty vector control pcDNA3 (without the $\alpha 5$ construct) was electroporated into CHO-B2 to generate CHO-P3 (Parent cell line). These cells were cultured under selection conditions as previously described.

CHO- $\alpha 5\beta 1$ /Ncad and CHO-Ncad Cell Lines

The CHO- $\alpha 5\beta 1$ /Ncad cell line was kindly provided from Dr. Corbett's library of cell lines. The engineering of this cell is described as a part of the thesis work by Elizabeth E.

Robinson [32]. The CHO-Ncad cell line engineering and development is described by Robinson et al., (Methods) [2].

Generation of Cell Lines with Variable Levels of Expression of The $\alpha 5$ Integrin Receptor

After constant selection with G418, we sorted positive cells for different levels of expression using Fluorescent Activated Cell Sorting (FACS) machine. Cells on culture dishes were wash with 4-ml of Phosphate Saline Buffer (PBS, pH 7.4 1x Gibco (Invitrogen™)). Then, cells were detached with 2-ml of 0.5% Trypsin EDTA (1x Gibco (Invitrogen™)) for 4 minutes at 37°C with sporadic tapping of the plate to help detach the cell on the surface of the tissue culture plate. Once cells were detached, 2-ml of complete media were added to stop the reaction. Cells were pooled into a 15-ml conical tube and centrifuged at 800 rpm for 4 minutes. The supernatant was removed via vacuum with a Pasteur glass pipette. The pellet was washed twice with 1-ml of ice-cold Hanks' Balanced Salt-Solution (HBSS) (1x Gibco (Invitrogen™)) and centrifuged again at 800 rpm for 4 minutes [33]. Following, cells were resuspended in 100- μ l of 1:100 dilution of primary anti-Integrin $\alpha 5$ /FnR Mouse receptor (CD49e) in ice-cold HBSS and incubated for 45 minutes in ice. The vial was tapped every 5 minutes to ensure homogeneous reactivity on all the cells. After incubation, cells were centrifuged at 800 rpm for 4 minutes. The supernatant was carefully removed and cells were washed twice with ice-cold HBSS. Then, the pellet was resuspended in 100- μ l of 1:100 dilution of secondary Alexa-Fluor 488 goat-anti-mouse IgG in ice-cold HBSS and incubated for 30 under dark conditions and in ice. After incubation in secondary antibody, cells were centrifuged at 800 rpm for 4 minutes. The supernatant was carefully removed and cells were washed

twice with 1-ml of ice cold HBSS. Cells were resuspended in 1-ml of ice cold HBSS and kept in ice. Sample was taken to the Flow Cytometry Facility at EOHSI (Rutgers University) for sorting of populations with marked differences in $\alpha 5$ subunit of the $\alpha 5 \beta 1$ heterocomplex on the cell surface. As controls for sorting we used, CHO-P3 (incubated with both primary and secondary antibodies) and CHO- $\alpha 5 \beta 1$ (incubated on secondary antibody only). After sorting, cells were plated on tissue culture dishes and grown to confluency. Stable and pure colonies of $\alpha 5 \beta 1$ -expressing cells were also generated through clonal dilution. Suspension of cells were made as to achieve 1 to 3 cells per 200- μ l. Aliquots of 200- μ l were then plated in a flat-bottom 96-well plate. Over time single cell colonies of cells with various levels of cell spreading morphologies were monitored. Once cell nodules formed, media was removed from the wells of interest. Wells were washed once with PBS. Nodules were trypsinized using short glass tubes and autoclaved-vaseline to isolate the nodule from the rest of the other unwanted nodules. 10- μ l of trypsin-EDTA was added into the tubing to dislodge the nodule into single cells. After 4 min on the 37°C heat block, 10- μ l of complete media was added to stop the trypsinization reaction. The cell suspension was directly added into regular tissue culture dishes. All sorted and clonal populations were analyzed for the $\alpha 5$ subunit in the $\alpha 5 \beta 1$ heterodimeric complex with flow cytometry as previously described.

Generation of CHO- $\alpha 5 \beta 1$ /Ncad Cell Lines with Variable Levels of Expression of The $\alpha 5 \beta 1$ Integrin Receptor and Constant N-cad.

Cells were grown to near confluency. Then, cells were washed with 4-ml of 1x PBS (pH 7.4 1x Gibco, Invitrogen™) and detached with 2-ml of 1x Trypsin EDTA (1x Gibco, Invitrogen™) for 4 minutes at 37°C with sporadic tapping of the plate to help detach the cell on the surface of the tissue culture plate. Once cells were detached, I added 2-ml of complete media to stop the reaction. Cells were pooled into a 15-ml conical tube and centrifuged at 800 rpm for 4 minutes. The supernatant was removed via vacuum with a Pasteur glass pipette. The pellet was washed twice with 1-ml of ice-cold HBSS and centrifuged again at 800 rpm for 4 minutes. Following, cells were resuspended in 100- μ l of 1:100 dilution of primary anti-Integrin α 5/FnR Mouse receptor (CD49e) in ice-cold HBSS and incubated for 45 minutes in ice. The vial was tapped every 5 minutes to ensure homogeneous reactivity on all the cells. After incubation, cells were centrifuged at 800 rpm for 4 minutes. The supernatant was carefully removed and cells were washed twice with ice-cold HBSS. Then, the pellet was resuspended in 100- μ l of 1:100 dilution of secondary Alexa-Fluor 488 goat-anti-mouse IgG in ice-cold HBSS and incubated for 30 under dark conditions and in ice. After incubation in secondary antibody, cells were centrifuged at 800 rpm for 4 minutes. The supernatant was carefully removed and cells were washed twice with 1-ml of ice cold HBSS. Cells were resuspended in 1-ml of ice-cold HBSS and kept in ice. Sample was taken to the Flow Cytometry Facility at EOHSI (Rutgers University) for sorting of populations with marked differences in α 5 subunit of the α 5 β 1 heterocomplex on the cell surface. For the purpose of this cell line, we gated cell populations at the left and right tails of mean peak value in order to achieve differences in receptor expression. After sorting, cells were plated on tissue culture dishes and grown to confluency.

Aggregate Formation and Hanging Drop

Cells were removed from near confluent 10-cm tissue culture plates with trypsin-EDTA. They were wash twice with PBS and resuspended at a concentration of 2.5×10^6 cells/ml in 1-ml of complete medium. 10- μ l aliquots of cell suspension were deposited on the underside of the top-lid of a 10-cm tissue culture dish. The bottom lid of the tissue culture plate was added 5-ml of PBS to maintain constant moisture inside the tissue culture plate. Following, the upper-lid was place on its regular position and the 10- μ l drops hanged from the top of the upper-lid pulled by gravity. This allows the suspension of cells to coalesce and interact under no influence of substrate other than the cellular interaction of the cells in the cell suspension. The drops were incubated under regular tissue conditions (37°C, 5% CO₂, and 80% Humidity) for 3 days allowing cells to coalesce and form aggregates. At day 3, the cell aggregates were transferred to 10-ml shaker flasks (Belko Glass, NJ) in 3-ml complete media and placed on an orbital shaker at 110 rpm for a range of time of 2-3 days. For our cells it was found that completely round spheroids formed after one and half days in the shaker. Spheroids had a size range of (500 to 600)- μ m in diameter. The hanging drop assay is a core procedure on all the experiments. We performed the same procedure of all the cells lines that were used in the course of this thesis. The following descriptions require of the hanging drop in order to address specific question about biological, rearrangement behaviors and biophysical properties of the $\alpha 5\beta 1$ -fibronectin mediated dynamics.

Serial-Eroding Aggregate Trypsinization Method

It was observed that regular incubation of aggregates with 100- μ l of trypsin for up to 10 minutes at 37° C water bath and up and down pipetting caused the cells to spit a gelatinous material described as nuclear material [34], to become non-viable, and still leave large fragments of cells in the cell suspension. In our experimental experience, this was correlated to the significant loss of the α 5 signal during FACS determination of the integrin receptor due to reduced cell number in the cell suspension. Aggregates of cells when it comes to trypsinization can be thought as a multilayered structure, since the cells making the aggregate would dislodge at different rates from the main aggregate as the trypsin works its way into the aggregate. During that time, single cells expend the same time, as the trypsin works its way into deeper cells in the aggregate, causing single cells to be overexposed to such harsh conditions and increasing cell non-viability. Therefore, serial-eroding aggregate trypsinization takes care of this difference in trypsin exposure time during aggregate trypsinization. The following is a description of the method. We labeled Eppendorf tubes and pooled the aggregates into each tube. At the same time, we labeled 15-ml conical tubes containing 2-ml of complete media as collection tubes. 100- μ m of trypsin-EDTA were added into the Eppendorf tubes and were put in the 37° C water bath for 2 minutes. Using a pipette set to 100- μ l volume, the aggregates were mildly disrupted through mild vortexing. Then, a 100- μ l aliquot was taken from the tube and placed in the 15-ml conical tube with fresh complete media. Following, another 100- μ m of trypsin-EDTA was added to the Eppendorf tubes and put for 2 minutes incubation in the 37° C water bath. It was found that with this method we required a cumulative time of 6-8 minutes to achieve total disruption of aggregates into a cell suspension. Additionally, there was neglectable presence of the gelatinous material in suspension

during this process. Lastly, the peaks representing the cell populations were sharper and had a better area than the signal with the previous trypsinization process of aggregates. Therefore, this process was used for all the characterizations of integrin surface receptor expression of 3D aggregates.

Determination of $\alpha 5$ and N-cad Receptors Expression in 3D Aggregates

Since all our experiments were conducted on aggregates of cells, it is expected that the profile of expression of the heterodimeric complex of $\alpha 5\beta 1$ on the cell surface should represent that of the geometry of the cell system. Four levels of expression of the $\alpha 5$ subunit on CHO- $\alpha 5\beta 1$ and two levels of expression on CHO- $\alpha 5\beta 1$ /Ncad were processed to form aggregates (Described above). For each cell line, there were a total of 40 aggregates or hanging drop (10- μ l of 2.5×10^6 cells/ml. At day 3, all the aggregates were pooled into labeled 1-ml Eppendorf tubes and washed with 1-ml of 1x PBS. Then, centrifuged at 800 rpm for 4 min. The supernatant was carefully removed with a glass pipette under vacuum conditions. Then, we did serial-eroding aggregate trypsinization with trypsin-EDTA method (Described above). After all cells were pooled into the large 15-ml conical tube, as part of the serial-eroding aggregate method, the conical tubes were centrifuged at 800 rpm for 4 minutes. After this point, we followed the same procedure as described under “Generation of Cell Lines with Variable Levels of Expression of The $\alpha 5$ Integrin Receptor” to quantify the level of expression of the integrin receptor of cells in aggregates. However, for aggregation of CHO- $\alpha 5\beta 1$ /Ncad and CHO-Ncad, we did a variation to determine the level of expression of the N-cadherin receptor. To determine the level of expression of surface N-cadherin (Ncad), we used trypsin-calcium (1x

Trypsin/ 5 mM Ca^{2+}) since calcium ion provided protection from protease activity on the cadherin receptor [35]. After washing with 1-ml ice-cold PBS (twice), the pellet was resuspended in 100-ml of 1:100 dilution of primary rat anti-N-cadherin (Chicken) (NCD-2) (Stock 1 mg/ml) in ice-cold HBSS for 45 minutes in ice. Following, the pellet was washed twice with 1-ml ice-cold HBSS. Then, the pellet was incubated in secondary antibody, 1:100 Alexa Flour (FITC) goat-anti-rat IgG in ice-cold HBSS and incubated for 30 minutes. After incubation in secondary antibody, cells were centrifuged at 800 rpm for 4 minutes. The supernatant was carefully removed and cells were washed twice with 1-ml of ice-cold HBSS. Cells were resuspended in 1-ml of ice-cold HBSS and transferred to 10-ml FACS tubes and kept in ice. We then, determine the level of expression of the Ncad receptor using flow cytometry.

Tissue Surface Tensiometry (TST)

The cohesive strength of the aggregates, as a function of $\alpha 5\beta 1$ receptor expression or $\alpha 5\beta 1$ /Ncad was measured by TST. This method has been extensively described as a way to measure and differentiate the biophysical properties of tissue-aggregates [1, 2, 36-38]. Spherical aggregates with a size range of (400 – 500) μm in diameter were transferred into the inner chamber, pre-filled with complete CO_2 independent-media 1x Gibco (Invitrogen™), of the tissue surface tensiometer and carefully position on the lower compression plate (LCP) with the aided of an autoclaved Pasteur pipette. The inner chamber contained pre-warmed, de-gassed CO_2 -independent medium at 37°C . The upper compression plate (UCP), attached to a nickel-chromium wire, was then positioned above the aggregate and connected to a Cahn/Ventron model 2000 recording electrobalance.

The C-2000 electrobalance operates on the null principle to record the change in weight to a set value between the weights of (the chromium wire + UPC) to the weight of the counterbalance weight pan. The fulcrum of the balance arm has an armature within a permanent magnetic field. When it is in balance, the continuous electromagnetic induction keeps physically the arm in the set position as when one tares a balance. Hence, the position of the UPC is kept constant during the compression of an aggregate. Consequently, the voltage recorded is a measure of the compression force applied to the aggregates during regular TST measurements. The measurements were taken in the 10 mg scale, i.e. the whole range of the analog spans 10-mg, divided into 0.1-mg. We then are allowed to determine surface tension in the 0.1-dyne/cm range.

The UPC and LCP were pre-coated with poly-2-hydroxyethylmethacrylate (10-mg/ml Poly-HEMA in ethanol), which reduces the adhesion of cell towards surfaces. Compression was initiated by raising the LCP until the aggregate became compressed against the UPC. One monitors the amount of initial compressive force on the aggregate, looking at the voltage change on the paper tracing connected to the Cahn electrobalance. The change in aggregate shape or geometry was monitored in real-time through a 25x Nikon dissecting microscope equipped with a CCD video camera and connected to a Macintosh Power PC computer. Images of aggregates at equilibrium were captured, digitized and their geometries were analyzed using ImageJ software (N.I.H., Bethesda). Each aggregate was subjected to double compressions, the second greater than the first. Measurements of aggregate geometry and force at equilibrium were plug into the Young-Laplace Equation [37, 39] producing numerical values of tissue surface tensions (σ) in analogy to liquids.

$$\frac{F_{eq}}{\pi R_3^2} = \sigma \left(\frac{1}{R_1} + \frac{1}{R_2} \right)$$

The F_{eq} is the resistance force at equilibrium of the aggregate on the upper compression plate, πR_3^2 is the area of the surface of the aggregate where the force F is exerted, and R_1 and R_2 are the respective principal radii of curvature. Because R_1 , R_2 and the separation between the UCP and LCP (H) can be measured with greater accuracy than R_3 , the latter parameter was calculated using the equation below:

$$R_3 = (R_1 - R_2) + \sqrt{\left(R_2^2 - \left(\frac{H}{2} \right)^2 \right)}$$

The main assumption on the use of the Young-Laplace equation is that the pressure term, $\frac{F_{eq}}{\pi R_3^2}$, is balanced by the surface tension forces at the surface of a drop of fluid. In the case of aggregates, there must be finite contact angle between the aggregate and the plates and there should be symmetry between the left and right curvature of the aggregate under compression. The balance force to the pressure term is thought to come from the ability of cells to dissipate the compressive force and assume a more round position at equilibrium. Thus behaving as viscoelastic-liquids [12]. Lastly, we approximate the side boundaries of the compressed aggregates by spherical caps [37]. The reason why we use a double compression on a single aggregate is to determine the dependence/independence

to force of compression. For example, aggregates that behave as viscoelastic-liquids have surface tensions that are independent of force, $\sigma_2/\sigma_1 \sim 1$ and $\sigma_2/\sigma_1 \ll F_2/F_1$. On the other hand, aggregates with viscoelastic-solid properties have surface tensions that are force dependent, $\sigma_2/\sigma_1 > 1$ and $\sigma_2/\sigma_1 = F_2/F_1$. This is a very important guideline in our analysis since $\alpha 5\beta 1$ -fibronectin dynamics and chick embryonic tissues have been found to have such transitions in tissue-aggregate properties when time in culture is a variable in the system [2, 36]. In the same manner, we want to distinguish these dynamics as a function of $\alpha 5\beta 1$ surface receptor expression and soluble fibronectin concentration.

Quantification of Aggregate Compaction

Cells were removed from near-confluent 10-cm tissue culture dishes. To make hanging drops we follow the same procedure as described under “Aggregate Formation and Hanging Drop”. We used two different cell concentrations, 2.5×10^6 cells/ml and 5.0×10^6 cells/ml and hanging drops of 10- μ l. This makes aggregates that are approximately made up of 25,000 to 50,000 cells. For each level of expression of the $\alpha 5\beta 1$ integrin receptor, sets of 10 hanging drops were made for the following times: 2, 3, 4, and 5 days. At each time point, high contrast images of aggregates were capture using IPLab imaging software (Slanalytics Inc., Fairfax, VA) and bright-field microscope (Nikon Eclipse TE300). Images were calibrated in order to convert pixels into length scale using the image of the upper compression plate (UCP), which is 1.64 mm in diameter. The calibration and measurements were done with ImageJ Software (N.I.H., Bethesda) by drawing a perimeter around each aggregate and calculating the area of the aggregate. Data sets were processed and graphed using Microsoft Excel to calculate averages,

standard deviation, and SEM. In our analysis, compaction is defined as the area of the aggregate.

Determination of Soluble Fibronectin Utilization With The ELISA Method

We used the ELISA method to determine the concentration of soluble fibronectin during integrin-mediated fibronectin matrix formation. Particularly, we were interested in the rate of soluble fibronectin utilization and basal levels of soluble fibronectin as aggregate compaction levels-off. Since we wanted the samples to be analyzed on the same day, all samples of cell suspensions were prepared as a function of the end point. For example, day 5 was our end point. Thus, 5-day samples were prepared independent of 4-day samples, and so were 3-day samples. Thus, the soluble Fibronectin determination, as a function of $\alpha 5\beta 1$ expression and incubation time, was measured on a single day. This method avoided storing of the older samples, which could potentially cause precipitation of soluble fibronectin during regular freeze/thaw process. For every time-point, cells suspensions of cells were made at a concentration of 2.5×10^6 cells/ml as described under “Aggregate Formation and Hanging Drop”. However, we controlled the following aspects: i) cells were resuspended in pre-made complete media (10% Fn free Fetal Calf Serum) supplemented with rat plasma fibronectin (Calbiochem®). Each cell suspension had an initial concentration of 30- μ g/ml soluble fibronectin at each time point. In this experiment we sampled soluble fibronectin utilization for days 3, 4, and 5. At the end point day, the complete media from each aggregate was collected and pooled into labeled-Eppendorf tubes and put in ice while collecting the remaining samples. Prior to collecting the samples, Immuno 96 MicroWell™ Plates (Nunc™, Nalge Nunc

International) were blocked for 1 hour with 200- μ l of 1x PBS with 0.1% BSA. Then, plates were washed four times with washing solution (PBS with 0.05% Tween 20) and dry by impact on a soft mount of paper towels. The rat soluble fibronectin standard curve was prepared to be in a range of (30 to 5)- μ g/ml diluting volumes of stock rat plasma fibronectin 500- μ g/ml (Calbiochem®) diluted in Dulbecco's Modified Eagle Medium (DMEM) for a total volume of 350- μ l. 100- μ l triplicates of the standard curve concentrations of soluble rat plasma fibronectin were loaded into the wells of the blocked-immuno 96 microwell plate. As blanks, 100- μ l of DMEM was loaded in triplicates as well. Following, samples with the unknown concentration of rat soluble fibronectin (As a function of time and $\alpha 5\beta 1$ receptor expression) were loaded as 100- μ l duplicates onto the same plate. The samples were incubated at room temperature for 45 minutes. Following samples were individually suctioned using Pasteur pipettes under vacuum conditions to avoid cross contamination. The immuno-plate was washed four times with washing solution (PBS with 0.05% Tween 20) and dry by impact on a soft mount of paper towels. Next, each well in the immuno-plate was incubated with 100- μ l of 1:4,000 primary biotinylated rabbit polyclonal fibronectin antibody (abcam 6584, MA) were loaded with an 8-channel multichannel pipette and incubated for 45 minutes at room temperature. The immuno-plate was washed four times with washing solution (PBS with 0.05% Tween 20) and dry by impact on a soft mount of paper towels. After washing, the immuno-plate was incubated with 100- μ l of 1:10,000 secondary Streptavidin/Horseradish Peroxidase conjugate (Pierce, Illinois) using an 8-channel multichannel pipette. Plate was incubated for 15 minutes at room temperature. The immuno-plate was washed four times with washing solution (PBS with 0.05% Tween 20) and dry by impact on a soft mount of

paper towels. Then, using the 8-channel multichannel pipette 100- μ l of 3,3',5,5' Tetramethylbenzidine (TMB) liquid substrate, Sigma St. Louis, MO) was loaded into the wells of interest and put into a shaker (Brand here) for 5 minutes. The immuno-plate was covered with aluminum foil (The substrate is light sensitive). The change in color from clear to dark blue is due to the cleaving reaction of protein-bound horseradish peroxidase (HRP) on the 3,3',5,5' Tetramethylbenzidine (TMB) liquid substrate. At 5 minutes incubation with the TMB, 50- μ l of stop solution (2M H₂SO₄) was added. This caused a change in color from blue to yellow. The immuno-plate was covered with aluminum foil to prevent light exposure. The samples were measured at 450 nm using an iMark Microplate Absorbance Reader (Biorad TM) and quantified with a build-in excel export spreadsheet function.

Soluble Fibronectin Secretion by CHO-Cell lines

Using the Elisa method (As described previously), we made 30 10- μ l hanging drops for each level of the α 5 β 1-expression on the transfected CHO cells lines at a cell density of 2.5×10^6 cells/ml. The cells were incubated in Fn-free Fetal Calf Serum following method on [40] in order to determine the amount of hamster Fn from the cells and to avoid contributions from fetal calf serum (FCS) fibronectin, which have been found to have an average soluble fibronectin concentration of 30- μ g/ml [30]. At day 3, the collected media from all the hanging drops were assessed for soluble fibronectin concentration was assessed following the same parameters as under “Determination of Soluble Fibronectin Utilization With The ELISA Method”

Fibronectin Immunostaining on 2D Cell Cultures

CHO- $\alpha 5\beta 1$ cells were plated on glass coverslips at a density of 5×10^5 cells/ml. For each level of integrin expression, cells were incubated in fibronectin free media, complete media, and media containing 300- μ g/ml soluble fibronectin. The next day, cover slips were prepared for detection of insoluble fibronectin fibers. Each glass coverslips was washed with 500- μ l of phosphate buffer saline (PBS). Coverslips were fixed with fixative solution (4% paraformaldehyde and 0.1% Triton x100) for 15 minutes at room temperature. Upon removal of the fixative solution, the coverslips were blocked with blocking solution (0.1% bovine serum albumin (BSA) in PBS) for 30 minutes at room temperature. After blocking, coverslips were incubated in rabbit polyclonal anti-fibronectin primary antibody (anti-Fn AB6584) in a 1:100 dilution in blocking solution for 45 minutes. The cover slips were washed twice with 500- μ l of PBS. Then, the coverslips were incubated with a 1:100 dilution of secondary antibody Alexa Fluor 568 goat-anti-rabbit in blocking solution for 30 minutes. After washing twice with PBS, we stained the cell nuclei with DAPI at a 1:5,000 dilution of stock DAPI solution (5mg/ml in methanol) in blocking solution for 5 minutes. Coverslips were washed once. Cover slips were added flour saver reagent (Carbiochem, CA) to prevent fluorobleaching. As a final step, a coverslip was put on top and sealed with clear nail polish. Images were taken with an epi-fluorescent microscope (Nikon, Eclipse TE300) using the FITC and the DAPI filter.

Fibronectin Immunostaining of Frozen Tissue Sections

Frozen sections of CHO- $\alpha 5\beta 1$ cell aggregates were cut in sections (5- μ m thickness) by the Tissue Retrieval service at RWJUH and mounted on glass slides. The tissue sections

were stored at -80°C . For fibronectin immunostaining of fresh tissue sections, slides were left at room temperature for 10 minutes. A perimeter was outlined using a Pap pen (Zymed, CA) to keep the incubating solutions localized on the tissue sections. Samples were washed with cold-PBS. We followed the same procedure as described on “Fibronectin Immunostaining on 2D Cell Cultures”. However, the samples were placed in a humidifier chamber during incubation with primary and secondary antibodies.

Rearrangement Assay

In order to assess the rearrangement behavior of CHO- $\alpha 5\beta 1$ and CHO- $\alpha 5\beta 1/\text{Ncad}$, cells were detached from plates following regular trypsin procedure of 0.5% Trypsin-EDTA for integrin containing cell lines and trypsin-calcium (1x Trypsin/ 5 mM Ca^{2+}) for Ncad containing cells lines. Once detached, cells were washed twice with PBS, and counted to obtain a cell seeding density of 2.5×10^6 cells/ml. To label cells, we used two types of membrane intercalating dyes: PKH2 Green Fluorescent Cell Linker and PKH26 Red Fluorescent Cell Linker Sigma® (Following Manufacturers Specifications). The time of incubation for each intercalating dye was optimized due to the different intercalating rates of the fluorescent cell linkers. For example, for the same ratio of cell number to dye concentration, PKH2 Green was incubated for 3 minutes and PKH26 Red was incubated for 30 seconds. Using these times of incubations, we were able to create a close range of exposure time of 120-140 milliseconds between the red and green signal that was optimum for our rearrangement experiments. After labeling the cells, we took equal volumes of labeled cell suspensions and mixed them. We then centrifuged the mixture at 800 rpm and for 4 minutes. Then, we carefully removed the supernatant and the pellet

was resuspended in fresh complete media or in complete media with higher concentrations of rat plasma fibronectin to assess rearrangement in the presence of higher soluble fibronectin concentrations. 10-ml hanging drops were made following the same process described in “Aggregate Formation and Hanging Drop”. At day 3, we looked at the aggregates using an epi-fluorescence microscope (Nikon, Eclipse TE300) at 470 nm (green emission) and at 530 nm (red emission). Epi-fluorescence images were then merged using IPLab (Slanalytics Inc., Fairfax, VA).

Chapter 3 Bibliography

1. Foty, R.A. and M.S. Steinberg, The differential adhesion hypothesis: a direct evaluation. *Dev Biol*, 2005. **278**(1): p. 255-63.
2. Robinson, E.E., et al., Alpha5beta1 integrin mediates strong tissue cohesion. *J Cell Sci*, 2003. **116**(Pt 2): p. 377-86.
3. Foty, R.A. and M.S. Steinberg, Measurement of tumor cell cohesion and suppression of invasion by E- or P-cadherin. *Cancer Res*, 1997. **57**(22): p. 5033-6.
4. Townes, P.L. and J. Holtfreter, Directed movements and selective adhesion of embryonic amphibian cells *Journal of Experimental Zoology*, 1955. **28**(1): p. 53-120.
5. Steinberg, M.S., Mechanism of tissue reconstruction by dissociated cells. II. Time-course of events. *Science*, 1962. **137**: p. 762-3.
6. Steinberg, M.S., On the mechanism of tissue reconstruction by dissociated cells. I. Population kinetics, differential adhesiveness. and the absence of directed migration. *Proc Natl Acad Sci U S A*, 1962. **48**: p. 1577-82.
7. Steinberg, M.S., On the mechanism of tissue reconstruction by dissociated cells, III. Free energy relations and the reorganization of fused, heteronomic tissue fragments. *Proc Natl Acad Sci U S A*, 1962. **48**(10): p. 1769-76.
8. Steinberg, M.S., Reconstruction of tissues by dissociated cells. Some morphogenetic tissue movements and the sorting out of embryonic cells may have a common explanation. *Science*, 1963. **141**: p. 401-8.
9. Steinberg, M.S., Does differential adhesion govern self-assembly processes in histogenesis? Equilibrium configurations and the emergence of a hierarchy among populations of embryonic cells. *J Exp Zool*, 1970. **173**(4): p. 395-433.
10. Phillips, H.M. and M.S. Steinberg, Equilibrium measurements of embryonic chick cell adhesiveness. I. Shape equilibrium in centrifugal fields. *Proc Natl Acad Sci U S A*, 1969. **64**(1): p. 121-7.
11. Phillips, H.M., M.S. Steinberg, and B.H. Lipton, Embryonic tissues as elasticoviscous liquids. II. Direct evidence for cell slippage in centrifuged aggregates. *Dev Biol*, 1977. **59**(2): p. 124-34.
12. Phillips, H.M. and M.S. Steinberg, Embryonic tissues as elasticoviscous liquids. I. Rapid and slow shape changes in centrifuged cell aggregates. *J Cell Sci*, 1978. **30**: p. 1-20.
13. Wiseman, L.L., M.S. Steinberg, and H.M. Phillips, Experimental modulation of intercellular cohesiveness: reversal of tissue assembly patterns. *Dev Biol*, 1972. **28**(3): p. 498-517.
14. Forgacs, G., et al., Viscoelastic properties of living embryonic tissues: a quantitative study. *Biophys J*, 1998. **74**(5): p. 2227-34.
15. Mosher, D.F. and R.B. Johnson, In vitro formation of disulfide-bonded fibronectin multimers. *J Biol Chem*, 1983. **258**(10): p. 6595-601.

16. Li, R., et al., Activation of integrin $\alpha 5 \beta 1$ by modulation of transmembrane helix associations. *Science*, 2003. **300**(5620): p. 795-8.
17. Lu, C., J. Takagi, and T.A. Springer, Association of the membrane proximal regions of the α and β subunit cytoplasmic domains constrains an integrin in the inactive state. *J Biol Chem*, 2001. **276**(18): p. 14642-8.
18. Takagi, J., H.P. Erickson, and T.A. Springer, C-terminal opening mimics 'inside-out' activation of integrin $\alpha 5 \beta 1$. *Nat Struct Biol*, 2001. **8**(5): p. 412-6.
19. Coppolino, M.G. and S. Dedhar, Bi-directional signal transduction by integrin receptors. *Int J Biochem Cell Biol*, 2000. **32**(2): p. 171-88.
20. Humphries, M.J., et al., Integrin structure: heady advances in ligand binding, but activation still makes the knees wobble. *Trends Biochem Sci*, 2003. **28**(6): p. 313-20.
21. Ilic, D., et al., Reduced cell motility and enhanced focal adhesion contact formation in cells from FAK-deficient mice. *Nature*, 1995. **377**(6549): p. 539-44.
22. Hynes, R.O., The dynamic dialogue between cells and matrices: implications of fibronectin's elasticity. *Proc Natl Acad Sci U S A*, 1999. **96**(6): p. 2588-90.
23. Wu, C., et al., Integrin activation and cytoskeletal interaction are essential for the assembly of a fibronectin matrix. *Cell*, 1995. **83**(5): p. 715-24.
24. O'Toole, T.E., et al., Integrin cytoplasmic domains mediate inside-out signal transduction. *J Cell Biol*, 1994. **124**(6): p. 1047-59.
25. Hynes, R.O., Integrins: versatility, modulation, and signaling in cell adhesion. *Cell*, 1992. **69**(1): p. 11-25.
26. Schwarzbauer, J.E. and J.L. Sechler, Fibronectin fibrillogenesis: a paradigm for extracellular matrix assembly. *Curr Opin Cell Biol*, 1999. **11**(5): p. 622-7.
27. Sivasankar, S., et al., Direct molecular force measurements of multiple adhesive interactions between cadherin ectodomains. *Proc Natl Acad Sci U S A*, 1999. **96**(21): p. 11820-4.
28. Perret, E., et al., Fast dissociation kinetics between individual E-cadherin fragments revealed by flow chamber analysis. *EMBO J*, 2002. **21**(11): p. 2537-46.
29. Duguay, D., R.A. Foty, and M.S. Steinberg, Cadherin-mediated cell adhesion and tissue segregation: qualitative and quantitative determinants. *Dev Biol*, 2003. **253**(2): p. 309-23.
30. Hayman, E.G. and E. Ruoslahti, Distribution of fetal bovine serum fibronectin and endogenous rat cell fibronectin in extracellular matrix. *J Cell Biol*, 1979. **83**(1): p. 255-9.
31. Zhang, Z., et al., The $\alpha v \beta 1$ integrin functions as a fibronectin receptor but does not support fibronectin matrix assembly and cell migration on fibronectin. *J Cell Biol*, 1993. **122**(1): p. 235-42.
32. Robinson, E.E., $\alpha 5 \beta 1$ Integrin-Fibronectin Interaction Mediates Strong Tissue Cohesion, in Graduate School of Biomedical Sciences 2003, UMDNJ-Rutgers University Piscataway, NJ. p. 162.
33. Mould, A.P., et al., Regulation of integrin function: evidence that bivalent-cation-induced conformational changes lead to the unmasking of ligand-binding sites within integrin $\alpha 5 \beta 1$. *Biochem J*, 1998. **331** (Pt 3): p. 821-8.
34. Steinberg, M.S., "ECM": its nature, origin and function in cell aggregation. *Exp Cell Res*, 1963. **30**: p. 257-79.

35. Takeichi, M., The cadherins: cell-cell adhesion molecules controlling animal morphogenesis. *Development*, 1988. **102**(4): p. 639-55.
36. Foty, R.A., et al., Surface tensions of embryonic tissues predict their mutual envelopment behavior. *Development*, 1996. **122**(5): p. 1611-20.
37. Foty, R.A., et al., Liquid properties of embryonic tissues: Measurement of interfacial tensions. *Phys Rev Lett*, 1994. **72**(14): p. 2298-2301.
38. Schoetz, E.M., et al., Quantitative differences in tissue surface tension influence zebrafish germlayer positioning HFSP, 2008. **2**(1): p. 1-56.
39. Davies, J.T. and E.K. Rideal, *Interfacial Phenomena* by J.T. Davies and E.K. Rideal. 1961, New York and London: Academic Press. 480.
40. Corbett, S.A., et al., Covalent cross-linking of fibronectin to fibrin is required for maximal cell adhesion to a fibronectin-fibrin matrix. *J Biol Chem*, 1997. **272**(40): p. 24999-5005.
41. Rajaraman, R., S.P. Sunkara, and P.N. Rao, Morphological reverse transformation of Chinese hamster ovary (CHO) cells and surface fibronectin. *Cell Biol Int Rep*, 1980. **4**(10): p. 897-906.
42. Mao, Y. and J.E. Schwarzbauer, Fibronectin fibrillogenesis, a cell-mediated matrix assembly process. *Matrix Biol*, 2005. **24**(6): p. 389-99.
43. Robinson, E.E., R.A. Foty, and S.A. Corbett, Fibronectin matrix assembly regulates alpha5beta1-mediated cell cohesion. *Mol Biol Cell*, 2004. **15**(3): p. 973-81.
44. Erickson, H.P., Reversible unfolding of fibronectin type III and immunoglobulin domains provides the structural basis for stretch and elasticity of titin and fibronectin. *Proc Natl Acad Sci U S A*, 1994. **91**(21): p. 10114-8.
45. Armstrong, P.B., Ability of a Cell-Surface Protein Produced by Fibroblast to Modify Tissue Affinity Behaviour of Cardiac Myocytes. *Journal of Cell Science* 1980. **44**: p. 263-271.
46. Armstrong, P.B. and M.T. Armstrong, Immunofluorescent Histological Studies of the Role of Fibronectin in the Expression of the Associative Preference of Embryonic Tissues. *Journal of Cell Science*, 1981. **50**: p. 121-133.
47. Sottile, J. and J. Chandler, Fibronectin matrix turnover occurs through a caveolin-1-dependent process. *Mol Biol Cell*, 2005. **16**(2): p. 757-68.
48. Shi, F. and J. Sottile, Caveolin-1-dependent beta1 integrin endocytosis is a critical regulator of fibronectin turnover. *J Cell Sci*, 2008. **121**(Pt 14): p. 2360-71.
49. Aguirre, K.M., R.J. McCormick, and J.E. Schwarzbauer, Fibronectin self-association is mediated by complementary sites within the amino-terminal one-third of the molecule. *J Biol Chem*, 1994. **269**(45): p. 27863-8.
50. Hazan, R.B., et al., Exogenous expression of N-cadherin in breast cancer cells induces cell migration, invasion, and metastasis. *J Cell Biol*, 2000. **148**(4): p. 779-90.
51. Nakajima, S., et al., N-cadherin expression and epithelial-mesenchymal transition in pancreatic carcinoma. *Clin Cancer Res*, 2004. **10**(12 Pt 1): p. 4125-33.
52. Foty, R.A. and M.S. Steinberg, Cadherin-mediated cell-cell adhesion and tissue segregation in relation to malignancy. *Int J Dev Biol*, 2004. **48**(5-6): p. 397-409.
53. Jia, D., D. Dajusta, and R.A. Foty, Tissue surface tensions guide in vitro self-assembly of rodent pancreatic islet cells. *Dev Dyn*, 2007. **236**(8): p. 2039-49.

54. Armstrong, P.B. and M.T. Armstrong, A Role for Fibronectin in Cell Sorting. *Journal of Cell Science*, 1984. **69**: p. 179-197.

Chapter 4

Conclusions and Outlook

In the work presented here, we investigated the effect of type of adhesive system on the material and rearrangement properties of cells. To achieve this end, we used two approaches: *in silico* modeling to determine the effect of attractive/repulsive cues and the effect of range of interaction on cellular rearrangement and structure formation and *in vitro* validation of the *in silico* concept of range of interaction, which is defined as the effect of cells interacting through fibronectin matrix or ECM.

In our *in vitro* system, we had the ability to vary cell-ECM and cell-cell/cell-ECM interactions during cellular aggregation. The motivation of this work is based on long-standing questions about complex behaviors of embryonic tissues during the validation of the DAH and the likelihood that during development embryonic tissues actively use any of the available nodes of adhesion, e.g. cell-cell, cell-ECM, and cell-cell/cell-ECM, to achieve material and rearrangement properties effecting cellular morphogenesis.

In chapter 1, we made an ample description of current literature on computational aims to understand morphogenesis and the biological relevance of the work presented here. We particularly reviewed the historical perspective on the effect of *in vitro* cell-cell and cell-ECM interactions of engineered and embryonic cells in 3D geometries, in addition to the theoretical framework of the Differential Adhesion Hypothesis (DAH).

In chapter 2, our simulations demonstrated that mechanical interactions alone could spontaneously generate a few specific building blocks. This being the case, it is difficult to hold the view that evolution could have proceeded without at some point sampling these building blocks. This leaves it unclear which structures may be produced by chemical pre-patterns in additions to the tendency of cells to self-assemble using membrane-generated attractive/repulsive cues and the effect of the extracellular matrix.

Second, our simulations are considerably simplified, neglecting important effects including shape changes due to cytoskeletal forcing, feedback between external stresses and internal cellular functions, and even precise conservation of cellular volumes as agglomerates are compressed.

Certainly many of these shortcomings can be improved through computational embellishments and it would be important to establish whether the structures predicted in our simplified simulations are reproduced in more detailed and complicated models. Third, the simulations described in this section only used two components, while complex organ systems contain many more cell types, and even the earliest developmental processes progress from a three-part layer of endoderm, mesoderm and ectoderm cells. Thus it is desirable to investigate what self-assembled morphologies appear using more cell types. Finally, our simulations have exclusively been under steady conditions, whereas in vitro development exhibits extensive temporal control over protein expression affecting everything from small-scale growth and migration to larger scale entire organ size and shape. Evidently considerable in silico work remains ahead to understand how structures emerge, grow, and change during normal development.

In chapter 3, we designed an experimental system to understand the effect of the ECM, as found in our simulations that the range of interaction between cells plays an active role in the aggregation and rearrangement of cells. Here, we have measured the mechanical properties of aggregates held through cell-ECM and cell-ECM/cell-cell interactions. We determined that the biphasic nature of the surface tension of aggregates held through $\alpha 5\beta 1$ -Fn adhesion is the result of a balance between the level of integrin expression at the cell surface and the available soluble fibronectin in the

microenvironment. This further causes effect on the degree of aggregation of these cells. Besides the mechanical properties of these aggregates, we determine the rearrangement dynamics of cell suspensions finding expected and unexpected morphologies.

As for the expected morphologies, N-cad expression causes the known internal sorting, as postulated by the DAH. However, unexpected morphologies such as peripheral sorting of cohesive populations are readily seen with cell-ECM interactions. We determined that this morphology, originally described in embryonic heart cell mixtures, depends on specific integrin receptor expression and sFn concentration. This work describes mechanical and rearrangement behaviors that are potentially found during wound healing, development, and stroma-epithelial boundary dynamics during cancer states. Future work requires the scrutiny and differentiation of cytoplasmic pathways controlling cytoskeletal rearrangement during cell-ECM and cell-cell. Particularly, it would be of interest to correlate the different tissue properties and rearrangement behaviors as the result of receptor-mediated adhesion and highly regulated cytoskeletal dynamics.

Bibliography

1. Steinberg, M.S., On the mechanism of tissue reconstruction by dissociated cells. I. Population kinetics, differential adhesiveness. and the absence of directed migration. *Proc Natl Acad Sci U S A*, 1962. **48**: p. 1577-82.
2. Steinberg, M.S., Reconstruction of tissues by dissociated cells. Some morphogenetic tissue movements and the sorting out of embryonic cells may have a common explanation. *Science*, 1963. **141**: p. 401-8.
3. Steinberg, M.S., "ECM": its nature, origin and function in cell aggregation. *Exp Cell Res*, 1963. **30**: p. 257-79.
4. Steinberg, M.S., Does differential adhesion govern self-assembly processes in histogenesis? Equilibrium configurations and the emergence of a hierarchy among populations of embryonic cells. *J Exp Zool*, 1970. **173**(4): p. 395-433.
5. Steinberg, M.S., Cell-cell recognition in multicellular assembly: levels of specificity. *Symp Soc Exp Biol*, 1978. **32**: p. 25-49.
6. Foty, R.A., et al., Liquid properties of embryonic tissues: Measurement of interfacial tensions. *Phys Rev Lett*, 1994. **72**(14): p. 2298-2301.
7. Foty, R.A., et al., Surface tensions of embryonic tissues predict their mutual envelopment behavior. *Development*, 1996. **122**(5): p. 1611-20.
8. Foty, R.A. and M.S. Steinberg, The differential adhesion hypothesis: a direct evaluation. *Dev Biol*, 2005. **278**(1): p. 255-63.
9. Jia, D., D. Dajusta, and R.A. Foty, Tissue surface tensions guide in vitro self-assembly of rodent pancreatic islet cells. *Dev Dyn*, 2007. **236**(8): p. 2039-49.
10. Foty, R.A. and M.S. Steinberg, Measurement of tumor cell cohesion and suppression of invasion by E- or P-cadherin. *Cancer Res*, 1997. **57**(22): p. 5033-6.
11. Duguay, D., R.A. Foty, and M.S. Steinberg, Cadherin-mediated cell adhesion and tissue segregation: qualitative and quantitative determinants. *Dev Biol*, 2003. **253**(2): p. 309-23.
12. Ryan, P.L., et al., Tissue spreading on implantable substrates is a competitive outcome of cell-cell vs. cell-substratum adhesivity. *Proc Natl Acad Sci U S A*, 2001. **98**(8): p. 4323-7.
13. Townes, P.L. and J. Holtfreter, Directed movements and selective adhesion of embryonic amphibian cells *Journal of Experimental Zoology*, 1955. **28**(1): p. 53-120.
14. Steinberg, M.S. and M. Takeichi, Experimental specification of cell sorting, tissue spreading, and specific spatial patterning by quantitative differences in cadherin expression. *Proc Natl Acad Sci U S A*, 1994. **91**(1): p. 206-9.
15. Robinson, E.E., et al., Alpha5beta1 integrin mediates strong tissue cohesion. *J Cell Sci*, 2003. **116**(Pt 2): p. 377-86.
16. Robinson, E.E., R.A. Foty, and S.A. Corbett, Fibronectin matrix assembly regulates alpha5beta1-mediated cell cohesion. *Mol Biol Cell*, 2004. **15**(3): p. 973-81.
17. Watson, A.J., et al., Gene expression regulating blastocyst formation. *Theriogenology*, 1999. **51**(1): p. 117-33.

18. Pey, R., et al., Increase of intracellular Ca^{2+} and relocation of E-cadherin during experimental decompaction of mouse embryos. *Proc Natl Acad Sci U S A*, 1998. **95**(22): p. 12977-82.
19. Lauffenburger, D.A. and A. Wells, Getting a grip: new insights for cell adhesion and traction. *Nat Cell Biol*, 2001. **3**(5): p. E110-2.
20. Potts, J.R. and I.D. Campbell, Fibronectin structure and assembly. *Curr Opin Cell Biol*, 1994. **6**(5): p. 648-55.
21. Clark, K., et al., A specific $\alpha 5 \beta 1$ -integrin conformation promotes directional integrin translocation and fibronectin matrix formation. *J Cell Sci*, 2005. **118**(Pt 2): p. 291-300.
22. Johnson, K.E., T. Darribere, and J.C. Boucaut, Mesodermal cell adhesion to fibronectin-rich fibrillar extracellular matrix is required for normal *Rana pipiens* gastrulation. *J Exp Zool*, 1993. **265**(1): p. 40-53.
23. Darribere, T., et al., In vivo analyses of integrin beta 1 subunit function in fibronectin matrix assembly. *J Cell Biol*, 1990. **110**(5): p. 1813-23.
24. Darribere, T., et al., Distinct regions of human fibronectin are essential for fibril assembly in an in vivo developing system. *Dev Dyn*, 1992. **194**(1): p. 63-70.
25. Wiseman, L.L., M.S. Steinberg, and H.M. Phillips, Experimental modulation of intercellular cohesiveness: reversal of tissue assembly patterns. *Dev Biol*, 1972. **28**(3): p. 498-517.
26. Armstrong, P.B., Ability of a Cell-Surface Protein Produced by Fibroblast to Modify Tissue Affinity Behaviour of Cardiac Myocytes. *Journal of Cell Science* 1980. **44**: p. 263-271.
27. Armstrong, P.B. and M.T. Armstrong, Immunofluorescent Histological Studies of the Role of Fibronectin in the Expression of the Associative Preference of Embryonic Tissues. *Journal of Cell Science*, 1981. **50**: p. 121-133.
28. Steinberg, M.S., On the Mechanism of Tissue Reconstruction by Dissociated Cells, Iii. Free Energy Relations and the Reorganization of Fused, Heteronomic Tissue Fragments. *Proc Natl Acad Sci U S A*, 1962. **48**(10): p. 1769-76.
29. Phillips, H.M. and M.S. Steinberg, Embryonic tissues as elasticoviscous liquids. I. Rapid and slow shape changes in centrifuged cell aggregates. *J Cell Sci*, 1978. **30**: p. 1-20.
30. Ermentrout, G.B. and L. Edelstein-Keshet, Cellular automata approaches to biological modeling. *J Theor Biol*, 1993. **160**(1): p. 97-133.
31. Sulsky, D., S. Childress, and J.K. Percus, A model of cell sorting. *J Theor Biol*, 1984. **106**(3): p. 275-301.
32. Gordon, R., On stochastic growth and form. *Proc Natl Acad Sci U S A*, 1966. **56**(5): p. 1497-504.
33. Odell, G.M., et al., The mechanical basis of morphogenesis. I. Epithelial folding and invagination. *Dev Biol*, 1981. **85**(2): p. 446-62.
34. Sales, T.R., Unidimensional games, propitious environments, and maximum diversity. *Phys Rev E Stat Phys Plasmas Fluids Relat Interdiscip Topics*, 1993. **48**(4): p. 2418-2421.
35. E. R. Berlekamp, J.H.C., and R.K. Guy, Winning Ways for your Mathematical Play. Vol. 2. 1982, New York: Academic
36. Wolpert, L., Principles of Development 1998: Oxford University Press.

37. Yakoby, N., et al., *Drosophila* eggshell is patterned by sequential action of feedforward and feedback loops. *Development*, 2008. **135**(2): p. 343-51.
38. Goel, N.S. and G. Rogers, Computer simulation of engulfment and other movements of embryonic tissues. *J Theor Biol*, 1978. **71**(1): p. 103-40.
39. Rogers, G. and N.S. Goel, Computer simulation of cellular movements: cell-sorting, cellular migration through a mass of cells and contact inhibition. *J Theor Biol*, 1978. **71**(1): p. 141-66.
40. Goel, N.S. and A.G. Leith, Self-sorting of anisotropic cells. *J Theor Biol*, 1970. **28**(3): p. 469-82.
41. Leith, A.G. and N.S. Goel, Simulation of movement of cells during self-sorting. *J Theor Biol*, 1971. **33**(1): p. 171-88.
42. Graner, F. and J.A. Glazier, Simulation of biological cell sorting using a two-dimensional extended Potts model. *Phys Rev Lett*, 1992. **69**(13): p. 2013-2016.
43. Antonelli, P.L., T.D. Rogers, and M.A. Willard, Geometry and the exchange principle in cell aggregation kinetics. *J Theor Biol*, 1973. **41**(1): p. 1-21.
44. Armstrong, P.B. and D. Parenti, Cell sorting in the presence of cytochalasin B. *J Cell Biol*, 1972. **55**(3): p. 542-53.
45. Mombach, J.C., et al., Quantitative comparison between differential adhesion models and cell sorting in the presence and absence of fluctuations. *Phys Rev Lett*, 1995. **75**(11): p. 2244-2247.
46. Agarwal, P., Cellular segregation and engulfment simulations using the cell programming language. *J Theor Biol*, 1995. **176**(1): p. 79-89.
47. Arthur, W., D'Arcy Thompson and the theory of transformations. *Nat Rev Genet*, 2006. **7**(5): p. 401-6.
48. Hulpiau, P. and F. van Roy, Molecular evolution of the cadherin superfamily. *Int J Biochem Cell Biol*, 2009. **41**(2): p. 349-69.
49. Takeichi, M., Functional correlation between cell adhesive properties and some cell surface proteins. *J Cell Biol*, 1977. **75**(2 Pt 1): p. 464-74.
50. Zhurinsky, J., M. Shtutman, and A. Ben-Ze'ev, Plakoglobin and beta-catenin: protein interactions, regulation and biological roles. *J Cell Sci*, 2000. **113** (Pt 18): p. 3127-39.
51. Niessen, C.M., Tight junctions/adherens junctions: basic structure and function. *J Invest Dermatol*, 2007. **127**(11): p. 2525-32.
52. Holthofer, B., et al., Structure and function of desmosomes. *Int Rev Cytol*, 2007. **264**: p. 65-163.
53. Calera, M.R., A. Venkatakrishnan, and A. Kazlauskas, VE-cadherin increases the half-life of VEGF receptor 2. *Exp Cell Res*, 2004. **300**(1): p. 248-56.
54. Zhang, Y., et al., Resolving cadherin interactions and binding cooperativity at the single-molecule level. *Proc Natl Acad Sci U S A*, 2009. **106**(1): p. 109-14.
55. Nelson, W.J., Regulation of cell-cell adhesion by the cadherin-catenin complex. *Biochem Soc Trans*, 2008. **36**(Pt 2): p. 149-55.
56. Gumbiner, B.M., Regulation of cadherin adhesive activity. *J Cell Biol*, 2000. **148**(3): p. 399-404.
57. Kemler, R., Classical cadherins. *Semin Cell Biol*, 1992. **3**(3): p. 149-55.
58. Ivanov, D.B., M.P. Philippova, and V.A. Tkachuk, Structure and functions of classical cadherins. *Biochemistry (Mosc)*, 2001. **66**(10): p. 1174-86.

59. Alberts, B., et al., *Molecular Biology of the Cell*. 2002, NY: Taylor and Francis Group
60. Brackenbury, R., U. Rutishauser, and G.M. Edelman, Distinct calcium-independent and calcium-dependent adhesion systems of chicken embryo cells. *Proc Natl Acad Sci U S A*, 1981. **78**(1): p. 387-91.
61. Wang, B., et al., Alternative splicing of human NrCAM in neural and nonneural tissues. *Mol Cell Neurosci*, 1998. **10**(5-6): p. 287-95.
62. Friedlander, D.R., R. Brackenbury, and G.M. Edelman, Conversion of embryonic form to adult forms of N-CAM in vitro: results from de novo synthesis of adult forms. *J Cell Biol*, 1985. **101**(2): p. 412-9.
63. Acheson, A., J.L. Sunshine, and U. Rutishauser, NCAM polysialic acid can regulate both cell-cell and cell-substrate interactions. *J Cell Biol*, 1991. **114**(1): p. 143-53.
64. Aberle, H., H. Schwartz, and R. Kemler, Cadherin-catenin complex: protein interactions and their implications for cadherin function. *J Cell Biochem*, 1996. **61**(4): p. 514-23.
65. Bell, G.I., Models for the specific adhesion of cells to cells. *Science*, 1978. **200**(4342): p. 618-27.
66. Pagan, R., et al., Vimentin filaments follow the preexisting cytokeratin network during epithelial-mesenchymal transition of cultured neonatal rat hepatocytes. *Exp Cell Res*, 1996. **222**(2): p. 333-44.
67. Bajpai, S., et al., α -Catenin mediates initial E-cadherin-dependent cell-cell recognition and subsequent bond strengthening. *Proc Natl Acad Sci U S A*, 2008. **105**(47): p. 18331-6.
68. Tinkle, C.L., et al., New insights into cadherin function in epidermal sheet formation and maintenance of tissue integrity. *Proc Natl Acad Sci U S A*, 2008. **105**(40): p. 15405-10.
69. Jaiswal, M., N. Agrawal, and P. Sinha, Fat and Wingless signaling oppositely regulate epithelial cell-cell adhesion and distal wing development in *Drosophila*. *Development*, 2006. **133**(5): p. 925-35.
70. Lauffenburger, D.A. and L.G. Griffith, Who's got pull around here? Cell organization in development and tissue engineering. *Proc Natl Acad Sci U S A*, 2001. **98**(8): p. 4282-4.
71. Sottile, J. and D.C. Hocking, Fibronectin polymerization regulates the composition and stability of extracellular matrix fibrils and cell-matrix adhesions. *Mol Biol Cell*, 2002. **13**(10): p. 3546-59.
72. Alfandari, D., et al., Integrin $\alpha 5 \beta 1$ supports the migration of *Xenopus* cranial neural crest on fibronectin. *Dev Biol*, 2003. **260**(2): p. 449-64.
73. Sottile, J., D.C. Hocking, and P.J. Swiatek, Fibronectin matrix assembly enhances adhesion-dependent cell growth. *J Cell Sci*, 1998. **111** (Pt 19): p. 2933-43.
74. Shoulders, M.D. and R.T. Raines, Collagen Structure and Stability. *Annu Rev Biochem*, 2009.
75. Faull, R.J., et al., Affinity modulation of integrin $\alpha 5 \beta 1$: regulation of the functional response by soluble fibronectin. *J Cell Biol*, 1993. **121**(1): p. 155-62.
76. Bernfield, M., et al., Functions of cell surface heparan sulfate proteoglycans. *Annu Rev Biochem*, 1999. **68**: p. 729-77.

77. Lu, X.L., V.C. Mow, and X.E. Guo, Proteoglycans and mechanical behavior of condylar cartilage. *J Dent Res*, 2009. **88**(3): p. 244-8.
78. Viidik, A., C.C. Danielson, and H. Oxlund, On fundamental and phenomenological models, structure and mechanical properties of collagen, elastin and glycosaminoglycan complexes. *Biorheology*, 1982. **19**(3): p. 437-51.
79. Dhaliwal, J.S. and S.C. Kaufman, Corneal collagen cross-linking: a confocal, electron, and light microscopy study of eye bank corneas. *Cornea*, 2009. **28**(1): p. 62-7.
80. Robins, S.P., M. Shimokomaki, and A.J. Bailey, The chemistry of the collagen cross-links. Age-related changes in the reducible components of intact bovine collagen fibres. *Biochem J*, 1973. **131**(4): p. 771-80.
81. Gardiner, G.A., Jr., J. Bonn, and K.L. Sullivan, Quantification of elastic recoil after balloon angioplasty in the iliac arteries. *J Vasc Interv Radiol*, 2001. **12**(12): p. 1389-93.
82. Farand, P., A. Garon, and G.E. Plante, Structure of large arteries: orientation of elastin in rabbit aortic internal elastic lamina and in the elastic lamellae of aortic media. *Microvasc Res*, 2007. **73**(2): p. 95-9.
83. Lillie, M.A. and J.M. Gosline, Mechanical properties of elastin along the thoracic aorta in the pig. *J Biomech*, 2007. **40**(10): p. 2214-21.
84. Mizuno, T., et al., Overexpression of elastin fragments in infarcted myocardium attenuates scar expansion and heart dysfunction. *Am J Physiol Heart Circ Physiol*, 2005. **288**(6): p. H2819-27.
85. Fukumoto, S., et al., Laminin alpha5 is required for dental epithelium growth and polarity and the development of tooth bud and shape. *J Biol Chem*, 2006. **281**(8): p. 5008-16.
86. E. Ruoslahti, E.E., *Methods in Enzymology, Extracellular matrix Components*. . Vol. 245. 1994: Academic Press.
87. Ruoslahti, E. and A. Vaheri, Interaction of soluble fibroblast surface antigen with fibrinogen and fibrin. *J Exp Med*, 1975. **141**(2): p. 497-501.
88. Mosesson, M.W. and R.A. Umfleet, The cold-insoluble globulin of human plasma. I. Purification, primary characterization, and relationship to fibrinogen and other cold-insoluble fraction components. *J Biol Chem*, 1970. **245**(21): p. 5728-36.
89. Wilson, C.L. and J.E. Schwarzbauer, The alternatively spliced V region contributes to the differential incorporation of plasma and cellular fibronectins into fibrin clots. *J Cell Biol*, 1992. **119**(4): p. 923-33.
90. Stroka, K.M. and H. Aranda-Espinoza, Neutrophils display biphasic relationship between migration and substrate stiffness. *Cell Motil Cytoskeleton*, 2009.
91. Pankov, R. and K.M. Yamada, Fibronectin at a glance. *J Cell Sci*, 2002. **115**(Pt 20): p. 3861-3.
92. Hynes, R.O., Integrins: versatility, modulation, and signaling in cell adhesion. *Cell*, 1992. **69**(1): p. 11-25.
93. Petersen, T.E., et al., Partial primary structure of bovine plasma fibronectin: three types of internal homology. *Proc Natl Acad Sci U S A*, 1983. **80**(1): p. 137-41.

94. Hormann, H. and V. Jelinic, Fibronectin, VII. Binding of cold-insoluble globulin and of denatured collagen by macrophages. *Hoppe Seylers Z Physiol Chem*, 1980. **361**(3): p. 379-87.
95. Richter, H., M. Seidl, and H. Hormann, Location of heparin-binding sites of fibronectin. Detection of a hitherto unrecognized transamidase sensitive site. *Hoppe Seylers Z Physiol Chem*, 1981. **362**(4): p. 399-408.
96. Mosher, D.F. and R.A. Proctor, Binding and factor XIIIa-mediated cross-linking of a 27-kilodalton fragment of fibronectin to *Staphylococcus aureus*. *Science*, 1980. **209**(4459): p. 927-9.
97. Skorstengaard, K., H.C. Thogersen, and T.E. Petersen, Complete primary structure of the collagen-binding domain of bovine fibronectin. *Eur J Biochem*, 1984. **140**(2): p. 235-43.
98. Verfaillie, C.M., et al., Adhesion of committed human hematopoietic progenitors to synthetic peptides from the C-terminal heparin-binding domain of fibronectin: cooperation between the integrin alpha 4 beta 1 and the CD44 adhesion receptor. *Blood*, 1994. **84**(6): p. 1802-11.
99. Pierschbacher, M.D. and E. Ruoslahti, Cell attachment activity of fibronectin can be duplicated by small synthetic fragments of the molecule. *Nature*, 1984. **309**(5963): p. 30-3.
100. Schwarzbauer, J.E., Identification of the fibronectin sequences required for assembly of a fibrillar matrix. *J Cell Biol*, 1991. **113**(6): p. 1463-73.
101. Mao, Y. and J.E. Schwarzbauer, Fibronectin fibrillogenesis, a cell-mediated matrix assembly process. *Matrix Biol*, 2005. **24**(6): p. 389-99.
102. Mosher, D.F. and R.B. Johnson, In vitro formation of disulfide-bonded fibronectin multimers. *J Biol Chem*, 1983. **258**(10): p. 6595-601.
103. Langenbach, K.J. and J. Sottile, Identification of protein-disulfide isomerase activity in fibronectin. *J Biol Chem*, 1999. **274**(11): p. 7032-8.
104. Alexander, S.S., Jr., G. Colonna, and H. Edelhoch, The structure and stability of human plasma cold-insoluble globulin. *J Biol Chem*, 1979. **254**(5): p. 1501-5.
105. Principles of Biochemistry Second edition ed. 1992, New York Worth Publishers, Inc.
106. Sottile, J. and S. Wiley, Assembly of amino-terminal fibronectin dimers into the extracellular matrix. *J Biol Chem*, 1994. **269**(25): p. 17192-8.
107. Erickson, H.P., Reversible unfolding of fibronectin type III and immunoglobulin domains provides the structural basis for stretch and elasticity of titin and fibronectin. *Proc Natl Acad Sci U S A*, 1994. **91**(21): p. 10114-8.
108. Li, L., et al., Mechanical unfolding intermediates observed by single-molecule force spectroscopy in a fibronectin type III module. *J Mol Biol*, 2005. **345**(4): p. 817-26.
109. Gao, M., et al., Structure and functional significance of mechanically unfolded fibronectin type III intermediates. *Proc Natl Acad Sci U S A*, 2003. **100**(25): p. 14784-9.
110. Hynes, R.O., The dynamic dialogue between cells and matrices: implications of fibronectin's elasticity. *Proc Natl Acad Sci U S A*, 1999. **96**(6): p. 2588-90.
111. Schwarzbauer, J.E. and J.L. Sechler, Fibronectin fibrillogenesis: a paradigm for extracellular matrix assembly. *Curr Opin Cell Biol*, 1999. **11**(5): p. 622-7.

112. Vakonakis, I., et al., Interdomain association in fibronectin: insight into cryptic sites and fibrillogenesis. *EMBO J*, 2007. **26**(10): p. 2575-83.
113. Ohashi, T., D.P. Kiehart, and H.P. Erickson, Dual labeling of the fibronectin matrix and actin cytoskeleton with green fluorescent protein variants. *J Cell Sci*, 2002. **115**(Pt 6): p. 1221-9.
114. Davidson, L.A., et al., Live imaging of cell protrusive activity, and extracellular matrix assembly and remodeling during morphogenesis in the frog, *Xenopus laevis*. *Dev Dyn*, 2008. **237**(10): p. 2684-92.
115. Erickson, H.P., Stretching fibronectin. *J Muscle Res Cell Motil*, 2002. **23**(5-6): p. 575-80.
116. Mould, A.P., et al., Regulation of integrin function: evidence that bivalent-cation-induced conformational changes lead to the unmasking of ligand-binding sites within integrin $\alpha 5 \beta 1$. *Biochem J*, 1998. **331** (Pt 3): p. 821-8.
117. Sheets, E.D., R. Simson, and K. Jacobson, New insights into membrane dynamics from the analysis of cell surface interactions by physical methods. *Curr Opin Cell Biol*, 1995. **7**(5): p. 707-14.
118. Wiseman, P.W., et al., Spatial mapping of integrin interactions and dynamics during cell migration by image correlation microscopy. *J Cell Sci*, 2004. **117**(Pt 23): p. 5521-34.
119. Balaban, N.Q., et al., Force and focal adhesion assembly: a close relationship studied using elastic micropatterned substrates. *Nat Cell Biol*, 2001. **3**(5): p. 466-72.
120. Ballestrem, C., et al., Marching at the front and dragging behind: differential $\alpha V \beta 3$ -integrin turnover regulates focal adhesion behavior. *J Cell Biol*, 2001. **155**(7): p. 1319-32.
121. Coussen, F., et al., Trimers of the fibronectin cell adhesion domain localize to actin filament bundles and undergo rearward translocation. *J Cell Sci*, 2002. **115**(Pt 12): p. 2581-90.
122. Cuevas, B.D., et al., MEKK1 regulates calpain-dependent proteolysis of focal adhesion proteins for rear-end detachment of migrating fibroblasts. *EMBO J*, 2003. **22**(13): p. 3346-55.
123. Li, R., et al., Activation of integrin $\alpha IIb \beta 3$ by modulation of transmembrane helix associations. *Science*, 2003. **300**(5620): p. 795-8.
124. Lu, C., J. Takagi, and T.A. Springer, Association of the membrane proximal regions of the α and β subunit cytoplasmic domains constrains an integrin in the inactive state. *J Biol Chem*, 2001. **276**(18): p. 14642-8.
125. Takagi, J., H.P. Erickson, and T.A. Springer, C-terminal opening mimics 'inside-out' activation of integrin $\alpha 5 \beta 1$. *Nat Struct Biol*, 2001. **8**(5): p. 412-6.
126. Coppelino, M.G. and S. Dedhar, Bi-directional signal transduction by integrin receptors. *Int J Biochem Cell Biol*, 2000. **32**(2): p. 171-88.
127. O'Toole, T.E., et al., Integrin cytoplasmic domains mediate inside-out signal transduction. *J Cell Biol*, 1994. **124**(6): p. 1047-59.
128. Humphries, M.J., et al., Integrin structure: heady advances in ligand binding, but activation still makes the knees wobble. *Trends Biochem Sci*, 2003. **28**(6): p. 313-20.

129. Geiger, B., J.P. Spatz, and A.D. Bershadsky, Environmental sensing through focal adhesions. *Nat Rev Mol Cell Biol*, 2009. **10**(1): p. 21-33.
130. Cai, X., et al., Spatial and temporal regulation of focal adhesion kinase activity in living cells. *Mol Cell Biol*, 2008. **28**(1): p. 201-14.
131. Ilic, D., et al., Reduced cell motility and enhanced focal adhesion contact formation in cells from FAK-deficient mice. *Nature*, 1995. **377**(6549): p. 539-44.
132. Wu, C., et al., Integrin activation and cytoskeletal interaction are essential for the assembly of a fibronectin matrix. *Cell*, 1995. **83**(5): p. 715-24.
133. DiMilla, P.A., K. Barbee, and D.A. Lauffenburger, Mathematical model for the effects of adhesion and mechanics on cell migration speed. *Biophys J*, 1991. **60**(1): p. 15-37.
134. DiMilla, P.A., et al., Maximal migration of human smooth muscle cells on fibronectin and type IV collagen occurs at an intermediate attachment strength. *J Cell Biol*, 1993. **122**(3): p. 729-37.
135. Palecek, S.P., et al., Integrin-ligand binding properties govern cell migration speed through cell-substratum adhesiveness. *Nature*, 1997. **385**(6616): p. 537-40.
136. Zaman, M.H., et al., Computational model for cell migration in three-dimensional matrices. *Biophys J*, 2005. **89**(2): p. 1389-97.
138. Johnson, C.P., et al., Direct evidence that neural cell adhesion molecule (NCAM) polysialylation increases intermembrane repulsion and abrogates adhesion. *J Biol Chem*, 2005. **280**(1): p. 137-45.
139. Burgess, A., et al., Polysialic acid regulates the clustering, migration, and neuronal differentiation of progenitor cells in the adult hippocampus. *Dev Neurobiol*, 2008. **68**(14): p. 1580-90.
140. Xu, Q., et al., In vivo cell sorting in complementary segmental domains mediated by Eph receptors and ephrins. *Nature*, 1999. **399**(6733): p. 267-71.
141. Kullander, K. and R. Klein, Mechanisms and functions of Eph and ephrin signalling. *Nat Rev Mol Cell Biol*, 2002. **3**(7): p. 475-86.
142. Wilkinson, D.G., et al., Segmental expression of Hox-2 homoeobox-containing genes in the developing mouse hindbrain. *Nature*, 1989. **341**(6241): p. 405-9.
143. Stadler, H.S., K.M. Higgins, and M.R. Capecchi, Loss of Eph-receptor expression correlates with loss of cell adhesion and chondrogenic capacity in Hoxa13 mutant limbs. *Development*, 2001. **128**(21): p. 4177-88.
144. Chen, J. and H.E. Ruley, An enhancer element in the EphA2 (Eck) gene sufficient for rhombomere-specific expression is activated by HOXA1 and HOXB1 homeobox proteins. *J Biol Chem*, 1998. **273**(38): p. 24670-5.
145. Cooke, J.E., H.A. Kemp, and C.B. Moens, EphA4 is required for cell adhesion and rhombomere-boundary formation in the zebrafish. *Curr Biol*, 2005. **15**(6): p. 536-42.
146. Kemp, H.A., J.E. Cooke, and C.B. Moens, EphA4 and EfnB2a maintain rhombomere coherence by independently regulating intercalation of progenitor cells in the zebrafish neural keel. *Dev Biol*, 2009. **327**(2): p. 313-26.
147. Unified nomenclature for Eph family receptors and their ligands, the ephrins. Eph Nomenclature Committee. *Cell*, 1997. **90**(3): p. 403-4.
148. Palmer, A. and R. Klein, Multiple roles of ephrins in morphogenesis, neuronal networking, and brain function. *Genes Dev*, 2003. **17**(12): p. 1429-50.

149. Yang, N.Y., et al., The EphB4 receptor-tyrosine kinase promotes the migration of melanoma cells through Rho-mediated actin cytoskeleton reorganization. *J Biol Chem*, 2006. **281**(43): p. 32574-86.
150. Zhuang, G., et al., Regulation of EphA2 receptor endocytosis by SHIP2 lipid phosphatase via phosphatidylinositol 3-Kinase-dependent Rac1 activation. *J Biol Chem*, 2007. **282**(4): p. 2683-94.
151. Zimmer, M., et al., EphB-ephrinB bi-directional endocytosis terminates adhesion allowing contact mediated repulsion. *Nat Cell Biol*, 2003. **5**(10): p. 869-78.
152. Marston, D.J., S. Dickinson, and C.D. Nobes, Rac-dependent trans-endocytosis of ephrinBs regulates Eph-ephrin contact repulsion. *Nat Cell Biol*, 2003. **5**(10): p. 879-88.
153. Lin, K.T., et al., Ephrin-B2-induced cleavage of EphB2 receptor is mediated by matrix metalloproteinases to trigger cell repulsion. *J Biol Chem*, 2008. **283**(43): p. 28969-79.
154. Janes, P.W., et al., Adam meets Eph: an ADAM substrate recognition module acts as a molecular switch for ephrin cleavage in trans. *Cell*, 2005. **123**(2): p. 291-304.
155. Wilson, H.V., On some phenomena of coalescence and regeneration in sponges. *J. Exp. Zoo.*, 1907. **5**: p. 245-258.
156. Steinberg, M.S., In *Dynamical Phenomena at Interfaces, Surfaces and Membranes*, D. Baysens, N. Bocara, and G. Forgacs, Editors. 1993, Nova Science Commack, NY.
157. Phillips, H.M., M.S. Steinberg, and B.H. Lipton, Embryonic tissues as elasticoviscous liquids. II. Direct evidence for cell slippage in centrifuged aggregates. *Dev Biol*, 1977. **59**(2): p. 124-34.
158. Panorchan, P., et al., Single-molecule analysis of cadherin-mediated cell-cell adhesion. *J Cell Sci*, 2006. **119**(Pt 1): p. 66-74.
159. Foty, R.A., et al., Dexamethasone up-regulates cadherin expression and cohesion of HT-1080 human fibrosarcoma cells. *Cancer Res*, 1998. **58**(16): p. 3586-9.
160. Phillips, H.M. and M.S. Steinberg, Equilibrium measurements of embryonic chick cell adhesiveness. I. Shape equilibrium in centrifugal fields. *Proc Natl Acad Sci U S A*, 1969. **64**(1): p. 121-7.
161. Armstrong, P.B. and M.T. Armstrong, A Role for Fibronectin in Cell Sorting. *Journal of Cell Science*, 1984. **69**: p. 179-197.
162. Forgacs, G., et al., Viscoelastic properties of living embryonic tissues: a quantitative study. *Biophys J*, 1998. **74**(5): p. 2227-34.
163. Winters, B.S., S.R. Shepard, and R.A. Foty, Biophysical measurement of brain tumor cohesion. *Int J Cancer*, 2005. **114**(3): p. 371-9.
164. Winters, B.S., et al., Three-dimensional culture regulates Raf-1 expression to modulate fibronectin matrix assembly. *Mol Biol Cell*, 2006. **17**(8): p. 3386-96.
165. Abedin, M. and N. King, The premetazoan ancestry of cadherins. *Science*, 2008. **319**(5865): p. 946-8.
166. Escalante, R. and J.J. Vicente, Dictyostelium discoideum: a model system for differentiation and patterning. *Int J Dev Biol*, 2000. **44**(8): p. 819-35.
167. Vicker, M.G. and J.F. Grutsch, Dual chemotaxis signalling regulates Dictyostelium development: intercellular cyclic AMP pulses and intracellular F-

- actin disassembly waves induce each other. *Eur J Cell Biol*, 2008. **87**(10): p. 845-61.
168. Ti, Z.C., et al., Glycoprotein complexes interacting with cellulose in the "cell print" zones of the Dictyostelium discoideum extracellular matrix. *Dev Biol*, 1995. **168**(2): p. 332-41.
 169. Springer, W.R., D.N. Cooper, and S.H. Barondes, Discoidin I is implicated in cell-substratum attachment and ordered cell migration of Dictyostelium discoideum and resembles fibronectin. *Cell*, 1984. **39**(3 Pt 2): p. 557-64.
 170. Benoit, M., et al., Discrete interactions in cell adhesion measured by single-molecule force spectroscopy. *Nat Cell Biol*, 2000. **2**(6): p. 313-7.
 171. Alexandre, P., et al., Positive and negative regulations by FGF8 contribute to midbrain roof plate developmental plasticity. *Development*, 2006. **133**(15): p. 2905-13.
 172. Hoffmann, A.D., et al., sonic hedgehog is required in pulmonary endoderm for atrial septation. *Development*, 2009. **136**(10): p. 1761-70.
 173. van Es, S., et al., Universal signals control slime mold stalk formation. *Proc Natl Acad Sci U S A*, 1994. **91**(17): p. 8219-23.
 174. Kragtorp, K.A. and J.R. Miller, Integrin alpha5 is required for somite rotation and boundary formation in *Xenopus*. *Dev Dyn*, 2007. **236**(9): p. 2713-20.
 175. Kasemeier-Kulesa, J.C., et al., Eph/ephrins and N-cadherin coordinate to control the pattern of sympathetic ganglia. *Development*, 2006. **133**(24): p. 4839-47.
 176. Schoetz, E.M., et al., Quantitative differences in tissue surface tension influence zebrafish germlayer positioning HFSP, 2008. **2**(1): p. 1-56.
 177. Sweeney, D., N. Lindstrom, and J.A. Davies, Developmental plasticity and regenerative capacity in the renal ureteric bud/collecting duct system. *Development*, 2008. **135**(15): p. 2505-10.
 178. Greiner, T.U., et al., Rac1 regulates pancreatic islet morphogenesis. *BMC Dev Biol*, 2009. **9**: p. 2.
 179. Nelson, C.M., et al., Change in cell shape is required for matrix metalloproteinase-induced epithelial-mesenchymal transition of mammary epithelial cells. *J Cell Biochem*, 2008. **105**(1): p. 25-33.
 180. Discher, D.E., P. Janmey, and Y.L. Wang, Tissue cells feel and respond to the stiffness of their substrate. *Science*, 2005. **310**(5751): p. 1139-43.
 181. Beningo, K.A., M. Dembo, and Y.L. Wang, Responses of fibroblasts to anchorage of dorsal extracellular matrix receptors. *Proc Natl Acad Sci U S A*, 2004. **101**(52): p. 18024-9.
 182. Wang, S., et al., Three-dimensional primary hepatocyte culture in synthetic self-assembling peptide hydrogel. *Tissue Eng Part A*, 2008. **14**(2): p. 227-36.
 183. Alcaraz, J., et al., Laminin and biomimetic extracellular elasticity enhance functional differentiation in mammary epithelia. *EMBO J*, 2008. **27**(21): p. 2829-38.
 184. Gray, D.S., J. Tien, and C.S. Chen, Repositioning of cells by mechanotaxis on surfaces with micropatterned Young's modulus. *J Biomed Mater Res A*, 2003. **66**(3): p. 605-14.

185. Hadjipanayi, E., R.A. Brown, and V. Mudera, Interface integration of layered collagen scaffolds with defined matrix stiffness: implications for sheet-based tissue engineering. *J Tissue Eng Regen Med*, 2009. **3**(3): p. 230-41.

Curriculum Vitae

Carlos E. Caicedo-Carvajal

EDUCATION

RUTGERS UNIVERSITY/UMDNJ-RWJMS, Piscataway, NJ
PhD in Biomedical Engineering, October 2009

RUTGERS UNIVERSITY, New Brunswick, NJ
B.S., Biochemistry, May 2001

COUNTY COLLEGE OF MORRIS, Randolph, NJ
Associate Degree in Chemistry, May 1999

RESEARCH EXPERIENCE

RUTGERS UNIVERSITY/UMDNJ-RWJMS, Piscataway, NJ
Graduate Student, Biomedical Engineering Department/ Department of Surgery, 2005-2009

RUTGERS UNIVERSITY, Piscataway, NJ
Graduate Student, Chemical Engineering Department, 2003-2005

RUTGERS UNIVERSITY, Piscataway, NJ
Laboratory Technician, New Jersey Center for Biomaterials, 2001-2002

RUTGERS UNIVERSITY, Piscataway, NJ
Undergraduate, New Jersey Center for Biomaterials, 2000-2001
Undergraduate, Bristol-Myers Squibb Internship, Summer 1999

PUBLICATIONS

Shinbrot T, Y. Chun, C.E. Caicedo-Carvajal, R. Foty. Cellular Morphogenesis In Silico. Biophysical Journal. (In Print July, 2009)

Caicedo-Carvajal C.E. and T. Shinbrot. In silico zebrafish pattern formation (2008). Dev Biol. 15; 315(2):397-403

Caicedo-Carvajal C.E., Benjamin J. Glasser, and T. Shinbrot. Granular flow transitions on sinusoidal surfaces (2006). Journal of Fluid Mechanics. 556:253-269

Weber N, C.E. Caicedo-Carvajal, C. Nardin, and J. Kohn. Measurement of Protein Adsorption and Cell Adhesion onto Polymer Surfaces Using Immuno-Fluorescent Assays (IFA) and the QCM-D Technique: A Comparative Study (2004). Mat. Res. Soc. Symp. Proc. Vol. EXS-1 F5.25.1

TEACHING EXPERIENCE

Rutgers Upward Bound Summer Program 2004 – 2007

Rutgers Governor School Summer Program 2007

Rutgers Upward Bound Saturday School Fall 2006-Spring 2000